EPA-600/R-95-142a
September 1995

Statewide Mapping of Florida Soil Radon Potentials

Volume 1. Technical Report

by

Kirk K. Nielson, Rodger B. Holt, and Vern C. Rogers
Rogers & Associates Engineering Corporation
P.O. Box 330, Salt Lake City, UT 84110-0330

EPA Interagency Agreement RWFL 93378-01
Florida Department of Community Affairs Contract 94RD-30-13-00-22-003
University of Florida Subcontract (Acct. 1506481-12)

EPA Project Officer: David C. Sanchez
U. S. Environmental Protection Agency
National Risk Management Research Laboratory
Air Pollution Prevention and Control Division
Research Triangle Park, NC 27711

Prepared for:

Florida Department of Community Affairs
2740 Centerview Drive
Tallahassee, FL 32399
(DCA Project Officer: Mohammad Madani)

and

U. S. Environmental Protection Agency
Office of Research and Development
Washington, DC 20460

TECHNICAL REPORT DATA
(Please read Instructions on the reverse before comple

1. REPORT NO. EPA-600/R-95-142a	2.	3. PB96-104351
4. TITLE AND SUBTITLE Statewide Mapping of Florida Soil Radon Potentials, Volume 1. Technical Report		5. REPORT DATE September 1995
		6. PERFORMING ORGANIZATION CODE
7. AUTHOR(S) Kirk K. Nielson, Rodger B. Holt, and Vern C. Rogers		8. PERFORMING ORGANIZATION REPORT NO. RAE-9226/2-2R1
9. PERFORMING ORGANIZATION NAME AND ADDRESS Rogers and Associates Engineering Corporation P.O. Box 330 Salt Lake City, Utah 84110-0330		10. PROGRAM ELEMENT NO.
		11. CONTRACT/GRANT NO. EPA IAG RWFL 93378-01
12. SPONSORING AGENCY NAME AND ADDRESS **EPA, Office of Research and Development** **Air Pollution Prevention and Control Division** **Research Triangle Park, NC 27711**		13. TYPE OF REPORT AND PERIOD COVERED Final; 4/92 - 9/94
		14. SPONSORING AGENCY CODE **EPA/600/13**

15. SUPPLEMENTARY NOTES APPCD project officer is David C. Sanchez, Mail Drop 54, 919/541-2979. Volume 2 contains Appendices A-P.

16. ABSTRACT The report gives results of statewide mapping of Florida soil radon potentials. Statewide maps identify Florida regions with different levels of soil radon potential. The maps provide scientific estimates of regional radon potentials that can serve as a basis for implementing radon-protective residential building standards where they are needed. The maps were developed from state soil maps and surface geology maps, which divided the state into 3,919 regions with unique combinations of soil and geologic properties. The potentials of the soil profiles in each region to contribute to indoor radpon levels were calculated and used to classify each map region into one of seven tiers of radon potential. The maps were validated by comparisons with more than 1,000 radon flux measurements and with 9,038 indoor radon measurements from three data sets. The comparisons showed consistency between the measurements and the radon potential maps, with approximately the expected numbers of outlier points. Field investigations of the outlier data points showed trends associating certain construction details with positive or negative biases. Radon potentials were calculated using a mathematical model of radon generation and transport from the top 5 m of surface soils into a reference house. Upper confidence limits of 70, 90, and 95% were defined for the radon potentials, in addition to regional median values.

17. KEY WORDS AND DOCUMENT ANALYSIS

a. DESCRIPTORS	b. IDENTIFIERS/OPEN ENDED TERMS	c. COSATI Field/Group
Pollution	Pollution Control	13B
Radon	Stationary Sources	07B
Soils	Indoor Air	08G, 08M
Mapping		08B
Residential Buildings		13M
Building Codes		05D

18. DISTRIBUTION STATEMENT **Release to Public**	19. SECURITY CLASS *(This Report)* **Unclassified**	21. NO. OF PAGES 105
	20. SECURITY CLASS *(This page)* **Unclassified**	22. PRICE

EPA Form 2220-1 (9-73)

NOTICE

This document has been reviewed in accordance with U.S. Environmental Protection Agency policy and approved for publication. Mention of trade names or commercial products does not constitute endorsement or recommendation for use.

FOREWORD

The U.S. Environmental Protection Agency is charged by Congress with protecting the Nation's land, air, and water resources. Under a mandate of national environmental laws, the Agency strives to formulate and implement actions leading to a compatible balance between human activities and the ability of natural systems to support and nurture life. To meet this mandate, EPA's research program is providing data and technical support for solving environmental problems today and building a science knowledge base necessary to manage our ecological resources wisely, understand how pollutants affect our health, and prevent or reduce environmental risks in the future.

The National Risk Management Research Laboratory is the Agency's center for investigation of technological and management approaches for reducing risks from threats to human health and the environment. The focus of the Laboratory's research program is on methods for the prevention and control of pollution to air, land, water, and subsurface resources; protection of water quality in public water systems; remediation of contaminated sites and groundwater; and prevention and control of indoor air pollution. The goal of this research effort is to catalyze development and implementation of innovative, cost-effective environmental technologies; develop scientific and engineering information needed by EPA to support regulatory and policy decisions; and provide technical support and information transfer to ensure effective implementation of environmental regulations and strategies.

This publication has been produced as part of the Laboratory's strategic long-term research plan. It is published and made available by EPA's Office of Research and Development to assist the user community and to link researchers with their clients.

E. Timothy Oppelt, Director
National Risk Management Research Laboratory

ABSTRACT

This report documents the characterization of soil radon potentials to be used in state wide soil radon potential maps of Florida. The maps are designed to show from soil and geological features the areas that have different levels of radon potential. The soil radon potential maps have been proposed as a basis for implementing radon-protective building construction standards in areas of elevated radon risk and avoiding unnecessary regulations in areas of low radon risk. The soil radon potentials calculated in this report are revised from previous regional estimates of radon potentials to eliminate boundary faults.

Discrete areas (polygons) on the radon maps were defined from the digital intersection of State Soil Geographic Data Base (STATSGO) soil map units with digitized geological map units. The University of Florida GeoPlan Center defined the map polygons using a geographic information system with ArcInfo format. The GeoPlan Center also partitioned National Uranium Resource Evaluation (NURE) aeroradiometric data for each polygon.

Radon potentials of each map polygon were estimated from the radon source and transport properties of the soil profiles that comprise the region represented by the polygon. Radon source properties include soil radium concentrations and radon emanation coefficients. Soil radium concentrations were estimated from NURE aeroradiometric data for shallow horizons (surface to 2 or 2.5m depth), and from geological classifications of the soils for deep horizons (to 5m depth). Radon emanation coefficients were based on trends from nearly 400 measurements on county-survey soil samples from most counties throughout the state. Radon transport properties (water contents, radon diffusion coefficients, and air permeabilities) were estimated from soil profile physical data compiled for the STATSGO soil maps from Soil Conservation Service (SCS) data bases by the University of Florida Soil and Water Science Department. Summary soil data files characterized soil densities, particle size distributions, water drainage curves, high water table depths and durations, and other mechanical and hydrological data. Radon transport properties were calculated from these data.

Soil radon potentials are quantified as calculated annual average radon entry rates into a reference house. The radon potentials were computed by mathematically modeling the reference house, typical of Florida slab-on-grade single-family housing, as if it were located on each soil profile of each of the radon map polygons. The parameters characterizing the reference house were held constant for the calculation on each polygon in order to include only the varied soil effects on each radon potential calculation. The model calculations were based on the RAETRAD (RAdon Emanation and TRAnsport into Dwellings) model, but were conducted using a more specialized, benchmarked radon potential cartography algorithm named RnMAP. Both models calculated radon potentials as the rate of radon entry into the reference house. Annual units (mCi y^{-1}) were used for the radon potentials to emphasize the long-term average nature of the radon potential estimates.

Radon potentials were calculated and then averaged for each of several soil profiles in each polygon, at each of two or three seasonal water table depths. They also were calculated for low, intermediate, or elevated-radium geology classes for most of the state, and the applicable geologic classification was used afterward to select the appropriate values to use in representing each polygon. Separate radon potentials were calculated for the estimated median radium concentrations and soil conditions, and also for radium and soil conditions corresponding to the 75%, 90%, and 95% confidence limits for area distributions within each polygon. The confidence limits were calculated from the geometric means and geometric standard deviations of radium and soil transport properties for each map polygon. The radium distributions were estimated from multiple NURE data points in many of the polygons that intersected NURE flight lines. Radium estimates for polygons not intersected by NURE flight lines were extrapolated from the overall data for the geologic unit in which the polygon was located. Distributions of soil radon transport properties were estimated from the multiple soil profiles defined to comprise each STATSGO map unit.

The resulting radon potentials were partitioned into seven tiers of similar numerical values for display on the radon potential maps. The tiers corresponded to the 0-0.4, 0.4-1, 1-2, 2-3, 3-6, 6-12, and >12 mCi y^{-1} levels of radon potential. This set of tiers provided suitable range for using a uniform tier scale on all of the radon potential maps. Map polygons finally were colored according to the appropriate tier classification for intuitive visual interpretation. This report presents numerical values of the radon potentials computed for each map polygon for more quantitative interpretations of the maps. A radon potential of approximately 3 mCi y^{-1} corresponds to approximately 3.9 pCi L^{-1} of soil-related radon in the reference house.

Separate maps were plotted for the median (50%), 75%, 90%, and 95% confidence limits of radon potentials to give a better perspective of radon potentials in a given polygon (region). Regions with low potentials on both the median and higher-confidence-limit maps have reasonable assurance of having minimal indoor radon risk. Regions with high radon potentials on the median and higher-confidence-limit maps conversely have a relatively high probability of elevated indoor radon levels. Regions with low median radon potentials but high potentials for higher confidence limits are heterogeneous (low median; high geometric standard deviation) and may have generally low radon potentials but occasional to frequent anomalies with high radon potential. Special considerations may be needed to define radon-protective building needs in these areas.

Comparisons of calculated radon potentials with 2,930 state-wide land-based indoor radon measurements were consistent with the reference-house indoor radon accumulation rate of 1.3 pCi L^{-1} per mCi y^{-1} of soil radon potential, and with an ambient outdoor radon concentration of approximately 0.1 pCi L^{-1}. The geometric standard deviation (GSD) between measured indoor radon levels and those predicted from the maps was 1.9, which is the approximate level of precision associated with the calculated soil radon potentials. The total variation among measured indoor radon levels was partitioned to estimate a house variability of approximately GSD=3.2, an annual-average measurement uncertainty of approximately GSD=2.1, and soil variabilities averaging approximately GSD=2. Uncertainties are much higher in predicting an indoor radon level for a particular house than for predicting the median level in the reference

house for a given polygon.

The soil radon potential map data were validated by state-wide comparisons with over a thousand soil radon flux measurements at 330 locations and with 9,038 indoor radon measurements from three different data sets. The radon flux measurements averaged similar to the map predictions, but were scattered more widely than the map data (16 below and 18 above the central 95% range, compared to eight expected for each). The difference in scatter is caused by inadequate definition of the temporal variations in radon flux that are needed for comparing the 24-hour flux measurements to annual-average calculated values.

The Geomet land-based data set best represents all regions of Florida and agrees very well with the map predictions. The middle 95% of the map range included 95.4% of the 2,952 measurements, with 1.9% below and 2.7% above the mid-range, compared to 2.5% expected for each. The HRS residential and Geomet population data sets do not represent all regions in Florida, but they were compared with the map predictions anyway. The 2,095 measurements in the Geomet population-based set averaged slightly lower than map values, while the 3,938 measurements in the HRS residential data set averaged slightly higher than map values.

Over 250 houses with the greatest differences between measured and predicted indoor radon concentrations were investigated and found to show trends that offer further explanations. Houses above the 95% mid-range were nearly three times more likely to use slab-on-grade construction than to have crawl spaces, while the opposite trend was seen for houses below the mid-range. Similarly, houses above the 95% mid-range were about 50% more likely to use hollow-block construction than frame construction, and the opposite trend was also seen for houses below the mid-range. These trends are consistent with model predictions, and account for potential anomalies on a state-wide level. Considering the variations in both measurements and map calculations, the measurements give excellent overall state-wide validation of the radon maps.

ACKNOWLEDGEMENTS

This project was conducted under review and guidance from the Radon Potential Cartography Committee of the Florida Radon Research Program. Soil survey data bases, samples, and STATSGO soil mapping data were provided by Randall B. Brown, Willie G. Harris, and Ronald J. Kuehl of the University of Florida Soil and Water Science Department, Gainesville, FL. Aeroradiometric data tapes and interpretations of geologic maps were provided by James K. Otton of the U. S. Geological Survey, Denver, CO. Geologic maps were provided by Thomas M. Scott of the Florida Geological Survey, Tallahassee, FL. Geographic partitioning of aeroradiometric and radon measurement data, intersections of soil and geology maps, and plotting of all radon maps were performed by Stanley D. Latimer and Paul D. Zwick of the University of Florida GeoPlan Center, Gainesville, FL.

TABLE OF CONTENTS

TABLE OF CONTENTS
(Continued)

(*) All appendices are in Volume 2.

TABLE OF CONTENTS
(Continued)

LIST OF FIGURES

LIST OF FIGURES
(Continued)

LIST OF FIGURES
(Continued)

LIST OF TABLES

Section 1
INTRODUCTION

1.1 BACKGROUND

Radon (^{222}Rn) gas from the decay of naturally-occurring radium (^{226}Ra) in soils can enter indoors through building foundations. If enough radon enters and the building is inadequately ventilated, radon can accumulate to a level that poses significant risks of lung cancer with chronic exposure. The degree of health risk is proportional to the long-term average level of radon exposure. The U.S. Environmental Protection Agency (EPA) attributes 7,000 to 30,000 lung cancer fatalities annually to radon, and recommends remedial action if indoor levels average 4 picocuries per liter (pCi L^{-1}) or higher (EPA92a). Indoor radon levels average about 1.25 pCi L^{-1} in the United States, and about 1% of all U.S. homes exceed 8 pCi L^{-1} (EPA92b).

The Florida Department of Community Affairs (DCA), under the Florida Radon Research Program (FRRP), is developing radon-protective building standards to reduce radon-related health risks (San90, SBC90). If integrated into state-wide building codes, the standards could add an incremental cost for new construction. To minimize economic impacts and still protect public health, the radon-protective building standards may be applied regionally where soils have the potential to cause elevated indoor radon. Although radon data are highly variable, regional trends support the use of a geographic basis for the radon-protective building standards (Coh86, Nag87, Pea90, EPA92b).

State-wide mapping of soil radon potentials has been proposed for developing a systematic basis for regional building standards in Florida (Nie91a). Alternative radon mapping approaches were evaluated in an FRRP workshop (Nie91b), and the present conceptual approach was selected to best utilize existing resources and to minimize regional bias. The approach was tested on a detailed scale in Alachua County (Nie91c), and was revised for more general, systematic applications to larger areas (Nie94a,b). For regional and state-wide radon

mapping, the methods were further revised to exclude county boundary influences, to eliminate polygons smaller than one square mile, and to explicitly include soil variations within map polygons. Using the revised methods, ten regional maps were developed that covered the entire state of Florida (Nie94b). The regional maps demonstrated several boundary faults when combined to form a state map, however, and therefore required revision. This report describes the state-wide revision of the maps to eliminate the regional boundary influences and to correct an inconsistency in the aeroradiometric data set. For completeness, this report also documents the technical basis and methods used to generate the present maps.

Soil radon potentials depend mainly on soil radium concentrations, radon emanation fractions, moisture, air permeability, diffusivity, and density. Indoor air pressures also affect radon entry rates, and house ventilation affects the extent of radon accumulation. House properties such as floor and foundation construction and design also affect the relation between indoor radon levels and soil radon potential. Although indoor radon levels depend on house conditions as well as soil properties, the effects of soil properties can be separated for mapping of soil radon potentials by holding the house parameters constant.

Previous radon maps have generally displayed different tiers of measured indoor radon levels for geographic units such as county or township areas, ZIP-Code areas, or physiographic or geologic units. As reviewed in the FRRP radon mapping workshop and feasibility study (Nie91a,b), other mapping approaches also have included numerical radon indices, aeroradiometric gamma activity, uranium mineralization zones, and surface outcrops of radium-mineralized geological formations. Although these approaches show where elevated radon has been or may be observed, they are generally inadequate for undeveloped or sparsely-populated areas with limited data from previous radon testing. They also are indirect or imprecise predictors of indoor radon or of radon-protection needs for new construction. Maps aimed at optimizing testing programs or locating areas of highest observed indoor radon are already available for Florida (Nag87).

Effective radon-resistant construction methods have been developed (EPA86, Osb88, Mur90, Bre90, Cla91). Current use of these methods is mostly voluntary or liability-oriented,

however, because most building regulations have not addressed radon protection. Recent initiatives to implement radon-protective building codes have raised important policy issues (Nue90), including altered property values, zoning and enforcement boundaries, and the confidence with which radon levels can be predicted or generalized. Previous county-scale radon classifications in Florida (Nag87) have been challenged for failure to correlate with health effects (Von90). Prevalent theoretical and empirical studies support the predictability, avoidability, and health effects of indoor radon (EPA92a), and suggest benefits from institutional controls to limit human exposures. Radon-protective building technology has been demonstrated for new construction (Nit89) and for remedial action (Fin89, Sco88, Sco89). Active mitigation systems generally are most effective, but they are more costly and require more maintenance than passive systems installed during initial construction. Regulations have been successfully implemented in some places to require radon-resistant features in new construction (Swe86, Swe90).

1.2 OBJECTIVES AND TECHNICAL APPROACH

The objectives of mapping soil radon potentials in Florida are to provide a sound scientific basis for implementing radon-protective building standards where needed, and to avoid the cost of unnecessarily implementing the standards where they are not needed. The measure of *soil radon potential* is defined as a calculated annual-average rate of radon entry from soils into a reference house.

As identified previously (Nie91b,c), several institutional and scientific criteria were considered in defining the technical approach. First, the maps must identify as precisely as possible the regions that need radon-protective building features for reduced indoor radon concentrations. The maps should also avoid political and institutional boundaries (city, county, etc.) that are not radon-related. The maps should not be restrictively tied to a preconceived radon standard (i.e., 4 pCi L^{-1}), and they should minimize uncertainties from variations in time, house design, and occupancy.

The approach to achieve these objectives was developed in the FRRP Workshop on Radon Potential Mapping and later feasibility studies (Nie91a,b,c) to satisfy institutional and scientific goals and objectives. This approach separates the soil radon potential from other factors that influence indoor radon levels to include only the soil properties that affect the radon source and its availability. The approach consists of:

a. Regional definition of radon map polygons (geographic areas on a radon map) from existing soil and geologic maps.

b. Definition of the soil profiles associated with each radon map polygon, and their associated radon generation and transport properties.

c. Calculation of numeric radon potentials for individual soil profiles, and an area-weighted average to represent each radon map polygon.

d. Grouping map units with similar radon potentials and plotting the radon map polygons by color-coded radon potential tiers.

This general approach has been demonstrated in the preceding regional radon maps of Florida (Nie94b). It was also followed in the present revised state-wide mapping of Florida soil radon potentials.

1.2.1 Partitioning of Variations

The mapping approach used here separates the *soil* radon potential from other factors that influence indoor radon. Besides soil effects, indoor levels also are affected by *house* characteristics and by *time variations* in the soil and house properties. The *time variations* are not of interest because only long-term averages are important for radon exposures and their underlying radon source strengths and house radon resistance. The time variations are eliminated by using long-term average values for all time-variant parameters such as indoor air pressure, house ventilation, indoor radon levels, soil water contents, etc. Properties such as radium concentration, density, and porosity are virtually constant. Others, including soil air permeability and diffusivity, vary with time, but are dominated by moisture changes. Hence their values may be estimated from representative soil water contents.

Long-term average soil water contents under structures can be defined from the drained field capacity of the soil. This water content commonly is related to a prescribed soil capillary suction or matric potential (Lut79) that is independent of immediate rainfall conditions or surface drying. It can be predicted if necessary solely from the soil textural classification and porosity (Nie92a). The effects of varying water-table depths also are important for the shallow water tables encountered in Florida, and can be included in defining the soil water profiles from their capillary suction (Nie92a).

House variations are eliminated similarly to time variations by averaging over the house variables to define an invariant, reference house. Its properties approximate those of Florida single-family dwellings, and it can be modeled as if constructed in any source (soil profile) location. Soil radon potentials then are estimated for each map unit as the calculated rate of radon entry into the reference house at each defined source location, independent of house and occupant variations.

The partitioning of soil and house variations, suggested at the FRRP Workshop on Radon Potential Mapping (Nie91b), is illustrated by the two-stage modeling shown in Figure 1-1. As illustrated, all radon source and transport parameters are combined with the reference house parameters in the radon entry model to estimate soil radon potential in units of radon entry rate (radon activity per unit time). The resulting soil radon potential varies geographically only with soil radon generation and transport properties, and is independent of house and occupant variations that further broaden distributions of indoor radon concentrations. The soil radon potentials can be used separately in a radon balance model to estimate indoor radon concentrations. However, for mapping purposes, the geographic variation of soil radon potential is best described independent of house variations. Comparisons with indoor radon levels can be made by statistically comparing the medians and distributions of indoor data with the distributions of corresponding soil radon potentials. Such comparisons reveal the effects of house and occupant variability.

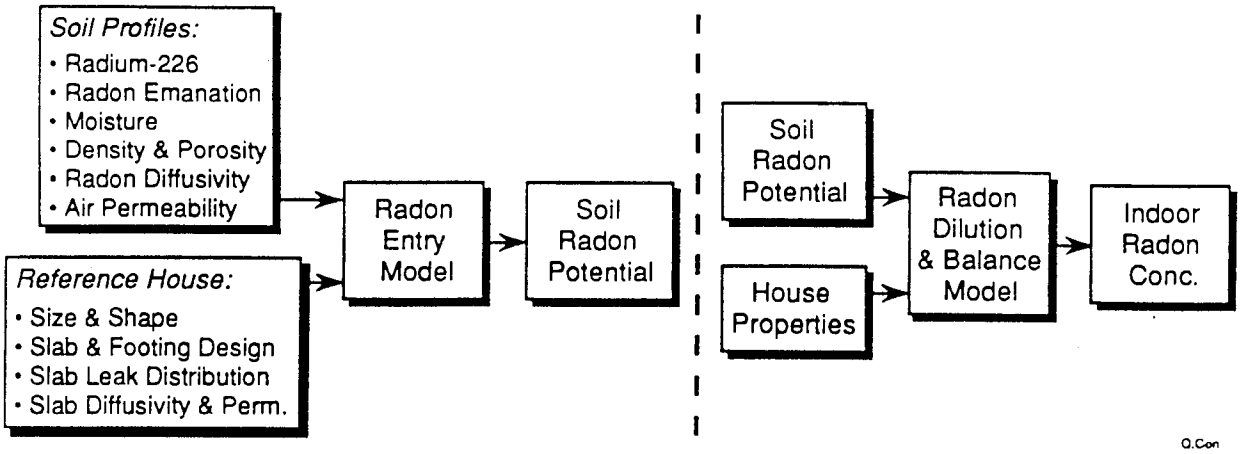

Figure 1-1. Partitioning of Radon Source and House Variations.

1.2.2 Definition of Radon Map Polygons

The map polygons used to represent geographic areas with different radon potentials were defined by the digital intersection of State Soil Geographic Data Base (STATSGO) soil maps with surface geology maps. This produced a soil radon profile map with polygons that were independent of institutional boundaries. Each polygon resulting from this intersection was numbered and characterized from its location and its particular combination of soil and geologic properties. The STATSGO soil maps (SCS91) provide summary digital coverage of soil units throughout Florida, based on higher-resolution soil survey data that presently are only digitized for a few counties in Florida. The STATSGO soil maps were chosen for their more complete, state-wide coverage and because the higher-resolution soil maps did not significantly improve estimates of soil radon potentials (Nie92b). The digital STATSGO map files provided by the University of Florida Soil and Water Science Department defined 165 different soil map units that occurred in multiple geographic areas that comprised several thousand soil map polygons in the state-wide STATSGO soil map.

The surface geology maps used in preparing the soil radon profile map were provided from newly-revised surface geology studies by the Florida Geological Survey. The maps were digitized and then intersected with the STATSGO soil maps by the University of Florida GeoPlan Center using a geographic information system with Arc-Info data formats. The geologic maps defined 46 geologic map units that occurred in multiple geographic areas that comprised several hundred geologic map polygons in the state-wide surface geology map. The U.S. Geological Survey analyzed the state-wide surface geology map and further categorized each geologic map unit into several tiers of radon production potential based on mineralogy, bore-hole data, and elevated radon occurrences. These classifications increased the total number of Florida geologic map units from 46 to 60.

The surface geology maps were revised from the versions used initially (Nie94b) in a few regions where geologic map faults at political (county) boundaries showed different unit designations across a boundary. In the cases where the faults could not be explained by known terrain features (river channels, topographic ridges, etc.), localized map sections were analyzed and revised by the Florida Geological Survey and the U.S. Geological Survey. The revised maps were then digitized and intersected with the STATSTO soil maps to obtain the present version of the soil radon profile maps.

The digital intersection of the soil and geology maps initially formed a soil radon profile map with more than twelve thousand polygons throughout Florida. Many of these were small, second-order polygons formed by the two different digital approximations of common boundaries. The second-order polygons were eliminated by merging all polygons with areas less than one square mile with adjacent polygons, since they represented border uncertainties rather than significant geographic areas. The resulting soil radon profile map contained 3,919 polygons, which are illustrated in regional sections by the maps in Appendix A.

Detailed soil profile properties for each map unit were defined from the unit's STATSGO soil designation, which was defined in turn as an area-weighted combination of several reference-pedon soil profiles. For each soil profile, Soil Conservation Service (SCS) data defined the detailed properties of the A, E, B, C, and other soil horizons from the top

surface to a depth of about 2.0-2.5 m. Deeper soils, extending to a 5-m depth (Figure 1-2), were characterized by extending the physical properties of the lowest SCS-characterized horizon to 5 m. Soil radium concentrations were defined from aeroradiometric data provided by the U.S. Geological Survey for the top interval (from the surface to approximately 2-2.5m depth) and from geological classification for the lower interval (extending to 5m depth), as described in more detail in Section 3.

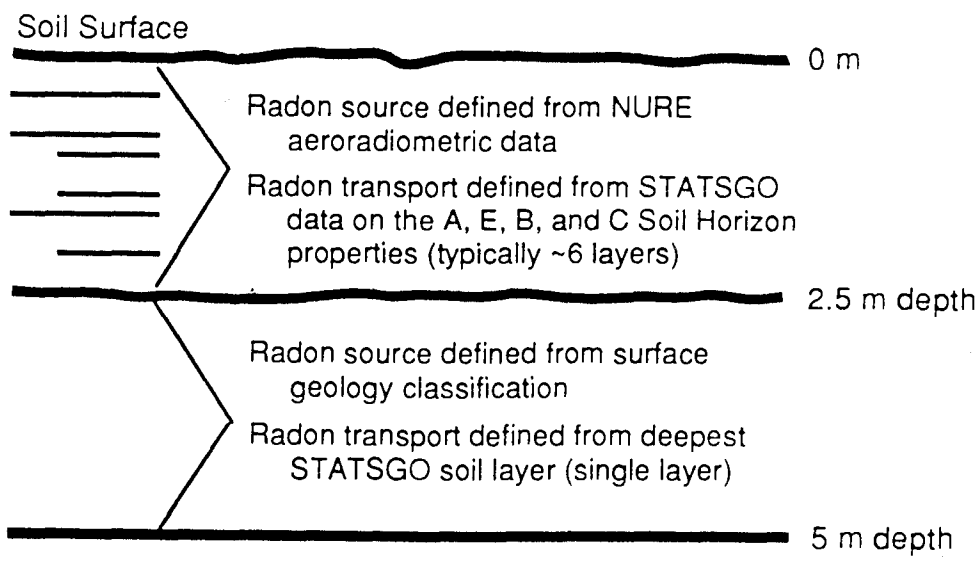

Figure 1-2. Representation of Soil Layers for Radon Potential Modeling

1.2.3 Modeling of Soil Radon Potentials

Soil radon potentials are the calculated rates of radon entry into a hypothetical reference house that is located over soil profiles defined from invariant or long-term averaged parameters. The potentials are expressed on an annual basis (mCi y^{-1}) instead of the previously-used short-

term basis (pCi s^{-1}, Naz89, Rog90) to emphasize the long-term time averaging of parameters. The potentials were also expressed on an annual basis because of the long-term, chronic nature of potential radon risks. The radon potentials can be converted to approximate indoor radon concentrations by dividing by the house volume and its ventilation rate, or by using a more detailed indoor radon balance model. The conversion of radon potential to indoor radon concentrations includes the broader uncertainties of house and possibly time variables, and is best done using a probabilistic approach.

Radon potentials were computed using the RnMAP computer code, a radon potential cartography algorithm that was developed from the radon entry efficiency model (Nie91d) and sensitivity analyses with the RAETRAD model (Nie94a). The RnMAP code uses detailed soil profile properties (density, porosity, water drainage properties, water table, radium concentration, radon emanation coefficient, radon diffusion coefficient, and air permeability) defined from SCS data and surrogates to compute the radon generation and transport profiles beneath the house, and the radon entry rates through its foundation. The approach uses the complete multi-phase radon theory (Rog91a) to include simultaneous radon transport by both diffusion and advection through both the intact foundation slab and through a modeled perimeter foundation crack (Figure 1-3). The reference house is defined to represent a rectangular single-story slab-on-grade house typical of Florida construction.

The state-wide calculations of soil radon potentials addressed in this report are based on data and parameter definitions developed cooperatively by several institutions working together in the Florida Radon Research Program. These institutions and their technical contributions are summarized in Figure 1-4.

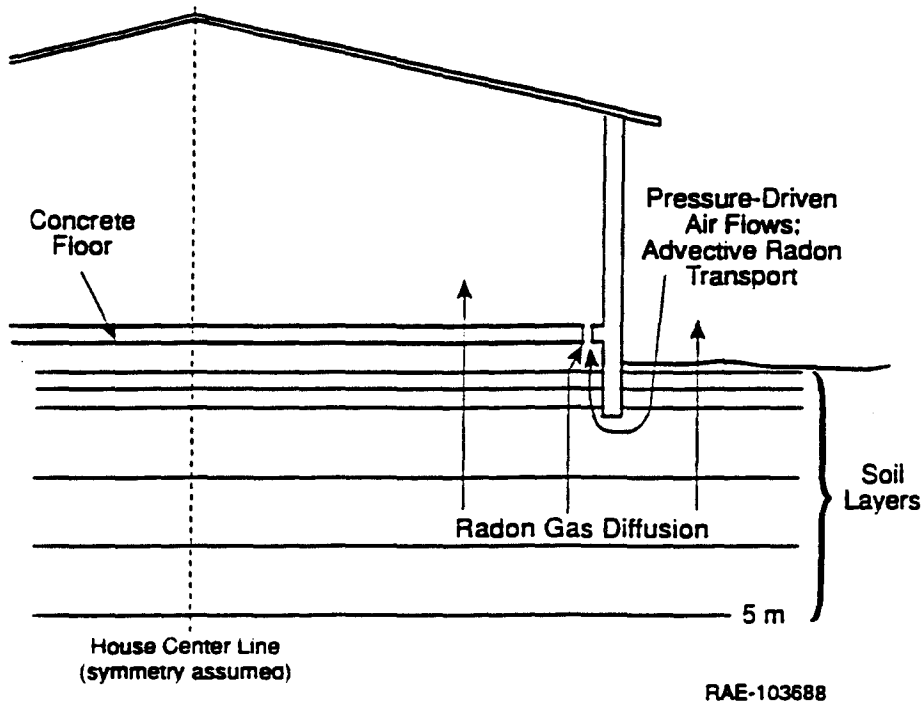

Figure 1-3. Diffusive and Advective Radon Entry Into the Reference House From the Underlying Soil Profile.

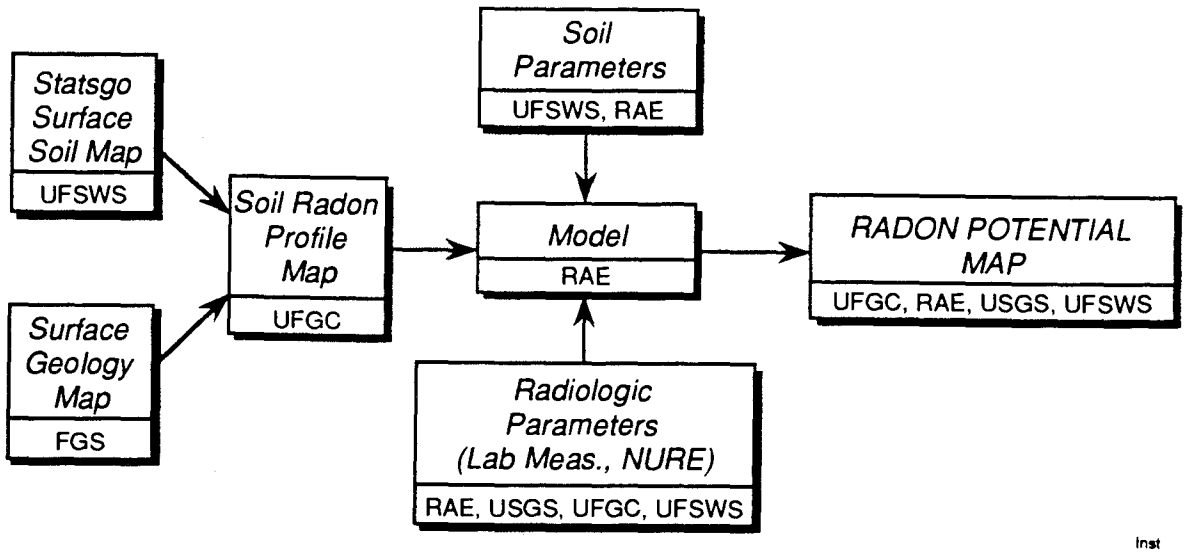

Figure 1-4 Tasks Performed by Cooperating Institutions for Development of the Soil Radon Potential Maps (UFSWS: Univ. of Florida Soil and Water Science Department; RAE: Rogers & Associates Engineering Corp.; UFGC: Univ. of Florida GeoPlan Center; USGS: U. S. Geological Survey; FGS: Florida Geological Survey).

1.3 SCOPE

This report presents the general approach, methods, and detailed basis data used to prepare state-wide soil radon potential maps of Florida. Section 2 presents the basic radon modeling, theory, and algorithms used to compute the soil radon potentials. Section 3 describes the radiological data and its analysis to define radon source terms. Section 4 describes calculation of the soil radon potentials for mapping, followed by a description of the production and intended interpretation of the radon maps in Section 5. Appendices B through I present detailed tables of the soil and radiological data used to characterize radon source and transport properties and also details of the laboratory measurements of soil radium and radon emanation coefficients.

Section 2
RADON ENTRY MODELING

Radon entry potentials were calculated for each soil profile under each water table condition using a radon potential cartography algorithm called RnMAP. The RnMAP code is a one-dimensional approximation of the more detailed RAETRAD code (RAdon Emanation and TRAnsport into Dwellings, Nie92b; Nie94a), which uses two-dimensional (elliptical-cylindrical) geometry to calculate radon generation and multiphase transport into houses from soils with varied moisture contents. This section summarizes the theoretical basis for RnMAP in estimating state-wide soil radon potentials.

2.1 RAETRAD NUMERICAL MODEL

Conceptually, radon gas is emanated from soil mineral grains, and can be transported through air-filled soil pores and foundation cracks and pores into the indoor environment. However, a more detailed model is required to represent the phase interactions and transport mechanisms of radon gas. For example, the emanated radon gas is distributed between the aqueous and gas phases of the soil pores and, when dry surfaces are encountered, it may also be adsorbed onto the solid mineral phase. Radon gas moves primarily by diffusion and advection mechanisms. Diffusion, driven by radon concentration gradients, is significant in the aqueous as well as the gas phase because of frequent intermittent blockages of soil pore segments by water. Advection, resulting from pressure-driven flow of soil gas, carries radon at the interstitial soil gas velocity. Both mechanisms establish new equilibria of radon concentrations along the transport route with local aqueous and solid phases in a chromatograph-like process.

The complete description of radon generation and transport is characterized by three coupled differential equations characterizing radon changes with time in the solid, liquid, and gas phases. With appropriate parameter definitions, these equations can be reduced to a single, multi-phase differential equation (Rog91a) that expresses radon concentrations in the air phase

as they commonly are measured. For steady-state calculations as used for soil radon potentials, this equation is written as:

$$\nabla \bullet f_a D \nabla (C_b/f_s) - \nabla \bullet [(K/\mu)(C_b/f_s)\, \nabla P] - \lambda C_b + R\rho\lambda E = 0 \qquad (1)$$

where ∇ = gradient operator

$f_a = p(1-S+Sk_H)$

p = soil porosity (dimensionless: cm^3 pore space per cm^3 bulk space)

S = soil water saturation fraction (dimensionless)

k_H = ^{222}Rn distribution coefficient (water/air) from Henry's Law (dimensionless)

D = diffusion coefficient for ^{222}Rn in soil pores ($cm^2\ s^{-1}$)

$C_b = f_s C_a$ = ^{222}Rn concentration in bulk soil space (pCi cm^{-3})

C_a = ^{222}Rn concentration in air-filled pore space (pCi cm^{-3})

$f_s = p(1-S+Sk_H)+\rho k_a$

ρ = soil bulk density (g cm^{-3}, dry basis)

$k_a = k_{ao} \exp(-bS)$

k_{ao} = dry-surface adsorption coefficient for ^{222}Rn ($cm^3\ g^{-1}$)

b = adsorption-moisture correlation constant (g cm^{-3})

K = bulk soil air permeability (cm^2)

μ = dynamic viscosity of air (Pa s)

∇P = air pressure gradient (Pa cm^{-1})

λ = ^{222}Rn decay constant ($2.1 \times 10^{-6}\ s^{-1}$)

R = soil ^{226}Ra concentration (pCi g^{-1})

E = total ^{222}Rn emanation coefficient (air + water) (dimensionless).

Equation (1) applies to gas-phase advective radon transport and to combined gas-phase and liquid-phase diffusive radon transport. The combined-phase diffusive transport is characterized by appropriate moisture- and porosity-dependent values of the pore-average diffusion coefficient, D (Rog91b). This approach is important to correctly characterize radon diffusion in unsaturated soil pores that may have small intermittent water blockages, but that still

may transmit significant radon flux (Nie84, Rog89). Liquid-phase advective radon transport is not addressed because it typically is negligible. The radon fluxes between different soil layers and at the soil surface are calculated as

$$F = -D\, f_a\, \nabla C_a + (K/\mu)\, \nabla P\, C_a, \qquad (2)$$

where F = bulk flux of ^{222}Rn (pCi cm^{-2} s^{-1}).

For RAETRAD calculations related to mapping, the radon adsorption characteristics of the soils were ignored, since they are negligible under the moisture conditions typical of Florida. Accordingly, the value for k_a was defined as zero in equation (1).

To compute radon entry into the reference house, RAETRAD uses an elliptical-cylindrical form of equations (1) and (2) (2-dimensional gradient operators). This approach provides a computationally-efficient alternative to three-dimensional algorithms. Three-dimensional algorithms have sometimes been used (Lou87), but give results similar to two-dimensional algorithms (Rev91). The present analyses also assume horizontal uniformity of the soil profiles. Because of the independence of soil air pressures from soil radon concentrations, RAETRAD computes the solution to Equation (1) in two steps. First, it computes the pressure gradients required for Equation (1) by separately solving the air flow equation, obtained from the equation of continuity and the equation-of-state for gases under isothermal expansion (Yua81):

$$\nabla \bullet \{[K/\mu p(1-S)]\, \nabla P]\} = 0 \qquad (3)$$

Then, using the resulting arrays of air flow velocities in the radial and vertical directions, $(K/\mu)\nabla P$, RAETRAD similarly solves equation (1) by substituting the computed velocities into equation (1). The boundary conditions for the finite-difference numerical calculations are: constant air pressure and radon concentration at the top surface of the house floor; constant air pressure and radon concentration (but different numerical values) at the top surface of the soil outside the house; and zero air velocity and radon flux at the center of symmetry, at the outer radial limit of the finite-difference grid, and at the bottom of the finite-difference grid.

The reference house, represented in Figure 1-3, was defined to have the approximate characteristics of Florida slab-on-grade single-family dwellings. The reference house consisted of a 28 x 54 ft (8.6 x 16.5 m) rectangular structure with nominal properties as listed in Table 2-1. Its volume is based on that of a median U.S. family dwelling (Naz88), and is similar to that of typical Florida houses (Acr90). A nominal 2.4-m (8-ft) ceiling height was used to estimate its area, which also is similar to other estimates of Florida floor slab areas (Acr90). The house ventilation rate is about half the median U.S. house ventilation rate (Naz88), based on measurements in Florida houses (Cum92). The floor crack location is chosen near the slab perimeter to approximate a slab/footing shrinkage crack that may occur with floating-slab construction inside concrete-block stem walls. The stem-wall footing penetrates 2 ft (61 cm) into the natural terrain, and contains an additional 1 ft (30 cm) of above-grade sandy fill soil beneath the slab. The fill soil has identical radiological properties to those of the surface soil at the site. The indoor pressure is typical of that resulting from thermal and wind-induced indoor pressures in U.S. homes (Naz87), and also of the average indoor pressures measured in a group of 70 Florida houses (Cum92) under average conditions. Concrete slab air permeabilities, radon diffusion coefficients, and other properties were estimated from data measured on Florida floor slabs (Rog95).

TABLE 2-1. DEFINITION OF REFERENCE HOUSE PARAMETERS FOR USE IN RADON ENTRY CALCULATIONS

House Area	143 m^2	Fill Soil Thickness	30 cm
House Dimensions	8.6 x 16.5 m	Indoor Pressure	-2.4 Pa
House Length/Width	1.9 (ratio)	Concrete Slab Thickness	10 cm
House Volume	350 m^3	Concrete Slab Porosity	0.22
House Ventilation Rate	0.25 h^{-1}	Concrete Slab $^{226}Ra \cdot$ Emanation	0.07 pCi g^{-1}
Floor Crack Width	0.5 cm	Exterior Footing Depth	61 cm
Floor Crack Location	slab perimeter	Concrete Air Permeability	1×10^{-11} cm^2
Crack Area Fraction	0.002	Concrete Rn Diffusion Coeff.	8×10^{-4} cm^2 s^{-1}

2.2 RADON POTENTIAL CARTOGRAPHY ALGORITHM

The detailed RAETRAD numerical model has been used for a previous prototype map of soil radon potentials in Alachua County (Nie91c), but uses a level of detail that is unnecessary for mapping soil radon potentials. In order to make the cartographic radon potential calculations computationally efficient and to better match them to their basis data, a specialized radon potential cartography algorithm was developed and incorporated into the RnMAP code. The algorithm was designed to utilize only vertical profile descriptions of soils, since horizontal uniformity was always assumed within the scale of a building site. RnMAP still incorporates the full two-dimensional geometry and advective-diffusive transport from the RAETRAD model, however, by using empirical constants fitted to RAETRAD analyses for the reference house. In this way, RnMAP preserves for different sites the correct parametric variations of radon potential, but avoids the duplicative calculation of detailed horizontal profiles around the same reference house.

The RnMAP code uses the multi-phase, one-dimensional RAECOM model (Radon Attenuation Effectiveness and Cover Optimization with Moisture Effects, Rog84) to compute the vertical radon profiles beneath the reference house, with boundary definitions to match the house-size related surface radon depletion near the house foundation. The rate of radon entry into the reference house then is computed using the radon entry efficiency model (Nie91d). The radon entry efficiency model explicitly includes advective and diffusive radon entry through cracks in the floor slab, and diffusive entry through the intact part of the slab. Using typical values of concrete permeability to air flow, advective entry through the intact part of the slab is negligible.

Radon entry into the reference house was modeled using the radon entry efficiency correlation derived previously (Nie91d), which gives the relationship:

$$Q = 10 \; [(C_s \, p_c \, D_c \, A_h)/t_c + (C_c \, p_s \, D_s \, A_c)/t_c + A_c \, C_c \, v] \qquad (4)$$

where Q = indoor radon entry rate (pCi s^{-1})

10 = unit conversion

C_s = area-weighted average sub-slab radon concentration (pCi L^{-1})

p_c = concrete effective total porosity

D_c = concrete radon diffusion coefficient (cm^2 s^{-1})

A_h = house floor area (m^2)

t_c = concrete floor thickness (cm)

C_c = radon concentration at the base of the floor crack (pCi L^{-1})

p_s = effective total porosity of the surface soil layer

D_s = radon diffusion coefficient of the surface soil layer (cm^2 s^{-1})

A_c = floor crack area (m^2)

v = air velocity through the floor crack (cm s^{-1})

The three terms in equation (4) correspond respectively to radon diffusion through the intact floor slab, radon diffusion through the perimeter floor crack, and advective movement of radon through the perimeter floor crack by pressure-driven air flow. The variables p_c, D_c, A_h, t_c, and A_c in equation (4) are defined as invariant properties of the reference house. The variables p_s and D_s are defined directly from the top of the soil profile on which the house is modeled. The remaining variables, C_s, C_c, and v are defined from empirical fits to numerical RAETRAD analyses.

The derivations of empirical expressions for C_s, C_c and v in equation (4) involved a series of RAETRAD analyses of reference houses of varying size over different soil types to establish the house size-dependence of sub-slab radon concentrations, and their interactions with soil texture. The analyses utilized a 5 pCi g^{-1} radium concentration in each of five soil textural types (sand, sandy loam, loam, clay loam, and clay). The water contents of each of the soils were defined to correspond to matric potentials of -0.3-bar (-30 kPa) (Nie92a). Soil permeabilities and diffusivities were defined by default correlations (Rog91b). The results of these analyses are presented in Table 2-2 in terms of the average sub-slab radon concentrations, the deep-soil radon concentrations, the radon concentrations beneath the floor crack, and the air velocity through the crack.

Table 2-2. Results of RAETRAD Analyses for Varying House Sizes and Soil Textural Classes

House Minor Radius (ft.)	Sub-Slab Radon Concentration (Area-Weighted Average, pCi L^{-1})				
	Sand	Sandy Loam	Loam	Clay Loam	Clay
4	3762	4797	4772	4329	2823
6	3926	4931	4943	4521	2945
8	4031	5000	5029	4616	2990
10	4104	5044	5077	4668	3007
13	4180	5085	5117	4709	3015
16	4236	5112	5137	4725	3017
20	4292	5134	5148	4735	3017
24	4334	5147	5153	4738	3017
30	4397	5158	5154	4739	3016
Deep-Soil Rn (pCi L^{-1}):	5246	7248	9353	10328	12747

House Minor Radius (ft.)	Radon Concentration under the Floor Crack (pCi L^{-1})				
	Sand	Sandy Loam	Loam	Clay Loam	Clay
4	3641	4408	3846	3094	1490
6	3761	4480	3905	3136	1502
8	3826	4509	3932	3155	1507
10	3862	4524	3946	3165	1510
13	3890	4536	3957	3173	1513
16	3905	4542	3963	3177	1514
20	3917	4547	3966	3179	1516
24	3923	4549	3968	3179	1517
30	3930	4552	3968	3179	1518

House Minor Radius (ft.)	Air Velocity Through the Floor Crack (cm s^{-1})				
	Sand	Sandy Loam	Loam	Clay Loam	Clay
4	3.18×10^{-3}	2.23×10^{-3}	5.13×10^{-4}	1.56×10^{-4}	4.54×10^{-6}
6	3.35×10^{-3}	2.40×10^{-3}	5.77×10^{-4}	1.76×10^{-4}	4.52×10^{-6}
8	3.45×10^{-3}	2.48×10^{-3}	6.12×10^{-4}	1.85×10^{-4}	4.40×10^{-6}
10	3.46×10^{-3}	2.52×10^{-3}	6.27×10^{-4}	1.90×10^{-4}	4.28×10^{-6}
13	3.48×10^{-3}	2.55×10^{-3}	6.40×10^{-4}	1.93×10^{-4}	4.11×10^{-6}
16	3.50×10^{-3}	2.58×10^{-3}	6.45×10^{-4}	1.94×10^{-4}	3.98×10^{-6}
20	3.51×10^{-3}	2.59×10^{-3}	6.47×10^{-4}	1.92×10^{-4}	3.85×10^{-6}
24	3.52×10^{-3}	2.60×10^{-3}	6.47×10^{-4}	1.90×10^{-4}	3.76×10^{-6}
30	3.53×10^{-3}	2.60×10^{-3}	6.43×10^{-4}	1.87×10^{-4}	3.67×10^{-6}

The RAETRAD analyses were interpreted by analyzing the ratio of the area-weighted average sub-slab radon concentration to the deep-soil radon concentration, C_s/C_d, as a function of house size and soil type. Figure 2-1 illustrates the regular trends resulting from these analyses. The curves in Figure 2-1 were fitted to the following exponential function of the house minor radius to obtain empirical parameters to represent the RAETRAD analyses:

$$C_s/C_d = 1 - \exp[-r / (b_o + b_1 r)] \tag{5}$$

where C_s = area-weighted average sub-slab radon concentration (pCi L^{-1})

C_d = deep-soil radon concentration (pCi L^{-1})

r = minor radius of the reference house (m)

b_0, b_1 = empirical fitting constants.

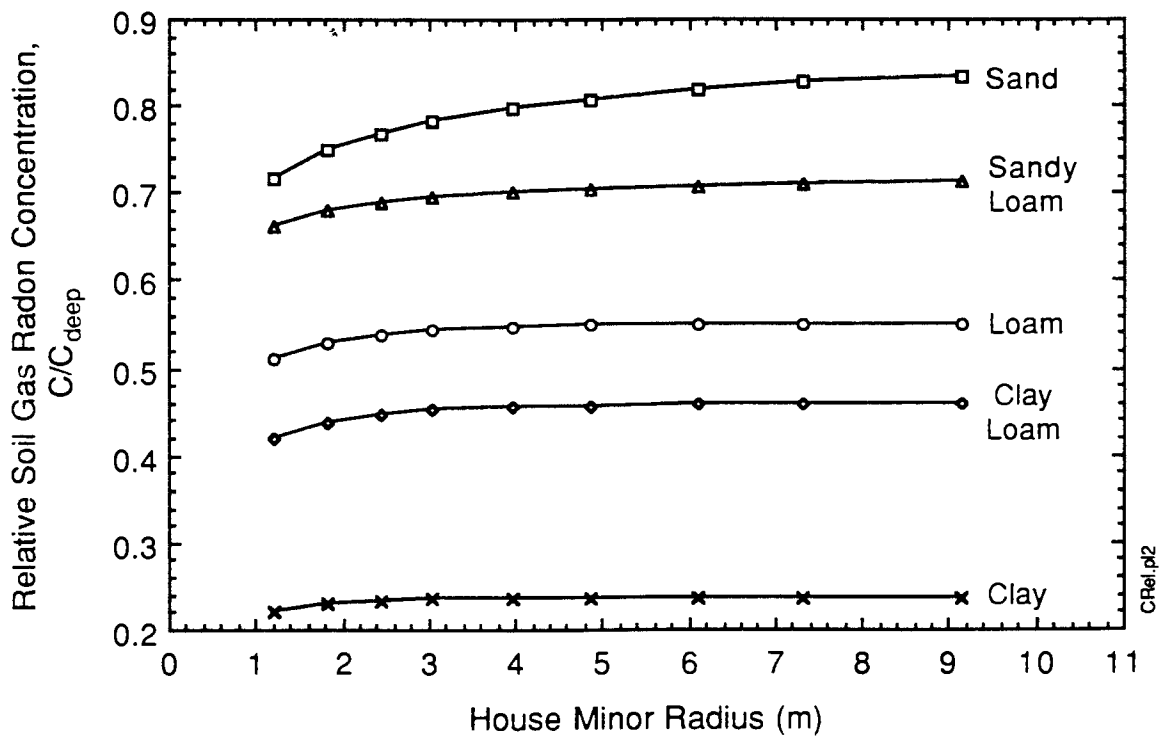

Figure 2-1. Relative Soil Gas Radon Concentrations as a Function of House Size for Five Soils.

The curve fitting was accomplished by transforming the data in Table 2-2 as

$$b = -r / \ln(1 - C_s/C_d)] \tag{6}$$

where $b = b_0 + b_1 r$.

The resulting values of b then were fitted as shown in Figure 2-2 to obtain the illustrated values of the fitting constants b_0 and b_1 for each of the five soil types.

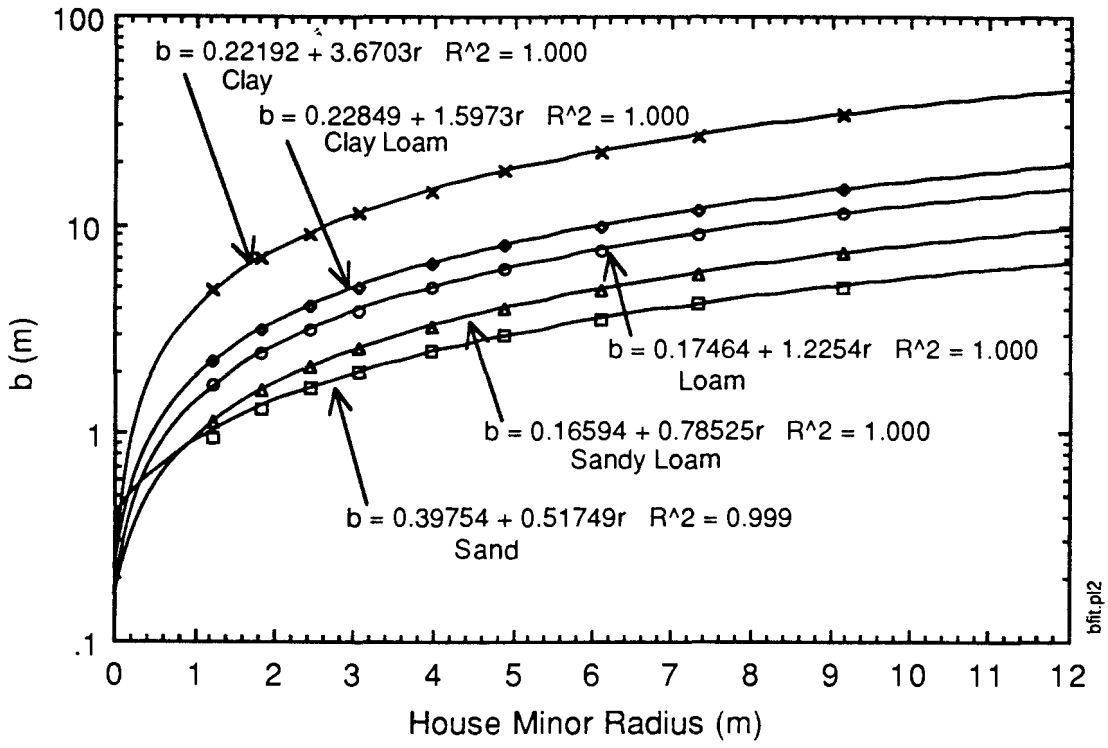

Figure 2-2. Fitting of the *b* Coefficients to House Radius for the Five Soils.

The fitting constants from Figure 2-2 were further fitted to obtain a continuous expression for all soils that did not depend on soil type. For this fitting, the five soils were represented by their radon diffusion coefficients, and were found to exhibit a regular dependence on the square-root of the diffusion coefficients, as illustrated in Figure 2-3. The resulting cubic equations, shown in Figure 2-3, were then used to represent the b_0 and b_1 constants for any soil based on its radon diffusion coefficient:

$$b_0 = 0.6178 + 8.368\sqrt{D} - 164\,D + 735.7\,D^{3/2}$$

$$b_1 = [-0.070645 + 10.6\sqrt{D} + 12.23\,D - 72.25\,D^{3/2}]^{-1} \tag{7}$$

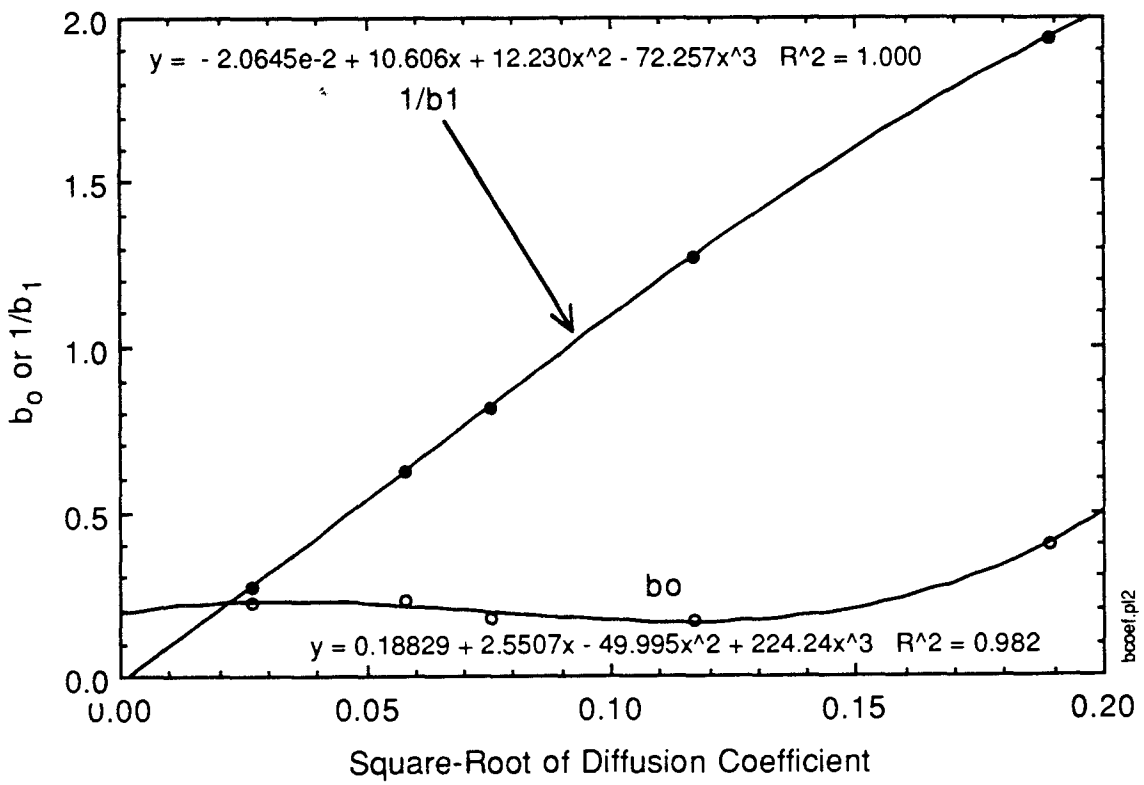

Figure 2-3. Estimation of the b_0 and b_1 Coefficients in Terms of the Radon Diffusion Coefficients of the Five Soils.

The average sub-slab radon concentration beneath a reference house was expressed in terms of the sub-slab radon concentration beneath an infinitely-large slab, so that a one-dimensional radon calculation (no radial dispersion) could be used to represent a finite-sized house. This utilized the large-house equivalent to equation (5), which neglects the b_0 constant,

$$C_{lg} / C_d = 1 - \exp[-1/b_1] \tag{8}$$

where C_{lg} = area-weighted average sub-slab radon concentration for a large house (pCi L^{-1}).

Combining equation (5) and equation (8) gives

$$C_s = C_{lg} \{1-\exp[-r/(b_0 + b_1 r)]\} / [1 - \exp(-1/b_1)], \tag{9}$$

which is the expression used to obtain C_s from a one-dimensional steady-state RAECOM analysis (Rog84) for the actual soil profile located beneath a concrete slab corresponding to the intact house floor.

The radon concentration immediately beneath the perimeter floor crack of the reference house is consistently lower than the area-weighted average sub-slab value (Table 2-2), despite the advective air flow, due to diffusive losses through the crack. The radon concentration at the base of the crack therefore was parameterized in a manner corresponding to the sub-slab average values, producing the fitting constants g_0 and g_1, as shown in Figure 2-4, which result from the relation

$$C_c/C_d = 1 - \exp[-r / (g_0 + g_1 r)] \tag{10}$$

where C_c = radon concentration at the base of the floor crack (pCi L^{-1}).

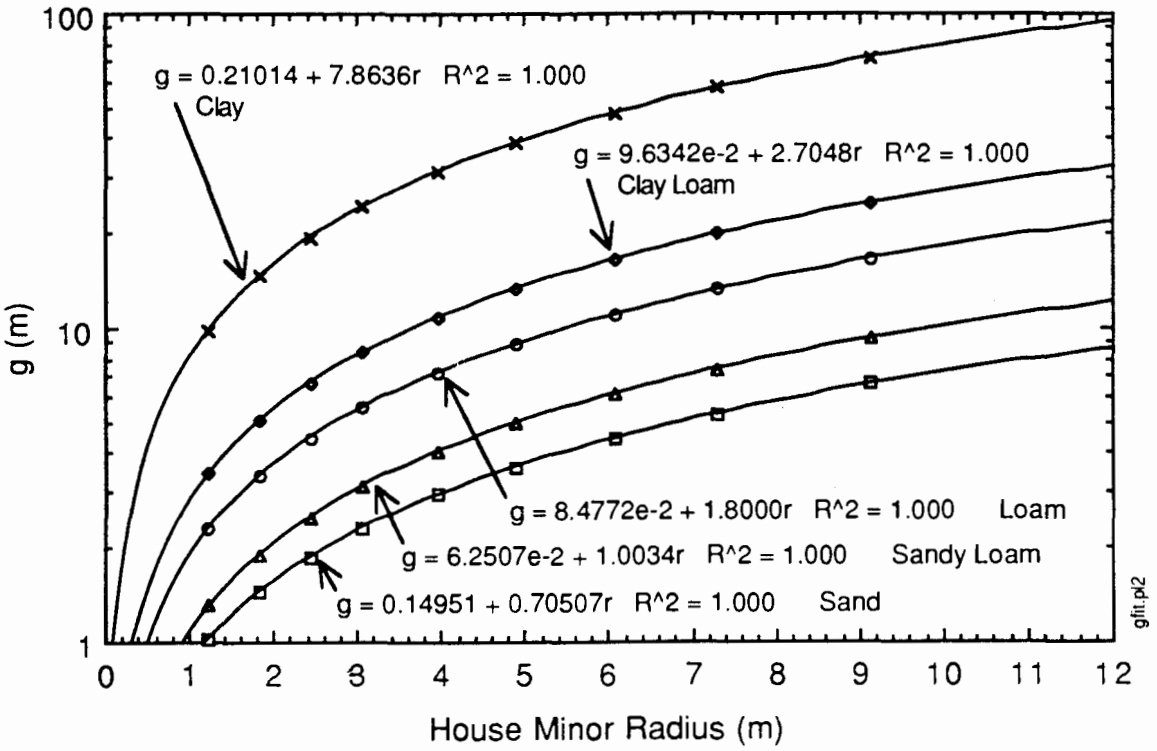

Figure 2-4. Fitting of the *g* Coefficients to House Radius for Each of the Five Soils.

Similarly fitting the constants g_0 and g_1 to the soil radon diffusion coefficients gives the relationships shown in Figure 2-5, from which the fitting constants are defined as

$$g_0 = 1.184 - 22.56\sqrt{D} + 157.5\,D - 305\,D^{3/2}$$

$$g_1 = [0.03249 + 0.7763\sqrt{D} + 111\,D - 405\,D^{3/2}]^{-1} \tag{11}$$

and the radon concentration at the base of the floor crack is computed as

$$C_c = C_{lg}\,\{1 - \exp[-r/(g_0 + g_1 r)]\} / [1 - \exp(-1/g_1)] \tag{12}$$

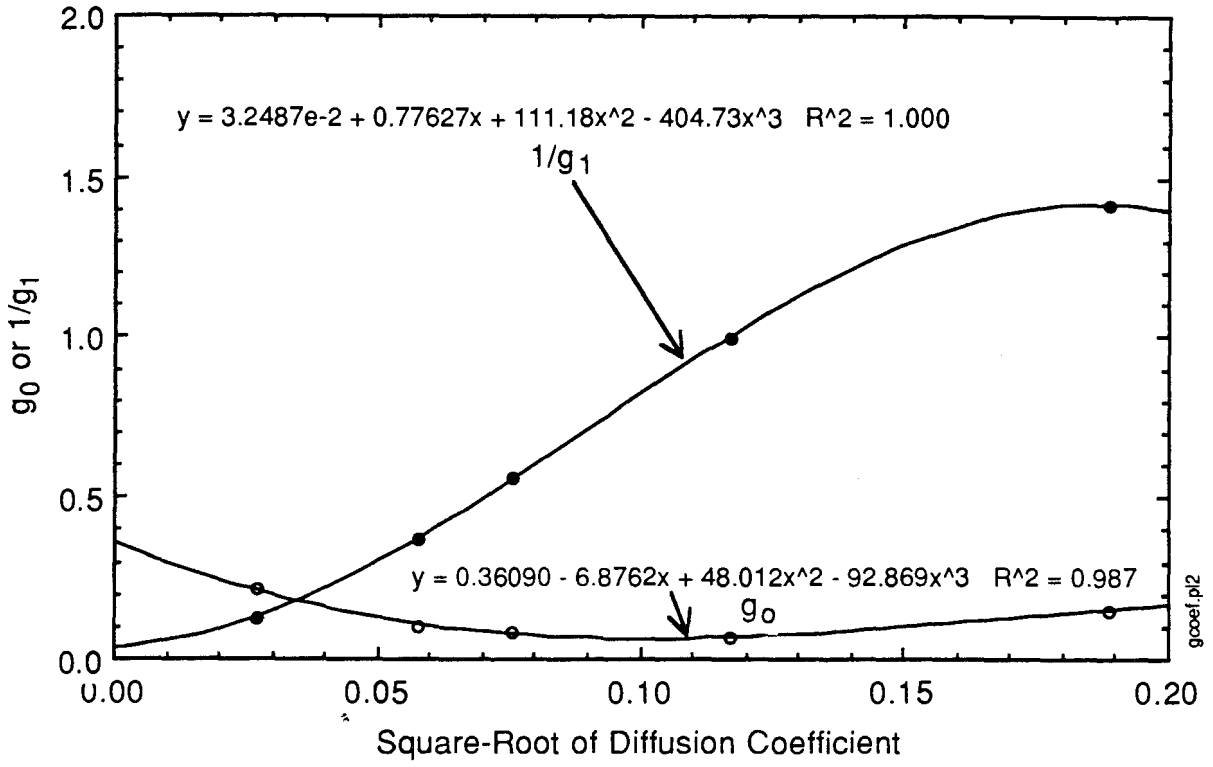

Figure 2-5. Estimation of the g_0 and g_1 Coefficients from the Diffusion Coefficients of the Five Soils.

The soil air velocities passing through the floor crack also were expressed as a function of the soil layer immediately beneath the crack. The velocities in Table 2-2 were found to depend mainly on the soil type (Figure 2-6), with very little dependence on the size of the house, particularly near the r = 4.9 m radius value. They were therefore fitted to the permeability function:

$$v = \exp(-fK), \tag{13}$$

where v = soil air velocity through the crack (cm s^{-1})

f = empirical fitting constant

K = soil air permeability (cm^2).

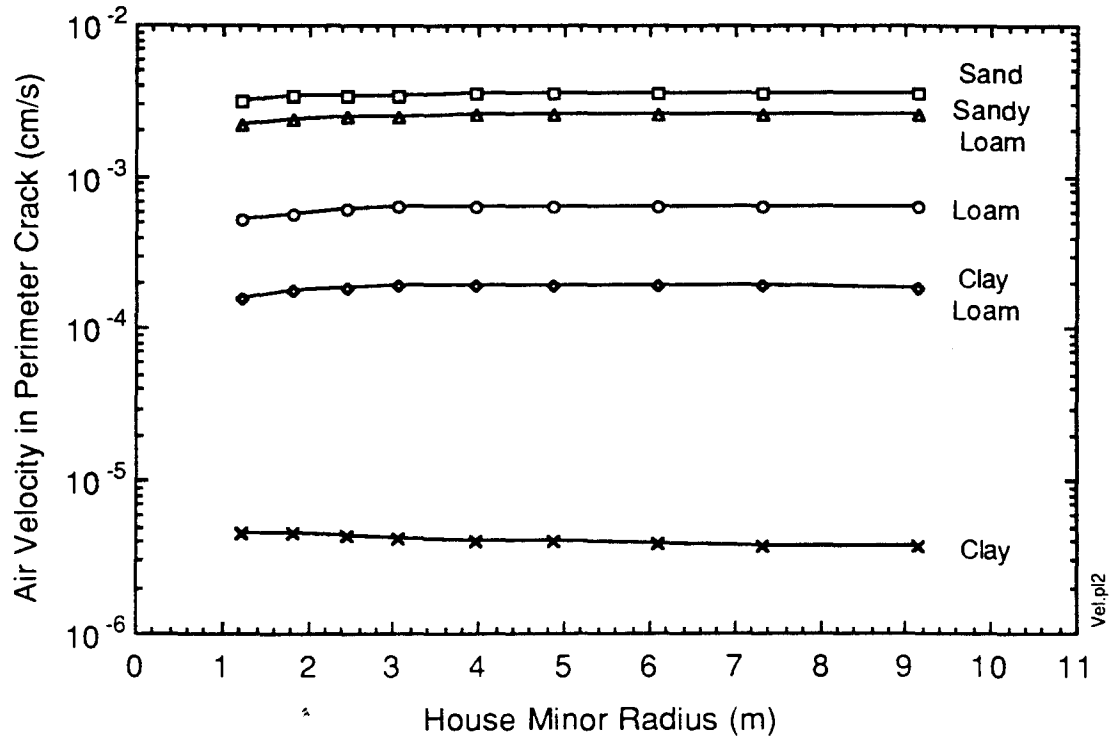

Figure 2-6. Variation of Air Velocities with House Radius for the Five Soils.

The least-squares fit, shown in Figure 2-7, indicates the fitting constant f also is a function of K, so that the quadratic fitting constants can be incorporated into equation (12) to give:

$$v = \exp[-e^{1.152} K^{1 - 0.9923 + 0.00284 \ln(K)}]. \tag{14}$$

Equation (14) therefore is used to calculate the air velocity in equation (4) for the floor crack.

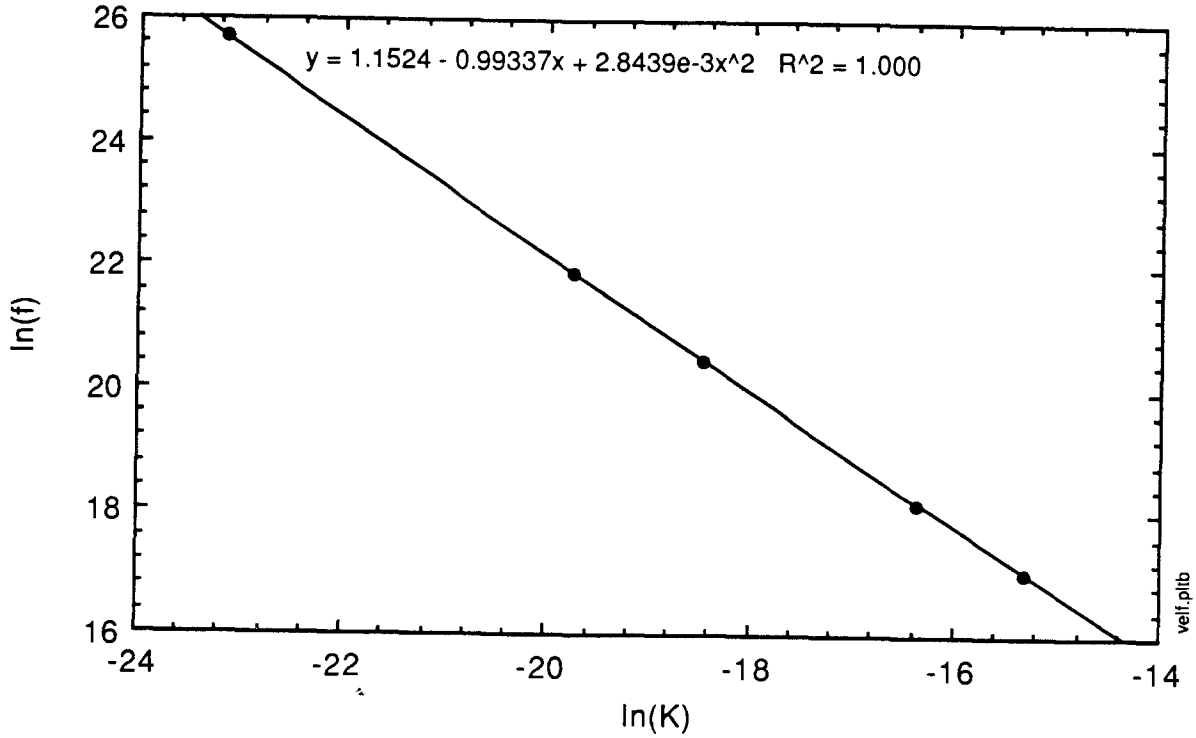

Figure 2-7. Fitting of the *f* Coefficient to the Air Permeabilities of the Five Soils.

The RnMAP computer code implements the above algorithms using equations (4), (9), (12), and (14). The basic logic of RnMAP is illustrated in Figure 2-8. After reading descriptive soil profile data, described further in Section 3, the RnMAP code starts a loop over four main cases of radon source strength for the radon entry calculations. These include a hot soil and cold soil case for each of two (hot and cold) geology configurations. The hot soil case was defined for the depth range (from surface to about 2-2.5m) defined by the SCS soil data, and was set equal to 4 pCi g^{-1} radium and 0.6 emanation. A radium content of 0.1 pCi g^{-1} and an emanation coefficient of 0.2 was used for the cold soils. The hot geology representing the remaining soils to the 5 m depth was defined by 4 pCi g^{-1} radium and 0.6 emanation, and the cold geology by 0.8 pCi g^{-1} radium and 0.32 emanation, consistent with the previous measurements and data for Florida (Appendix F).

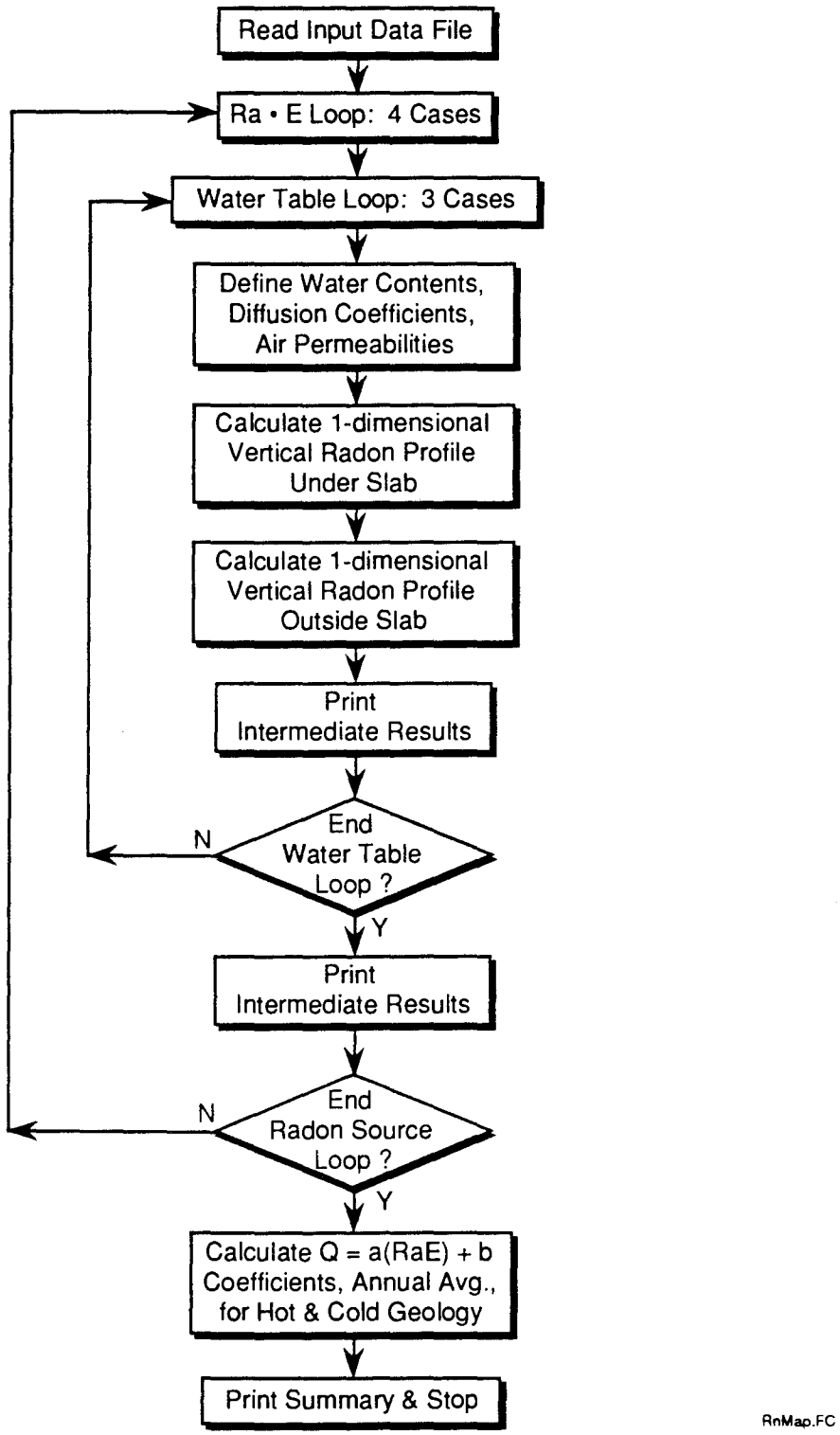

Figure 2-8. Summary Flowchart for the RnMAP Code.

A second loop in the RnMAP code (Figure 2-8) includes three different water table depths that were defined from the University of Florida/SCS estimate of the seasonal high water table depth and duration. The annual distribution of water table depths was estimated, as illustrated in Figure 2-9, as being 2 m deeper than the high water table depth during most of the part of the year not included in the reported high water table period. During two one-month transition periods between the high and low water table levels, the depth was approximated as only one meter deeper than the reported high water table level. For map units in which the water table was reported as >180 cm, the high water table level was estimated to be at the three meter depth for half of the year and at the five meter depth for the remainder of the year.

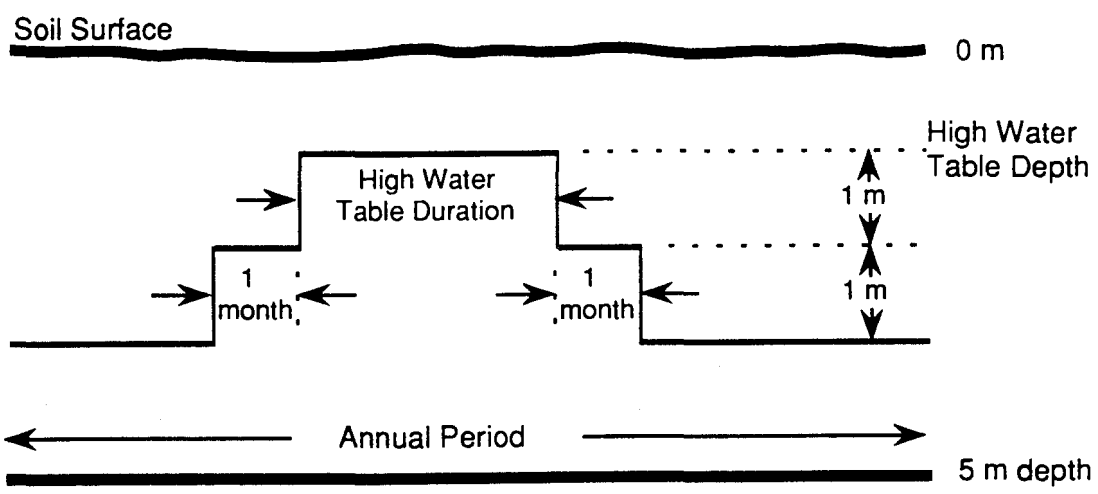

Figure 2-9. Modeling of Water Table Annual Distribution From the SCS High Water Table Depths and Durations.

After starting the two loops (Figure 2-8), the water contents were estimated for each layer of the soil profile from its distance above the water table. Soil water contents throughout the top five-meter soil profile were estimated directly from the soil water drainage data supplied by UFSWS. The height of each layer above the water table was set equal to the soil capillary suction and used to interpolate the SCS drainage curve data to determine the drained soil water content. Benchmark numerical calculations with the FEMWATER code (Yeh87, Sul88) indicate that sub-slab soil water matric potentials are well-approximated by the height above the water table for wet climates and shallow water tables as occur in most of Florida (Nie94b). Radon diffusion coefficients and permeabilities were defined for each soil horizon from the soil and water parameters (Rog91b).

Once inside the main loops (Figure 2-8), RnMAP calculates the vertical one-dimensional radon concentration profile for an infinitely-large (horizontal extent) slab with the RAECOM code algorithm (Rog84). The resulting sub-slab radon concentration then is used in equations (9) and (12) to obtain the parameters needed in equation (4). The air velocity for the crack similarly is estimated from equation (14) for use in equation (4).

The resulting radon entry rate then is printed with the vertical radon concentration profiles and related input data, and the code proceeds to the next calculation for a different water table depth. After completing the calculation for each of the intended water table depths, a summary of the annual-average radon entry values is printed, and the code proceeds to the next radon source term case. After completing each of the four radon source term cases and their summary printouts, the RnMAP code computes and prints linear coefficients for the key output parameters including the radon entry rates (soil radon potentials). The linear coefficients allow calculation of corresponding results in terms of any other values of the soil radium concentrations and emanation coefficients, and thus they serve as the basis to efficiently use the RnMAP results with the wide variety of soil radium concentrations estimated from National Uranium Resource Evaluation (NURE) aeroradiometric data. This is described in Section 3. A sample printout from RnMAP for one soil profile is presented in Appendix B.

Equations (9), (12), and (14), which comprise the input to equation (4) and the basis for the RnMAP code were benchmarked against RAETRAD analyses using the parameters defined in Table 2-1 for the reference house. Although RAETRAD cannot directly compute an infinitely-large house case, it can directly calculate the sub-slab and deep-soil radon concentrations that form the basis for equations (5) through (8), from which equation (9) is defined. For the 4.9-m radius reference house, the C_s/C_d ratios were calculated by equations (5) and (7) for sand, sandy loam, loam, clay loam, and clay. The resulting ratios then were divided by the corresponding ratios computed by RAETRAD, giving bias ratios of 1.006, 1.000, 0.999, 0.994, and 0.998 for the five respective soil types. Their average, 0.999 ± 0.004, shows no net bias in the equations, and the individual ratios show less than 1% bias for any of the soils.

Similar benchmarks for the radon concentration at the base of the floor crack also were examined using the same RAETRAD analyses on the same five soils. In this case, the ratios of radon at the crack to deep-soil radon (C_c/C_d) were computed from equations (10) and (11). The resulting bias ratios from dividing by their RAETRAD counterparts were 0.999, 0.999, 0.994, 1.004, and 0.994 for the same five respective soils. Their average, 0.998 ± 0.004, again shows no significant net bias, and individual ratios show less than 1% bias for any of the soils.

Benchmarks of soil air velocities through the crack also used the same RAETRAD analyses. In this case, the velocities from equation (14) were divided by the RAETRAD velocities for the same five soils, yielding bias ratios of 1.085, 0.884, 0.957, 1.140, and 0.956. Their average, 1.004 ± 0.105, indicates no significant net bias. However individual ratios indicate a typical 10% variation due to uncertainties in the empirical parameterization.

The combined benchmark of all of the empirical equations in equation (4), computed by RnMAP, against radon entry rates computed by RAETRAD also was analyzed for each of the five soils. The ratios of RnMAP to RAETRAD radon entry rates were 1.13, 1.02, 1.00, 1.02, and 1.08, respectively. Their mean, 1.05 ± 0.05, indicates an approximate 5% positive bias of RnMAP relative to RAETRAD, with a nominal 5% uncertainty. Although the bias is small enough to be acceptable, it also is explainable by the finite-difference method used in

RAETRAD compared to the exact analytical mathematics used in the RAECOM section of the RnMAP code. If infinitely-small numerical mesh units were used in RAETRAD, it would yield a slightly higher radon entry rate that approaches that calculated by RnMAP. The differences are well within the uncertainty of the other parameters used to represent radon potentials from soil profile data.

Section 3
RADON SOURCE AND TRANSPORT PARAMETERS

3.1 RADON SOURCE PARAMETERS

Radon source parameters were defined separately for the upper (surface to approx. 2-2.5m depth) and lower (extending to 5 m depth) zones of the soil profile, as illustrated in Figure 1-2. The radium concentration in the upper zone was defined from National Uranium Resource Evaluation (NURE) aeroradiometric data, while that in the lower zone was defined from geologic estimates and measured radium concentrations. Radon emanation coefficients were based on measured values as correlated to radium concentrations. This section describes the NURE data and the measured radium and radon emanation data that were used to estimate the radon source strengths.

3.1.1 NURE Data

Radon source parameters were defined from NURE aeroradiometric data as a vertically uniform source profile throughout the upper soil region (see Figure 1-2). The NURE data, measured on flight lines at 6-mile intervals with data recorded every second, give a data point corresponding to every 200-ft interval beneath each flight line. Details of the measurement procedures and results are published (EGG81).

Digital tapes of NURE data provided by USGS were used to digitally intersect the NURE flight lines with the radon map polygons. Figures A-1 through A-8 (Appendix A) show the flight lines superimposed on radon map polygons for different regions of the state. The partitioning of the NURE data was performed, with a geographic information system, by the University of Florida GeoPlan Center. The resulting partitioned NURE data were transferred to Rogers & Associates Engineering Corp. (RAE). RAE then calculated geometric means, geometric standard deviations, and the number of points associated with each radon map polygon. The NURE data, expressed in parts-per-million equivalent uranium (eU), were

converted to an equivalent ^{226}Ra concentration in pCi g^{-1} by dividing by the units conversion factor of 3.0 pCi g^{-1} per ppm eU. Table C-1 (Appendix C) presents a statistical summary of the resulting data.

Although Table C-1 contains data for most of the map polygons, some were not intersected by a NURE flight line, and therefore the NURE data did not directly represent them. These polygons were represented by the overall geometric mean and geometric standard deviation of the NURE values for the geology unit in which the polygon was classified. If an entire geology unit was not intersected by NURE flight lines, the inter-line polygons were defined from corresponding geometric means and standard deviations of NURE data for their STATSGO soil units.

3.1.2 Soil Radium and Emanation Data

Radon emanation coefficients for defining source terms in the upper and lower zones of the soil profiles (Figure 1-2) utilized empirical trends in emanation with soil radium. The trends were defined from radon emanation measurements on 301 samples from 12 counties in north-central Florida and 95 additional samples from the remaining Florida counties. The emanation-radium trend was used with NURE radium data to define source terms for the upper soil zone, and with geology-based estimates to define source terms for the lower soil zone. The geology-based radium estimates for the lower zone were divided into five classifications. The first was for low radium levels typical of Florida sands that are not influenced by elevated-radium mineralization. The second was for intermediate radium levels with mixed or intermittent mineralization by elevated-radium materials. The third was for elevated radium levels typical of certain Hawthorn and limestone units. The fourth was for high radium levels typical of the undisturbed parts of the Bone Valley Formation. The fifth was for high radium levels typical of the disturbed parts of the Bone Valley Formation.

As reviewed previously (Nie91c), there are few other data resources to characterize radium levels in Florida soils, and virtually no others that adequately characterize their associated radon emanation coefficients. Therefore the present radon emanation

measurements were made using soil samples archived from prior county soil surveys. These samples, which the University of Florida Soil and Water Science Department made available, were from documented reference pedon sites that corresponded directly to many of the physical-property data sets being used from the STATSGO soil data base. The samples therefore were representative of the STATSGO-defined soil profiles used to calculate soil radon potentials.

Improved, more-sensitive methods were developed (Appendix D) and used for the radon emanation measurements. They were shown (Appendix E) to be comparable to traditional emanation measurement methods (Aus78, Tha82, Wil91). Radium concentrations also were measured (Appendix F) in each sample as part of the emanation measurement procedure. Although the radium results from these measurements were used only indirectly, the emanation data and trends were used directly to define radon source terms.

The radon emanation measurements included three sets of samples. The first set, totaling 513 samples (3- or 4- digit sample numbers in Table F-1, Appendix F) included all available samples from Alachua County and many from Marion and St. Johns Counties. Forty additional samples in the first set were collected by the U.S. Geological Survey (USGS) and Florida Geological Survey (FGS) (A1 through A8 series in Table F-1) in supplemental field investigations for this study. The second set included 128 samples from Citrus, Clay, Duval, Flagler, Lake, Levy, Nassau, Putnam, and Volusia Counties. The third set included 95 samples from 38 additional counties. Samples in the third set were selected from University of Florida archives by gamma screening several hundred samples (four from each county, where available), and analyzing the samples with gamma intensities corresponding to approximately 1 pCi g^{-1} or higher. Radium and radon emanation measurements then were made on the selected samples by the methods described in Appendix C.

The samples were analyzed first for radium concentration. Radon emanation measurements then were made on all samples with radium concentrations exceeding 1 pCi g^{-1} plus a number of the lower-radium samples. Most low-radium samples were excluded because their radon emanation measurements typically have very high uncertainty. A total of 172

emanation measurements were performed on the first set of samples, and 29 were performed on the second set of samples. Emanation was measured on all 98 samples from the third set because they had already been screened to eliminate low-radium samples.

The results of the radium and radon emanation measurements are presented in Appendix F. The methods used to make the measurements are described in Appendix D. The sample moistures reported for the UFSWS samples represent water that was added to the air-dry archived samples to obtain field-representative radon emanation measurements. The radon emanation coefficients are generally low for dry samples, but exhibit higher values when a small quantity of water is present, consistent with previous observations (Nie82, Tha82). Sample moistures for the USGS/FGS samples represent field (as-received) moistures. Soil series designations were not provided for several of the sample sets.

The measured radium concentrations for all of the samples were log-normally distributed, with a geometric mean of 0.56 pCi g^{-1} and a geometric standard deviation (GSD) of 3.5 (Figure 3-1). The measured radium concentrations ranged from <0.3 pCi g^{-1}, the typical analytical detection limit, to 43 pCi g^{-1}. Approximately 73 percent of the measurements exceeded the analytical detection limit. Related quality control measurements on duplicate samples, standards, and blanks are presented in Appendix E.

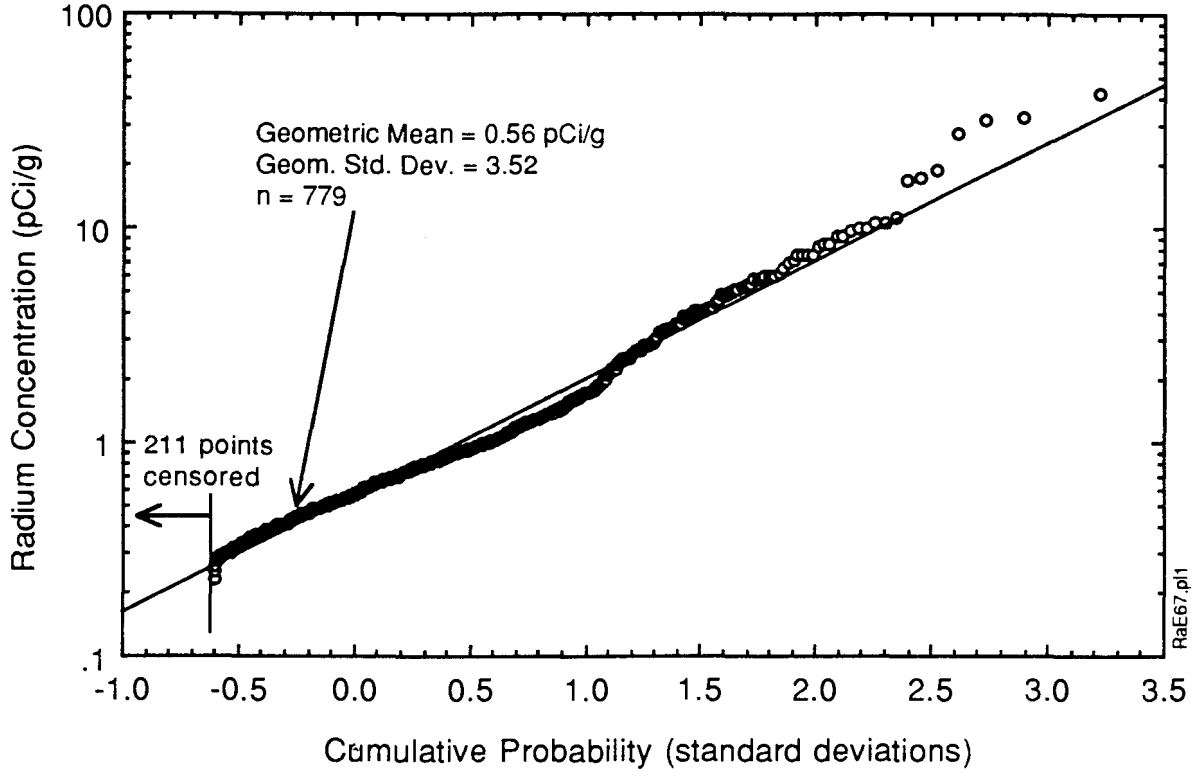

Figure 3-1. Cumulative probability distribution of measured soil radium concentrations in 779 Florida soil samples.

Radon emanation coefficients measured on the 296 samples (Tables F-1 through F-3 in Appendix F) ranged from 0.01 to 0.85, and averaged 0.44 ± 0.18 (mean ± standard deviation). Related quality control measurements for the emanation coefficients are presented in Appendix E. The relation between radon emanation and radium concentration was explored by plotting these parameters as illustrated in Figure 3-2 (open circles). As illustrated, the lowest emanation coefficients were only observed at low radium concentrations (generally <2 pCi g^{-1}), and the typically high emanation coefficients (0.4-0.7) were mainly observed at higher radium concentrations (1-30 pCi g^{-1}). The relation between emanation and radium concentration is consistent with two types of radium mineralization: primary mineralization that is of low radium concentration, distributed uniformly in the soil grains, and secondary mineralization that is of higher radium concentration, localized closer to pore and grain surfaces.

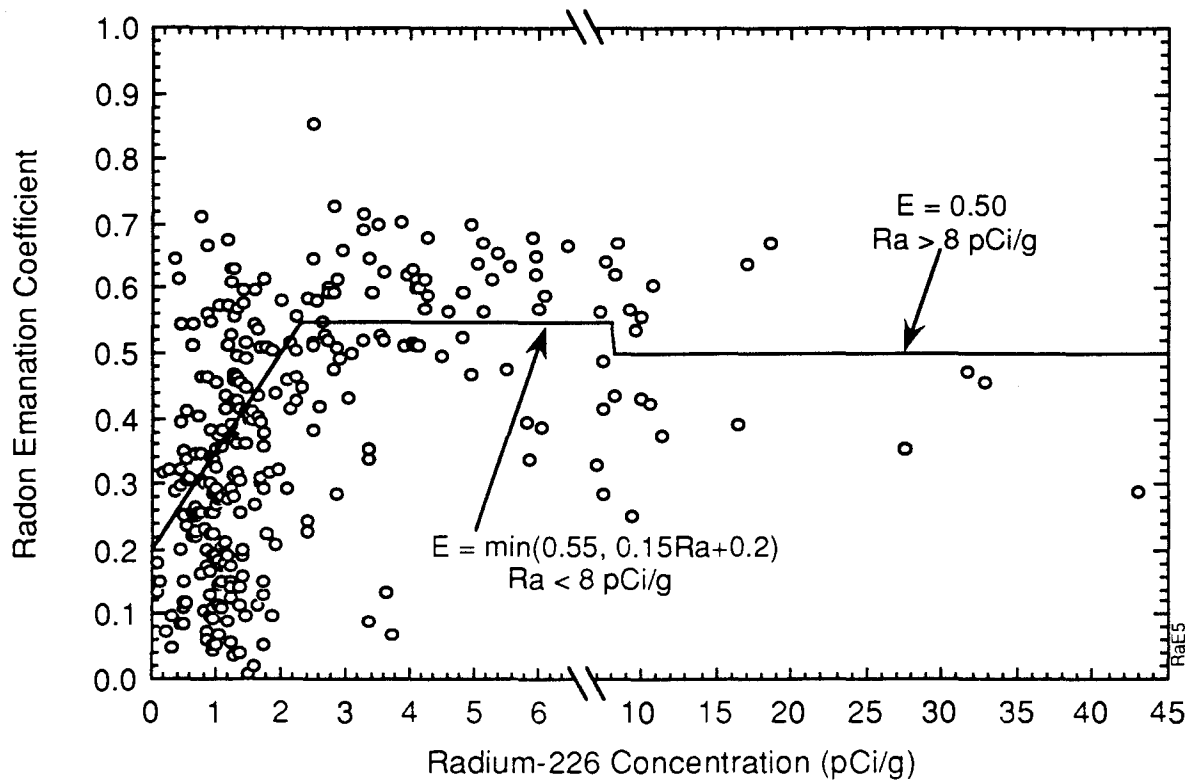

Figure 3-2. Comparison of radon emanation coefficients with soil radium concentrations for 296 samples of Florida soils.

The emanation trend lines in Figure 3-2 were defined mathematically for use with NURE radium values and geology-based deep-zone radium estimates as:

$$E = \min(0.55,\ 0.15\ Ra + 0.20), \quad Ra \le 8\ pCi\ g^{-1}$$
$$E = 0.50 \quad Ra > 8\ pCi\ g^{-1} \tag{15}$$

This approximation avoids the most extreme emanation values but still retains the general measured trends. Based on the five previously-defined geologic classifications, the radium concentrations representing the deep-zone soils were defined to be 0.8 pCi g^{-1} for the low-radium group, 1.8 pCi g^{-1} for the intermediate group, 4 pCi g^{-1} for the elevated-radium group,

8 pCi g^{-1} for the undisturbed parts of the Bone Valley Formation, and 20 pCi g^{-1} for the disturbed parts of the Bone Valley Formation.

3.2 RADON TRANSPORT PARAMETERS

Radon transport parameters were defined from soil profile properties associated with each of several reference pedon sites that were defined in the STATSGO data base to represent a particular STATSGO soil map unit. The reference pedon components of each of the STATSGO soil map units are listed in Appendix G. As indicated by these data, some of the soil components occur in more than one STATSGO map units. This illustrates the generalized nature of the STATSGO soil maps, which represent landscape areas by area-averaged composites of several different soil profiles. Although the individual profiles can be associated with more specific soil map units in the higher-resolution (1:24,000) individual county soil surveys (e.g., see Tho85), they are grouped according to commonly-associated soil types in the digitized STATSGO files used here.

The dominant soil components identified for each map unit were used to characterize the radon transport properties for radon potential modeling. Data files were assembled by the UFSWS from SCS data bases to define the physical properties of each horizon in each soil component. The data in Appendix H present the physical properties of each soil horizon in each respective reference pedon as they were used in computing radon transport parameters. In addition to the data in these tables, other information also was furnished, including the horizon identifications, complete textural data and classifications, and selected hydraulic properties. The data in Appendix H constitute the complete soil characterization input to the RnMAP code, which in turn calculated secondary parameters from these data.

Soil porosities computed in the RnMAP code were calculated from the densities given in column 2 of the Appendix H tables as:

$$p = 1 - \rho / \rho_g \tag{16}$$

where p = total soil porosity

ρ = soil bulk dry density (g cm^{-3})

ρ_g = soil specific gravity (nominally 2.7 g cm^{-3})

Soil water contents were estimated in the RnMAP code for each soil component and each horizon from the capillary drainage data in Appendix H. The capillary suction corresponding to the water content for sub-slab conditions was initially estimated by a series of 2-dimensional water balance calculations with the FEMWATER model (Yeh87, Sul88). These analyses are summarized for a water table in clay soil 5 m below the house in Figure 3-3. The capillary suction under the (11 m. wide) house is almost identically equal to the height above the water table (100 cm water column = -0.1 bar, etc) for a constant infiltration of 16 cm y^{-1}, which is typical for Gainesville, Florida (Tho64). Even outside of the house footprint the water suction is well-represented by the height above the water table. At lower infiltration rates and for sandier soils, the agreement is even better. For higher infiltration rates (3 times the typical Gainesville estimate), the dashed lines show a larger discrepancy outside the house, but excellent agreement under the house. The worst outside case shown in Figure 3-4 amounts to only a 1% higher water content outside the house than under it.

For deeper water tables, capillary suctions of -0.1 bars to -0.33 bars are commonly used (Tho85, Lut79) instead of the height above the water table. To examine the frequency of higher-suction matric potentials, a series of shallow-depth (30 cm) matric potential measurements was conducted throughout much of Florida. Forty-six measurements were made using a quick-draw portable tensiometer (Model 2900, Soil Moisture Equipment Corp., Santa Barbara, CA). They were made in multiple locations in or near Tampa, Ruskin, Sarasota, Punta Gorda, Bartow, Lakeland, Orlando, Ocala, Gainesville, Lake City, Madison, and Tallahassee.

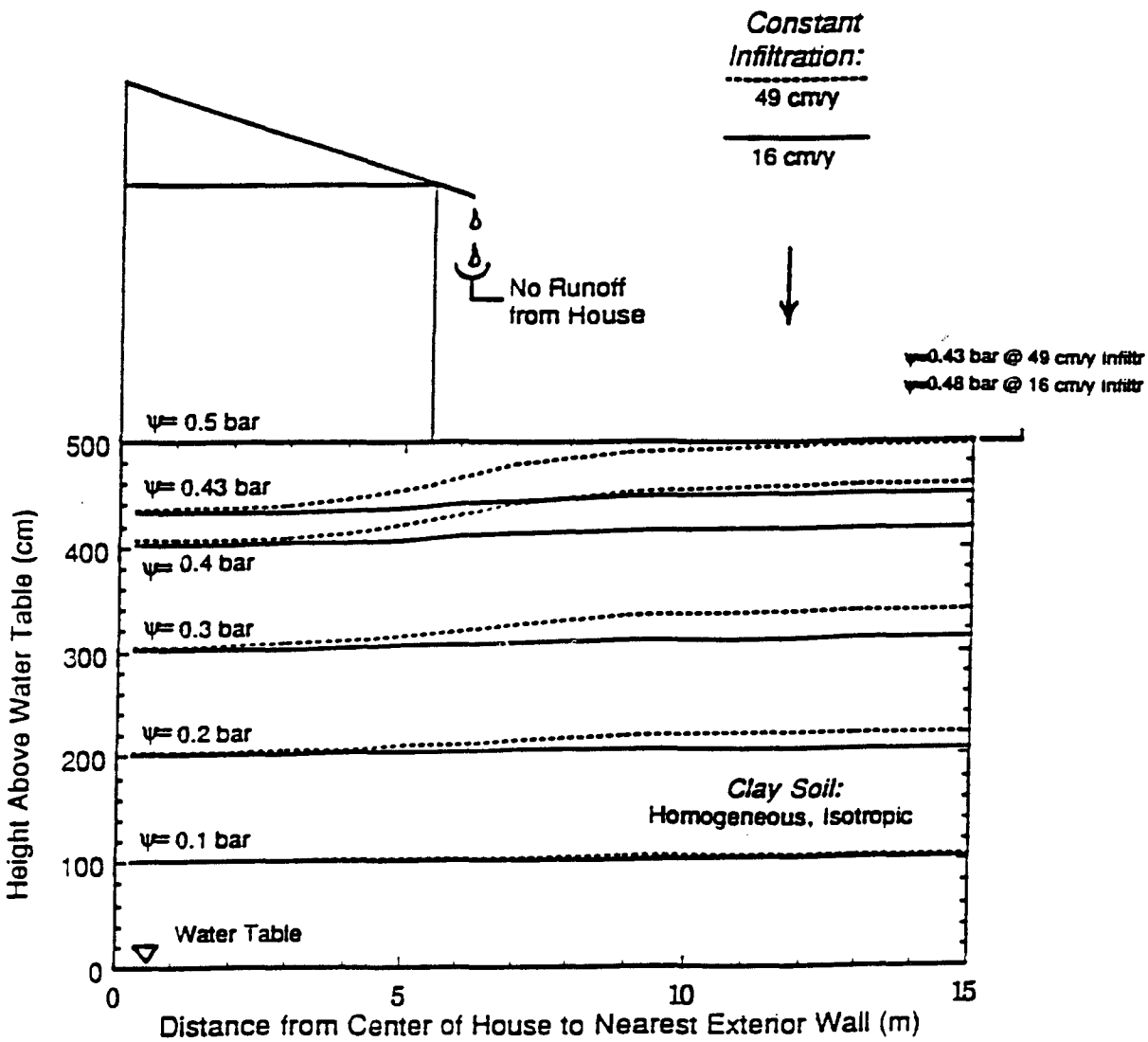

Figure 3-3. Water capillary suction profiles under and beside a house for normal (16 cm y^{-1}) and extreme infiltration.

The results of the capillary suction measurements (Figure 3-4) suggested two distributions, corresponding approximately to areas with estimated shallow water tables and deeper water tables. The shallow-depth case had a geometric mean matric potential of -0.06 bars (GSD=1.1), corresponding to a water table at only 60-cm below the measurement depth. The other group had a geometric mean matric potential of -0.21 bars (GSD=2.8), corresponding to approximately a 210-cm water table depth beneath the measurement point. The upper 7 points in Figure 3-4 were censored due to a suction gauge limit above this point. About 85% of the open-soil measurements were within the gauge range of <75 centibars, and 78% were within 50 centibars. The medians also approximated the -0.1 to -0.33 bar range

commonly used for sands and clays. An upper limit of -0.5 bars, therefore, was considered acceptable for mapping purposes. This is the limit afforded by the maximum 5-m water table depth represented in Figure 2-9 for the RnMAP calculations. For shallower depths of the water table, the actual depth is used, as suggested by the data in Figure 3-3.

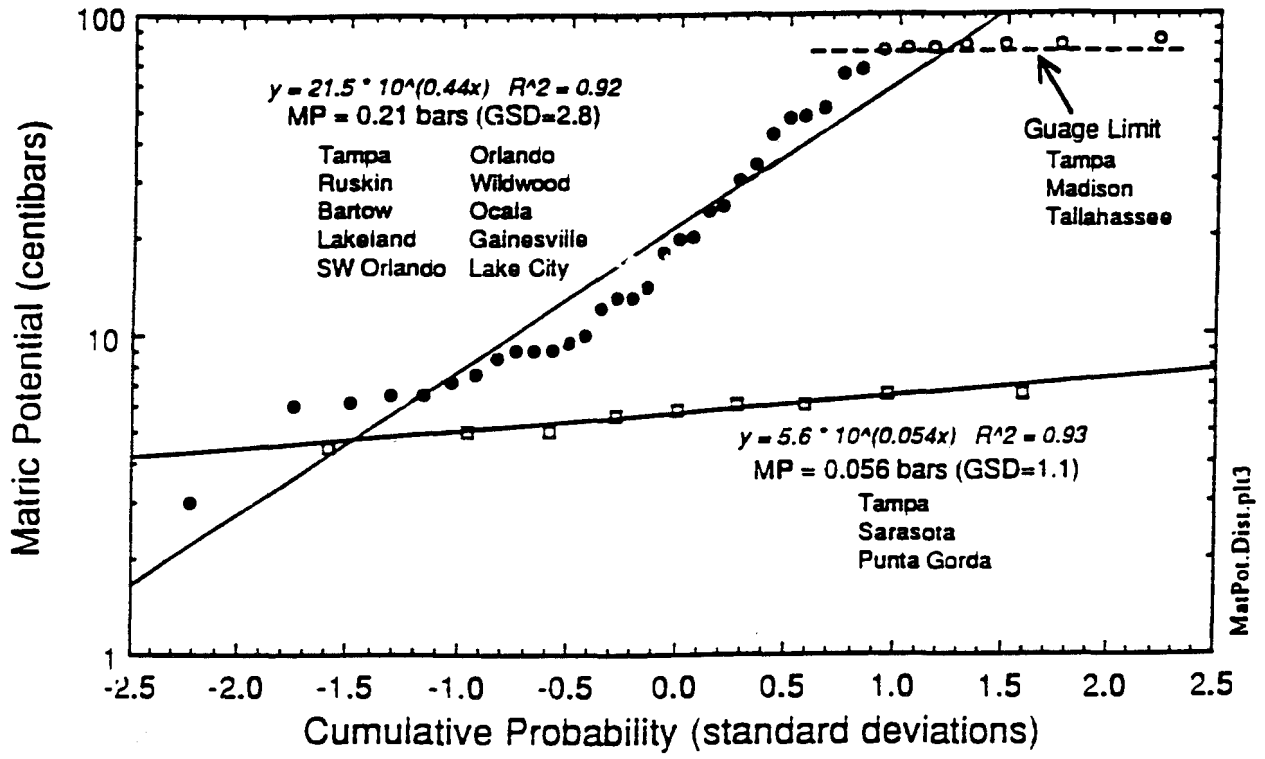

Figure 3-4. Measured water matric potentials at 46 locations in Florida.

Soil water contents for each horizon were interpolated from the water drainage curves in columns 5-15 of the Appendix H tables to obtain the water content for the specific height of the horizon above the water table. Separate values were computed for each seasonal level, and were used for separate seasonal radon calculations before averaging, as illustrated by the sample printout from RnMAP in Appendix B. Interpolation of the water content data in Appendix H was done on a log(suction) vs. moisture basis. Some of the water contents were supplied in the SCS data file on a weight-percent basis, and were converted to volume-

percent for consistency with the majority of the other SCS moisture data. The conversion between water contents on a weight-percent basis, a volume-percent basis, and fraction of saturation basis utilized the relationship

$$100S = M_v/p = \rho M_w/p \tag{17}$$

where S = fraction of water saturation

M_v = soil water content (volume percent)

M_w = soil water content (dry weight percent)

The high water table depths and durations in columns 16 and 17 of Appendix H were interpreted to characterize an approximate seasonal distribution of water tables as described in Section 2 (Figure 2-9). Soil horizon thicknesses in column 18 were used directly to define layers for the radon transport calculations in RnMAP. Soil particle diameters in column 19 were computed from detailed sieve analysis data in the SCS data files. Using standard sieve size definitions (SCS75), the arithmetic mean particle diameters were computed as required by RnMAP for definition of soil air permeabilities (Rog91b).

Soil radon diffusion coefficients were estimated from the water contents and porosities of the soils using a predictive correlation that is based on 1073 laboratory measurements of radon diffusion in re-compacted soils at moistures ranging from dryness to saturation (Rog91b). The soil textures ranged from sandy gravels to fine clays, and their densities covered the range of most of the Florida soil densities. The correlation exhibited a GSD between measured and calculated values of 2.0, and had the form

$$D = D_o\, p \exp(-6Sp - 6S^{14p}) \tag{18}$$

where D = diffusion coefficient for ^{222}Rn in soil pores ($cm^2\ s^{-1}$)

D_o = diffusion coefficient for ^{222}Rn in air (0.11 $cm^2\ s^{-1}$).

Soil air permeabilities were estimated similarly from the water contents, porosities, and particle diameters of the soils using a predictive correlation that was based on more than

a hundred in-situ field measurements of soil air permeability, including measurements in Florida (Rog91b). This correlation exhibited a GSD between measured and calculated values of 2.3, and had the form

$$K = 10^4 (p/500)^2 d^{4/3} \exp(-12S^4) \tag{19}$$

where K = bulk soil air permeability (cm^2)

d = arithmetic mean soil particle diameter, excluding >#4 mesh (m).

Section 4
CALCULATION OF RADON POTENTIALS FOR MAPS

Soil radon potentials were calculated for radon maps in two steps. The RnMAP code first computed the individual soil radon potentials for each soil component for which data were available. The RnMAP calculations used the fundamental soil property data from Table H-1. The RnMAP code internally averaged the resulting radon potentials over the two or three seasonal conditions to obtain annual average radon potentials for both low-radium and elevated-radium geology configurations and for two different (low-radium and elevated-radium) surface soil radium concentrations. For soils associated with the Bone Valley Formation, additional RnMAP runs were performed for the two higher-radium categories. In the second step, the radon potentials RnMAP computed were transferred into a spreadsheet (MicroSoft EXCEL®) for the following three additional calculations: (a) interpolation of the RnMAP results to correspond to the NURE-based top-zone radium concentrations in each polygon (defined from Table C-1); (b) area-weighted averaging of the resulting radon potentials according to the soil profiles used; and (c) selection of the appropriate geology class for each polygon for defining the lower-zone radon sources.

To simplify the second step, the soil radon potentials computed by RnMAP were summarized for each annual-averaged soil profile condition by several pairs of fitting coefficients. These corresponded to the following equation for a single soil profile:

$$Q = a \cdot (R \cdot E) + b, \tag{20}$$

where Q = soil radon potential (mCi y^{-1})

a,b = fitting coefficients computed by RnMAP

$R \cdot E$ = product of radium concentration (pCi g^{-1}) and radon emanation coefficient.

One *a,b* pair was computed for the low-radium geology case, one pair for the intermediate-radium geology case, and another pair for the elevated-radium geology case. Fitting coefficients were computed for the Bone Valley and disturbed Bone Valley cases for applicable

soils only. Sensitivity analyses with the RnMAP code showed that when the soil radium profiles were divided into two parts, as in Figure 1-2, the radon potential was a linear function of the radium·emanation product for the upper part of the profile, as long as the radium·emanation product in the lower part was held constant. Furthermore, identical *a* values were obtained for all geology definitions, and the *b* constants were directly proportional to the radium·emanation product for the lower soil zone. Radium concentrations used for the lower, geology-dominated soil zone in the RnMAP calculations were defined as described in Section 3.1. All radon emanation coefficients also were defined as described in section 3.1.

The *a* and *b* radon potential coefficients were entered into a spreadsheet on rows corresponding to their soil series (profile) name, as illustrated in Tables I-1 and I-2. The constants were ordered alphabetically by soil series name to form a look-up table that was in turn accessed by a second look-up table. In the second table the fractional area of the STATSGO unit occupied by each soil series (see Table G-1) was used to calculate the area-weighted average of the *a* and *b* coefficients for each STATSGO unit. With weighted averaging, the radon potentials for the different soil series were defined from equation (20) for a STATSGO map unit as:

$$Q_a = 0.01 \sum F_i \, [a_i \cdot (R \cdot E) + b_i] \tag{21}$$

where Q_a = soil radon potential for the polygon (mCi y^{-1})

F_i = normalized area % occupied by the soil component (%, $\Sigma F_i = 100$)

a_i, b_i = RnMAP fitting coefficients for soil series *i* for the polygon geology designation

R = soil radium concentration (pCi g^{-1})

E = radon emanation coefficient defined from equation (15).

The soil component areas from Table G-1 were used for area-weighted averaging of the a_i and b_i coefficients from Tables I-1 and I-2. However, these areas were first normalized upward to account for the missing minor soil components (generally those <10% of the STATSGO map unit) that were not defined in the STATSGO data sets (Table H-1).

The a_i and b_i coefficients in equation (21), listed in Tables I-1 and I-2, are distributed relatively narrowly for each STATSGO unit. In contrast to the log-normally distributed NURE radium data, a normal distribution better represents the a_i and b_i coefficients. Therefore, arithmetic means and standard deviations were computed in the area-weighted averaging of the coefficients to define a simpler form of equation (21). This simpler form better separates the soil-related coefficients from the radium and emanation parameters. The equation reads:

$$Q_a = A \cdot (R \cdot E) + B \tag{22}$$

where $A = (\Sigma F_i\, a_i) / \Sigma F_i$ = area-weighted mean of the a_i's
$B = (\Sigma F_i\, b_i) / \Sigma F_i$ = area-weighted mean of the b_i's.

The values of b_i appropriate to the polygon geology were used in equation (22). Values of a_i were independent of the different geology categories.

The area-weighted averages of the soil coefficients for each STATSGO soil unit finally were combined with the NURE radium and emanation estimates (see Table C-1) to calculate the soil radon potential for each map polygon. Combining equation (15) with equation (22) gave the following equation for the median radon potential for a map polygon:

$$Q_m = Q_1 + Q_2 + Q_3 \tag{23}$$

where Q_m = median soil radon potential for a map polygon (mCi y^{-1})

$Q_1 = 0.15\ A\ R^2$ $\quad R < 2.33$ pCi g^{-1}
$\quad = 0$ $\quad R > 2.33$ pCi g^{-1}
$Q_2 = 0.20\ A\ R$ $\quad R < 2.33$ pCi g^{-1}
$\quad = 0.55\ A\ R$ $\quad 2.33 < R < 8$ pCi g^{-1}
$\quad = 0.50\ A\ R$ $\quad R > 8$ pCi g^{-1}
$Q_3 = B$.

Before calculating and adding the three terms contributing to the radon potential in equation (23), the normal and log-normal distributions were first made consistent. Since the radium concentrations (R) typically had very wide log-normal distributions, their variations

usually dominated the narrower normal distributions of the soil parameters A and B. Therefore the means and standard deviations of the A and B parameters were used to compute approximately equivalent log-normal parameters for A and B. Q_m was then calculated using consistent, log-normal distributions for all parameters.

The geometric standard deviations used to approximate the arithmetic standard deviations for the soil parameters were estimated by linearizing standard expressions (Has75) as:

$$g_A = 1 + s_A/A \qquad (24)$$
$$g_B = 1 + s_B/B$$

where g_A = geometric standard deviation of the soil parameters a_i
s_A = arithmetic standard deviation of a_i ($s_A = \sqrt{\Sigma F_i\, a_i^2 - (\Sigma F_i\, a_i)^2}$)
g_B = geometric standard deviation of the soil parameters b_i
s_B = arithmetic standard deviation of b_i ($s_B = \sqrt{\Sigma F_i\, b_i^2 - (\Sigma F_i\, b_i)^2}$).

The corresponding geometric means used to approximate the arithmetic means of the soil parameters were estimated as (Has75):

$$G_A = A \exp\{-0.5\, [\ln(g_A)]^2\} \qquad (25)$$
$$G_B = B \exp\{-0.5\, [\ln(g_B)]^2\}$$

Soil radium concentrations were defined directly as the geometric means from Table C-1 for estimating the median, or 50% confidence limit of the radon potential for all polygons having a NURE-defined value. Estimates for polygons without NURE data were defined using the overall geometric mean for the geology unit associated with the polygon. In the few cases where the radium for an entire geology class was not defined with NURE data, the overall geometric mean for the polygon's STATSGO unit was used. Thus, the polygons with large, identical numbers of points in Table C-1 are not necessarily better-defined, but may be extrapolations to polygons that were not directly intersected by NURE flight lines. The geometric means and geometric standard deviations of the NURE radium data points were calculated as:

$$G_R = \exp[\Sigma \ln(r_i) / n] \tag{26}$$

and

$$g_R = \exp[\sqrt{\{\Sigma[\ln(r_i)]^2 - [\Sigma \ln(r_i)]^2/n\} / (n-1)}\ ] \tag{27}$$

where G_R = geometric mean of the NURE-estimated radium concentrations (pCi g^{-1})
r_i = NURE estimate of radium concentration at a single point (pCi g^{-1})
n = number of NURE points in a map polygon
g_R = geometric standard deviation of the NURE-estimated radium concentrations.

The Q_1 and Q_2 terms in equation (23) were computed by using geometric means (G_A and G_R) directly for the indicated A and R parameters. The resulting Q_1 and Q_2 terms were therefore medians (geometric means) of log-normal distributions, with associated geometric standard deviations that were calculated as:

$$g_{Q1} = \exp\{\sqrt{[\ln(g_A)]^2 + 2[\ln(g_R)]^2}\} \tag{28}$$

$$g_{Q2} = \exp\{\sqrt{[\ln(g_A)]^2 + [\ln(g_R)]^2}\} \tag{29}$$

where g_{Q1}, g_{Q2} = respective geometric standard deviations of Q_1 and Q_2.

The number of degrees of freedom associated with the Q_1 and Q_2 distributions was defined as the minimum of the degrees of freedom for either their radium or soil parameter components. Since the soil components were computed as area-weighted averages, their degrees of freedom were considered large, and the number of degrees of freedom was defined from the number of NURE points in the radium distribution.

The addition of the Q_1, Q_2, and Q_3 components of the soil radon potential posed a more difficult problem, since the sum of two or more independent, log-normally distributed variables does not necessarily yield either a normal or log-normal distribution. Although the central-limit theorem suggests that the distribution of the sums should approach normality (Dev87), other studies suggest that the sums may be nearly log-normal (Mit68). Tests with map data indicated that neither distribution adequately describes the median or distribution of the sums for the necessary range of cases. Figure 4-1 illustrates an example of the three

components of Q for a map polygon calculated previously (Nie93a). As illustrated, the sum of the medians of the three distributions (0.325) is only about two-thirds of the median of the distribution of random sums from the Q_1, Q_2, and Q_3 distributions as calculated by Monte-Carlo methods. For comparison, the sum of the arithmetic means of the three distributions is 1.5, more than three times higher than the expected median. Although approximate methods have been proposed for adding independent, log-normally-distributed variables (Mit68, Bar76), the problem is presently best-addressed by Monte-Carlo calculations (Gil93).

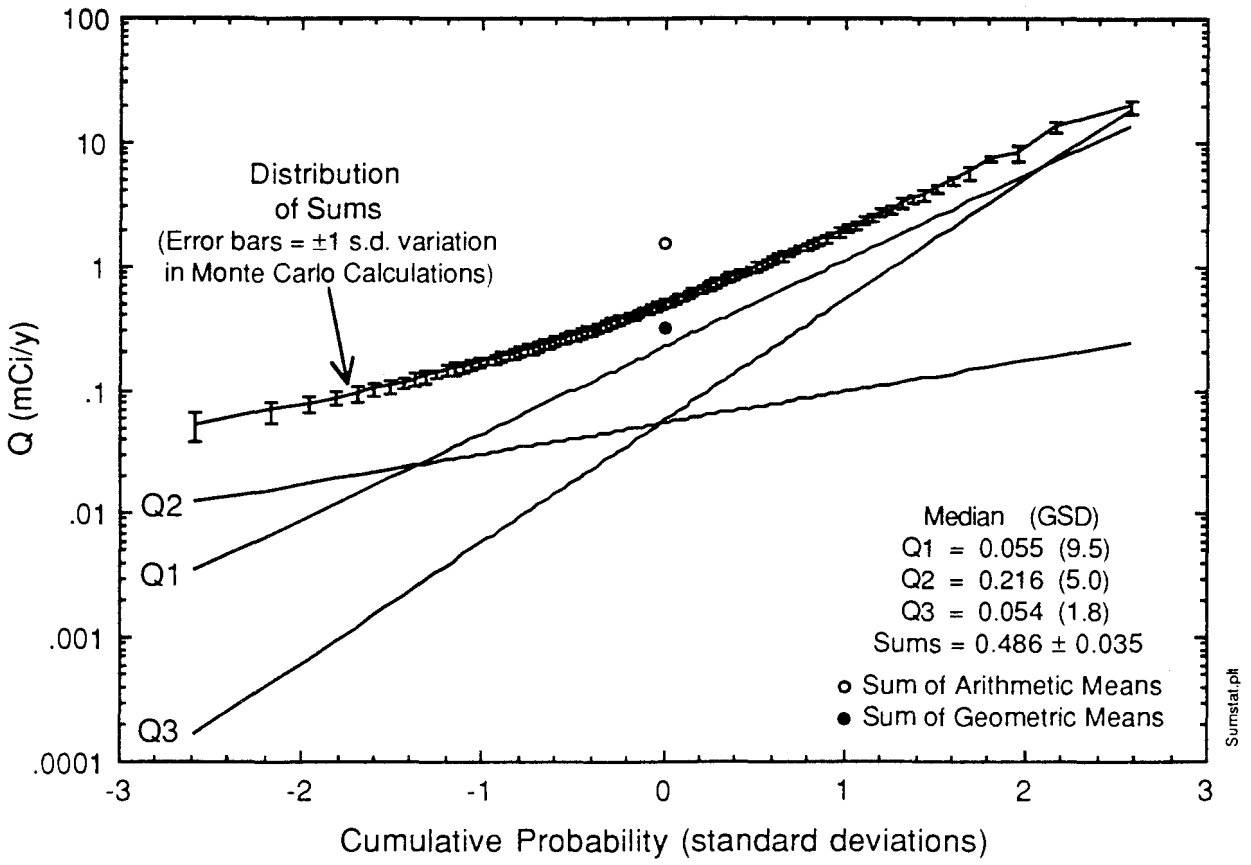

Figure 4-1. Distribution of the random sums of the log-normally distributed variables Q_1, Q_2 and Q_3.

For adding the Q_1, Q_2, and Q_3 variables in equation (23), the distribution of the sum was estimated in the following manner. One hundred points of equal probability were computed to represent each of the three distributions, as illustrated by the straight lines in Figure 4-1. The points in each distribution were then randomly shuffled and successive

single points from each were added together to obtain a 100-point random distribution of the sums, which is also illustrated in Figure 4-1. This process was repeated nine times for each sum to reduce the uncertainty in the mean of the sum by a factor of three. The individual distributions of the sums had a relatively uniform coefficient of variation throughout the required range of confidence limits (50% to 95%) of about 7.6%, which was reduced to about 2.5% by averaging the nine replicate distributions.

The composite distribution of Q was finally used to estimate soil radon potentials at various confidence limits. The value for the median, or 50% confidence limit, was defined for the composite distribution (see Figure 4-1) as the value at zero standard deviations from the center. The values for 75%, 90%, and 95% confidence limits were defined from the same composite distribution at positive probability levels defined from student's t-statistic (Nat66) at the desired confidence level and degrees of freedom. The number of degrees of freedom used to calculate the t-position in the distribution of Q was estimated from the degrees of freedom of the Q_1, Q_2 and Q_3 components as:

$$\upsilon = [\Sigma(f_i/n_i)]^{-1} \tag{30}$$

where υ = degrees of freedom for the composite estimate of variability

$f_i = Q_i / \Sigma Q_i$

n_i = number of degrees of freedom for component i.

The positions in the Monte Carlo distribution of sums that corresponded to the chosen "t" values were interpolated between the calculated distribution points to obtain the desired confidence limits for the radon potentials. For example, the polygon used to create Figure 4-1 was estimated from equation (30) to have υ=2021 degrees of freedom, which corresponds to a t-statistic of 1.282 for a 90% confidence limit. The soil radon potential was therefore interpolated between points calculated at +1.254 and +1.311 standard deviations above the median to obtain the 90% confidence limit for the radon potential map.

Soil radon potentials were estimated for the 50% (median), 75%, 90%, and 95% confidence limits for mapping purposes. The "t" statistics used in the calculations were

obtained from internal spreadsheet functions found to correspond to standard tables of values (Nat66). The Monte Carlo calculations also were performed by spreadsheet calculations using a macro instruction set and the spreadsheet random number generator. It should be noted that the geometric standard deviations used in equations (24), (27), (28), and (29) reflect variations among *individual* NURE observations and *individual* soil series within a map polygon. The calculations therefore give confidence limits for ***individual localized areas*** in order to reach the stated radon potentials. Since the spatial resolution of the NURE measurements is on the order of 0.25 square miles, and NURE variations dominate the total radon potential variations, the calculated confidence limits potentially apply to maxima over localized areas as small as 0.25 square miles (0.65 km^2). Soil and geology units are much larger, however, and the one square mile (2.6 km^2) minimum polygon size is estimated to better represent the nominal map resolution.

The calculated radon potentials are presented in columns 7-10 of Table J-1. The definitions of the geology classes for selecting the appropriate *b* coefficients for each polygon are presented in Table 4-1. The geology definitions are based on geologic descriptions and recommendations from the USGS, and are also summarized in Table 4-1. The resulting calculated estimates of soil radon potentials were sorted by polygon number and submitted to the University of Florida GeoPlan Center for plotting on maps.

Table 4-1
Geologic description and radium category of Florida Geologic Units

Class	Description	Category
Qa1	Anastasia Formation	Low
Qal1	Alluvium deposits	Low
Qbd1	Beach ridge dune sands	Low
Qbda1	Beach ridge dune sands over Anastasia formation	Low
Qd1	Dune sands	Low
Qh1	Quartz sands and lagoonal deposits	Low
Qk1	Key Largo limestone	Low
Qm1	Miami limestone	Low
Qm2	Miami limestone	Intermediate
Qq1	Undifferentiated Pleistocene and Holocene coastal deposits	Low
Qr1	Fluvial, lacustrine sands, clay, marl, and peat	Low
Qsu1	Undifferentiated shell beds	Low
Qsu2	Undifferentiated shell beds	Intermediate
Qtd1	Dune-like quartz sands	Low
Qtma1	Transitional unit between Qa and Qm	Low
Qtr1	Trail Ridge quartz sands	Low
Qtu1	Undifferentiated older quartz sands	Low
Qtu2	Undifferentiated older quartz sands	Intermediate
Qtu3	Undifferentiated older quartz sands	Elevated
Qtuk2	Undifferentiated sands on karstic limestone	Intermediate
Qu1	Undifferentiated quartz sand	Low
Qu2	Undifferentiated quartz sand	Intermediate
Quc1	Undifferentiated quartz sand from cypresshead	Low
Qul1	Lagoonal sands, clay, and shell	Low
Tab1	Alum bluff formation	Low
Tap1	Avon Park formation	Low
Tap2	Avon Park formation	Intermediate
Tc1	Cypresshead formation	Low
Tc3	Cypresshead formation	Elevated
Tchat1	Chattahoochee formation	Low
Tci1	Citronelle	Low
Th1	Hawthorn group phosphatic sediments	Low
Th2	Hawthorn group phosphatic sediments	Intermediate
Th3	Hawthorn group phosphatic sediments	Elevated
Tha2	Tampa member, Arcadia formation	Intermediate
That2	Tampa member, Arcadia formation (limestone/dolostone)	Intermediate
Thcc1	Charleton Coosawhatchie formation (Hawthorn group)	Low
Thpb4	Bone Valley formation (undisturbed)	High
Thpb5	Bone Valley formation (disturbed)	High
Thpr2	Peace River formation	Intermediate
Ths1	Hawthorn group phosphatic sediments	Low
Ths2	Hawthorn group phosphatic sediments	Intermediate
Tht1	Tampa member, Arcadia formation (phosphatic sediments)	Low

(Continued)

Table 4-1 (continued)
Geologic description and radium category of Florida Geologic Units

Class	Description	Category
Tic1	Intercoastal formation	Low
Tjb1	Jackson bluff formation	Low
Tko2	Extremely karstified Ocala limestone	Intermediate
Tmc1	Miccosukee formation	Low
Tmc2	Miccosukee formation	Intermediate
To2	Ocala group (Crystal River limestone)	Intermediate
Tre1	Residuum on Eocene limestones and siliclastics	Low
Trm1	Residuum on Miocene limestones and siliclastics	Low
Tro1	Residuum on Oligocene-Miocene limestones and siliclastics	Low
Ts1	Suwannee limestone	Low
Ts2	Suwannee limestone	Intermediate
Tsk2	Karstified Suwannee limestone	Intermediate
Tsm1	Undifferentiated Suwannee and Marianna limestone	Low
Tsm2	Undifferentiated Suwannee and Marianna limestone	Intermediate
Tt2	Tamiami formation	Intermediate
Twh1	Weathered Hawthorn group	Low
Twh3	Weathered Hawthorn group	Elevated

Section 5
PRODUCTION AND INTERPRETATION OF THE RADON MAPS

Soil radon potential maps were produced by displaying each radon map polygon in a color corresponding to its calculated radon potential. Since the radon potentials for each polygon were calculated as a statistical distribution, it was possible to prepare separate maps to show different confidence limits of the radon potentials. Data were therefore prepared for mapping the median, 75%, 90%, and 95% confidence limits of the calculated soil radon potentials. To display the numerical radon potentials by corresponding colors, the numerical data were grouped into several tiers of similar values, and different colors were assigned to each tier. Although this approach sacrifices the numerical detail associated with each polygon, it helps illustrate regional trends and anomalies. The numerical details are still preserved, however, by using Table J-1 to examine any particular polygons of interest.

The calculated soil radon potential distributions were compared with indoor radon measurements to help clarify the general relationship between the calculated radon potentials and observed indoor radon levels. Although a theoretical, linear relationship is predicted from simulations of radon entry into the map reference house, large variations caused by construction and occupancy differences and temporal variations obscure the relationship. Calculated radon potentials were compared with the Geomet land-based indoor radon data (Nag87) to help identify the magnitudes of the variations from calculated values and to attempt to partition them among soil-related and house/occupant-related sources.

5.1 DEFINITION OF RADON MAP TIERS

The boundaries between different tiers of soil radon potential were defined from analyses of the distributions of all of the calculated radon potentials. Figure 5-1 summarizes these distributions using cumulative probability plots. The higher confidence limits (i.e., 90%, 95%) have consistently higher values than the lower ones, as expected, and tend to exhibit a slightly broader distribution than the values for the 50% confidence limit. As

illustrated, there are no significant breaks in the distributions that suggest consistent natural cut points. Therefore an arbitrary but consistent set of tier cut points was defined that would display the soil radon potentials in several different color categories.

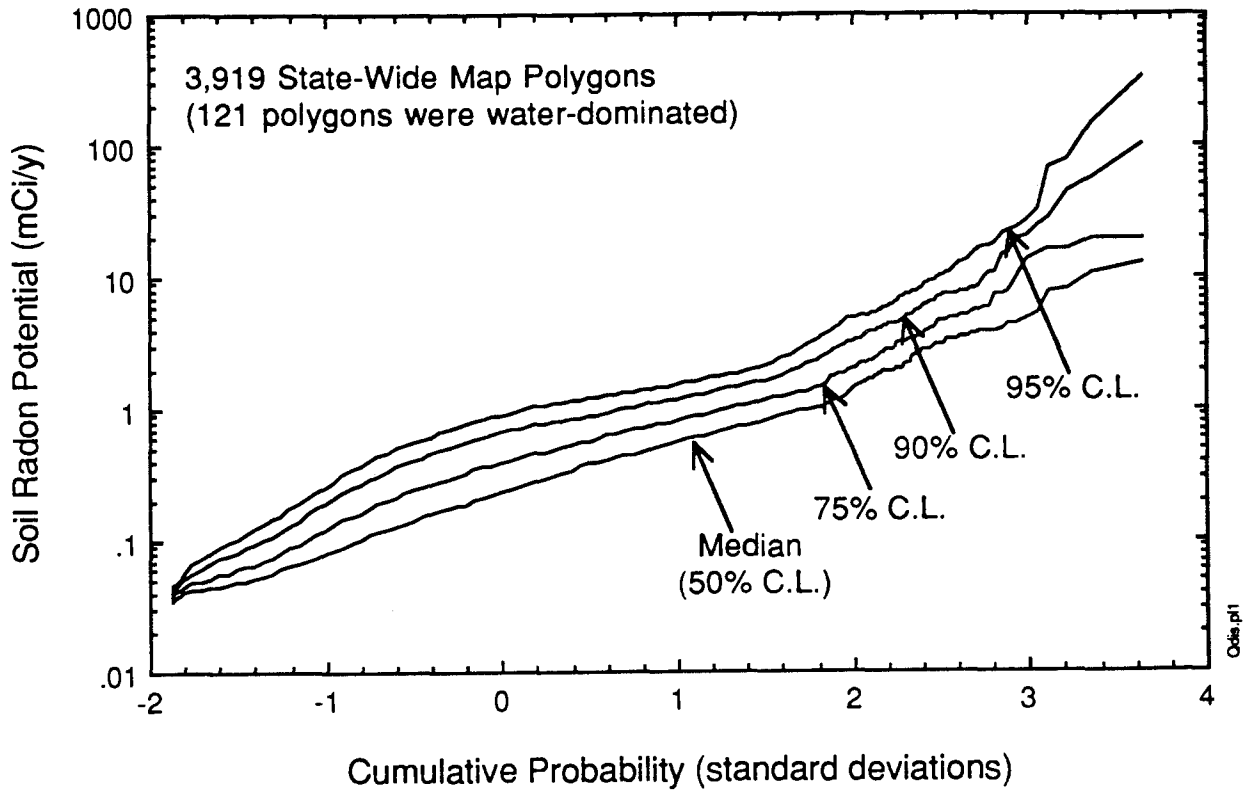

Figure 5-1. Cumulative probability distributions of the soil radon potentials for all map polygons in Florida.

The definition of cut points for the radon potential map tiers recognized the approximate log-normal distributions shown in Figure 5-1, and centered the narrowest tiers in the low range where most of the data occurred. The only pre-selected tier boundary was defined at a radon potential of 3 mCi y^{-1}, which approximates for the reference house the EPA indoor radon criterion of 4 pCi L^{-1} (EPA92a). Tier boundaries above this level increased exponentially by successive factors of two, and two lower levels both decreased by units of 1 mCi y^{-1}. The low range from zero to 1 mCi y^{-1} was further divided at 0.4 mCi y^{-1} because of the large amount of data in this range. Table 5-1 shows the numbers and percentages of

polygons that fall into each of the seven tiers at the 50%, 75%, 90%, and 95% confidence limits. Although these tier definitions provide little separation among most of the lower radon potentials, they accommodate the higher radon potentials observed in several areas of the state.

Table 5-1. Radon Potential Polygon Distributions Among Seven Tiers.

Tier	Radon Potential (mCi y^{-1})	50% Confidence Limit		75% Confidence Limit	
		No. of Polygons	Percent of Polygons	No. of Polygons	Percent of Polygons
1	0.0 - 0.4	2834	72.3	2036	52.0
2	0.4 - 1	945	24.1	1521	38.8
3	1 - 2	95	2.4	278	7.1
4	2 - 3	19	0.5	37	0.9
5	3 - 6	22	0.6	37	0.9
6	6 - 12	3	0.1	4	0.1
7	>12	1	0.0	6	0.2

Tier	Radon Potential (mCi y^{-1})	90% Confidence Limit		95% Confidence Limit	
		No. of Polygons	Percent of Polygons	No. of Polygons	Percent of Polygons
1	0.0 - 0.4	1225	31.3	904	23.1
2	0.4 - 1	1780	45.4	1291	32.9
3	1 - 2	737	18.8	1435	36.6
4	2 - 3	74	1.9	127	3.2
5	3 - 6	73	1.9	110	2.8
6	6 - 12	21	0.5	34	0.9
7	>12	9	0.2	18	0.5

It should be recognized that the radon potential maps show the potential soil radon contribution to the reference house (annual average basis) as if it were located on the soil profiles in different parts of the state. Indoor radon concentrations also depend strongly on house and occupant characteristics and their changes in time. Important house variables include the ventilation (dilution) of radon in indoor air, the ambient indoor air pressure, and

the house foundation design and construction and its susceptibility to radon penetration. Models that represent these parameters and their variations are complex. However, a simple approximate equation estimates the nominal indoor radon concentration that could occur in the *reference house* over soil profiles with a given radon potential. The approximate indoor radon concentration in the reference house is:

$$C_h = 114\ Q / (V_h\ \lambda_h) + C_{out}, \tag{31}$$

where C_h = indoor radon concentration (pCi L^{-1})

114 = unit conversion (pCi L^{-1} h^{-1} per mCi m^{-3} y^{-1})

Q = potential radon entry rate (mCi y^{-1})

V_h = house volume (m^3)

λ_h = house ventilation rate (h^{-1})

C_{out} = outdoor radon concentration (pCi L^{-1}).

This relation suggests that soil with a radon potential of about 3 mCi y^{-1} would cause an indoor radon concentration of 3.9 pCi L^{-1} in the reference house if no other radon sources were present (using the house volume and ventilation rate in Table 2-1). This gives a ratio for the reference house of 1.3 pCi L^{-1} of indoor radon, delivered from the slab and soil, for every mCi y^{-1} of calculated soil radon potential. Since ambient levels of radon in outdoor air generally add an additional 0.1-0.4 pCi L^{-1} (Ner88) to the levels caused by foundation soils, the 3 mCi y^{-1} cut point approximates the 4 pCi L^{-1} concentration for total indoor radon.

Figures 5-2 and 5-3 illustrate two of the soil radon potential maps for the median (50% confidence limit) case and the 95% confidence limit case, respectively. Although the 50% confidence limit map in Figure 5-2 suggests that only a few of the polygon areas have sufficient radon potential to exceed 4 pCi L^{-1} in the reference house, soil and house variabilities cause the reference house to approach and exceed 4 pCi L^{-1} in many additional areas at the 95% confidence limit. For this reason, the two maps together give a more complete picture. The median map in Figure 5-2 shows the commonly-expected levels while the 95% map shows the levels at the upper end of the range that includes all but the top 5% of the land areas. As illustrated by Figure 5-3, radon potentials in a much larger part of the

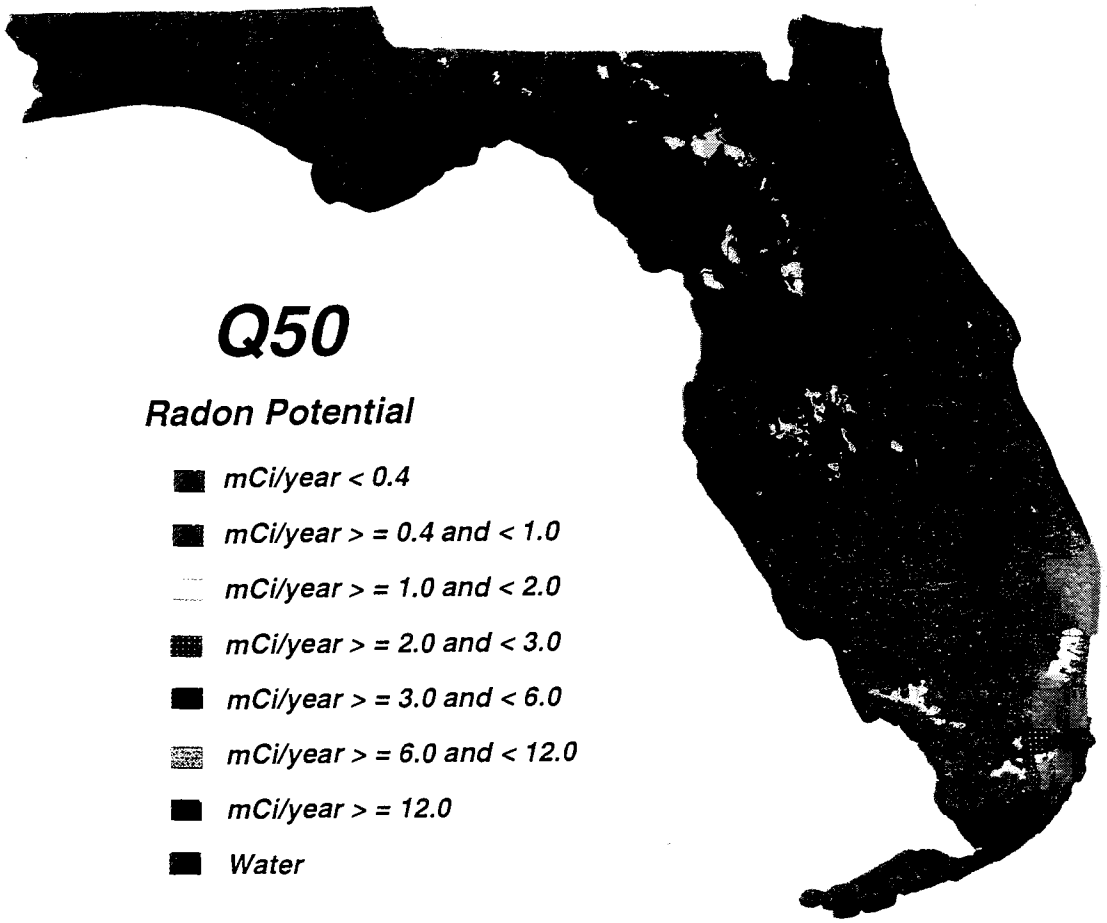

Figure 5-2. Florida median (50% confidence limit) map of soil radon potentials.

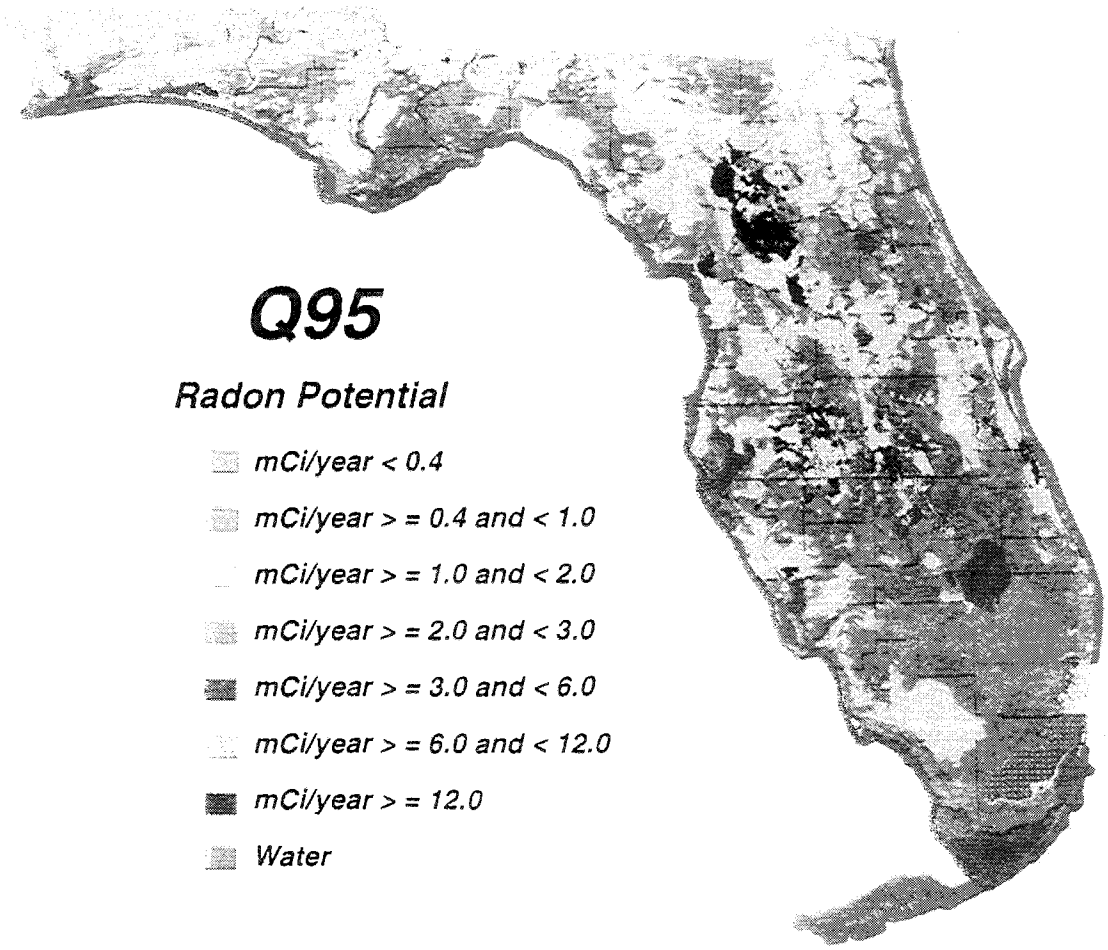

Figure 5-3. Florida 95% confidence limit map of soil radon potentials.

Preceding page blank

state would cause the reference house to have levels that approach, and in some areas exceed, 4 pCi L^{-1} in a small (approximately 5%) part of polygon land areas.

The interpretation of the soil radon potential maps is conceptually simplified by assuming a uniform density of residential housing (corresponding to the reference house) in the mapped areas. The 50% confidence limit map then shows that approximately half of the houses in a red area would exceed 4 pCi L^{-1}, and that approximately half in any other color tier would similarly exceed the corresponding level calculated by equation (31) from the mapped radon potential. The 95% confidence limit map shows more conservatively the regions in which approximately 5% of the houses would exceed the corresponding limits. For new construction (of a reference house), any red and pink color tiers on the two maps show the respective areas in which a 50% and 5% chance of exceeding 4 pCi L^{-1} may be expected. As implied, the first four color tiers show areas corresponding to lower radon potentials. The 75% confidence limit and 90% confidence limit maps (not shown here) show the corresponding respective areas in which 25% and 10% of new (reference) houses may exceed corresponding levels under the same assumptions.

5.2 INTERPRETATION OF THE RADON MAPS

Interpretation of the soil radon potential maps requires an understanding of their various sources of uncertainty. The large total variations between mapped soil radon potentials and short-term measurements are illustrated by the scatter plot in Figure 5-4. This plot compares indoor radon concentrations from the Geomet state-wide land-based radon survey (Nag87) with corresponding soil radon potentials, and shows the uncertainties associated with the simple linear relationship in equation (31). The map coordinates for each indoor radon measurement were used in the University of Florida's geographic information system (GIS) to find the corresponding map polygons, from which the soil radon potentials were identified. The comparisons utilized 2,930 of the 2,952 measurements in the land-based data set. The remaining 22 were excluded because they occurred in polygons dominated by water (lakes), precluding quantitative estimates of their radon potential. The logarithm of

Preceding page blank

the indoor radon data were fitted by least-squares to the radon potentials to estimate the slope and intercept for the following equation, which corresponds to equation (31):

$$C_h = xQ + C_{out}, \tag{32}$$

where x = fitted slope of the C_h vs. Q data (pCi L^{-1} per mCi y^{-1}).

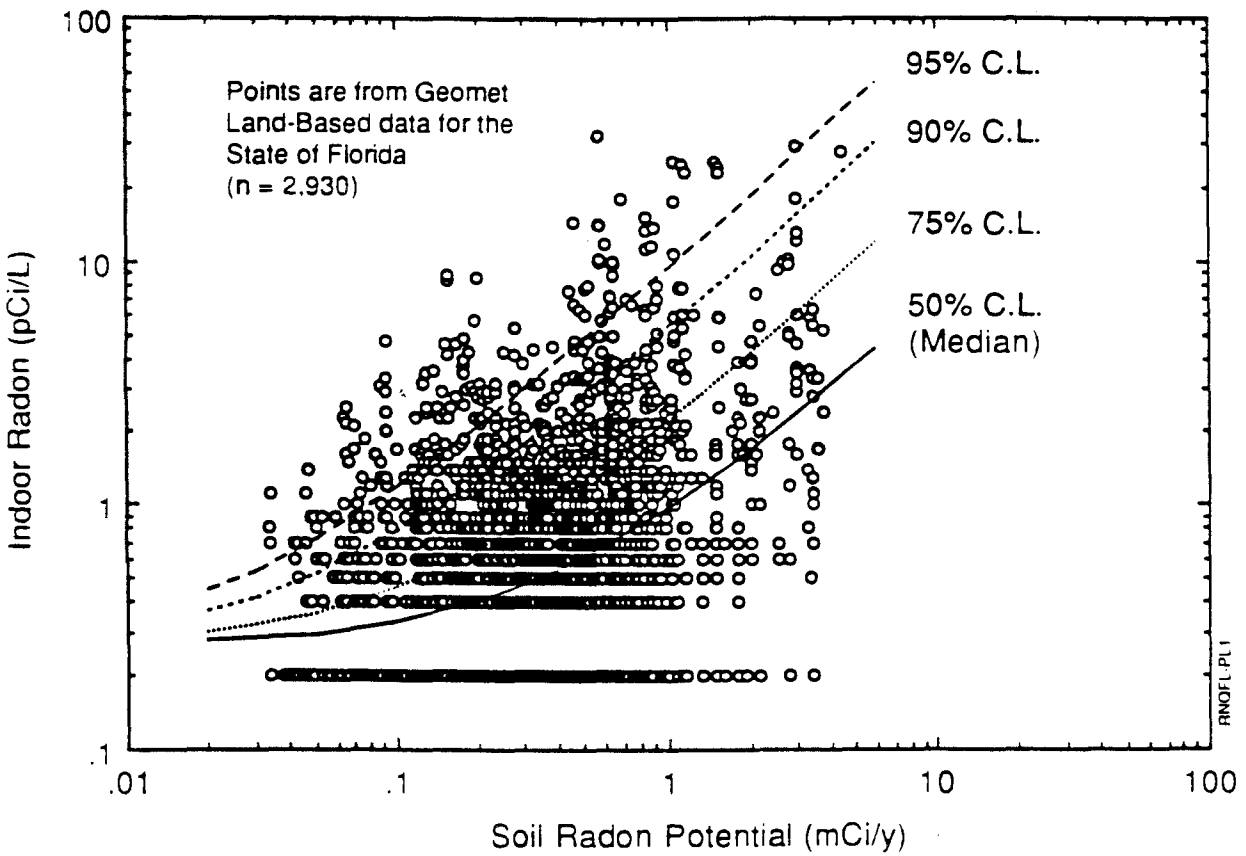

Figure 5-4. Comparison of measured indoor radon levels with mapped soil radon potentials.

The least-squares fit to the median radon potentials yielded the numerical values x=0.7 pCi L^{-1} per mCi y^{-1} and C_{out} = 0.26 pCi L^{-1}, both of which are reasonable values. The value x = 0.7 is about 47% lower than the value of 1.3 pCi L^{-1} per mCi y^{-1} calculated for the

reference house in Section 5-1. Inaccuracy in the fitted values is caused in part by the predominantly low radon potentials, which lower the soil-related indoor radon to approximately the outdoor levels in many cases. The apparent lower, narrower distributions of soil radon potentials give a relatively insensitive measure of the value of x. The value of C_{out}=0.26 pCi L^{-1} is also within the natural background range, reported from 0.1 to 0.4 pCi L^{-1}, with large variability (Ner88).

The GSD between the pairs of measured radon levels and the values calculated by equation (32) from the mapped soil radon potentials was 1.93. This is estimated to be the approximate overall precision of the mapped soil radon potentials. The total variations among the measured indoor radon levels were partitioned between geographic soil variations and combined house/occupant and measurement variations by modifying equation (32) to obtain:

$$C_h = C_{out} + x_{50}\, Q_{50} \left\{\exp[\sqrt{(\ln g_s)^2 + (\ln g_h)^2}\,]\right\}^{t_n}, \qquad (33)$$

where x_{50} = median ratio of indoor radon to soil radon potential (pCi L^{-1} per mCi y^{-1})

Q_{50} = median soil radon potential (mCi y^{-1})

g_s = geometric standard deviation from soil profile (location) differences

g_h = geometric standard deviation from house and measurement variations

t_n = t-statistic.

The total variations of the measured values from the median line in Figure 5-4 were partitioned by quadratically subtracting the soil variations, as in equation (33), to find the corresponding value of g_h that matched the observed spread in the data. The geometric standard deviations estimated from NURE and soil variations for each map polygon were estimated from the calculated soil radon potentials (Appendix F) as $g_s=\exp[\ln(Q_p/Q_{50})/t_p]$ to give average estimates of g_s = 1.91 for the 75% confidence limit, g_s = 1.98 for the 90% confidence limit, and g_s = 2.05 for the 95% confidence limit. A value of g_h = 4.0 was then found to match the total variation, as illustrated in Figure 5-4 for the calculated confidence limits. Using a previous estimate of g_m = 2.08 for the measurement uncertainty in estimating annual-average radon concentrations from charcoal canister measurements (Roe90), the value of g_h can be further partitioned to estimate a GSD of approximately 3.2 for house/occupant variations alone. A

corresponding numerical summary in Table 5-2 shows that the data are reasonably consistent in approximating the calculated confidence intervals.

Table 5-2. Comparison of Calculated and Measured Radon Statistics

	Calculated	Observed	
t_n	% > C.L.	Fraction > C.L.	Percent > C.L.
0.000	50%	1419/2930	48.4%
0.674	25%	800/2930	27.3%
1.282	10%	290/2930	9.9%
1.645	5%	131/2930	4.5%

The precision of median mapped radon potentials (GSD=1.93) is considerably better than the total variation among indoor radon levels, and also is better than the partitioned estimates of either soil or house variations. This fact illustrates the advantage of defining soil radon potentials with the present approach. It also illustrates the higher uncertainties in trying to predict the indoor radon level in any particular house compared to the map prediction of the median level in the reference house for a given polygon.

Averaging the measured radon concentrations in Figure 5-4 by their map tier, as defined in Section 5.1, gives the geometric means and geometric standard deviations shown in Figure 5-5. As expected, the medians for each tier are close to the calculated line for the 50% confidence limit. These analyses illustrate the uncertainties in estimating actual indoor radon levels from soil radon potentials.

The mapped soil radon potentials represent the effects of different soils on the *reference* house. For the reference house, the annual-average indoor radon concentration in picocuries per liter (pCi L^{-1}) is approximately 1.3 times the soil radon potential (in mCi y^{-1}). Thus, soil-related radon in the reference house would average approximately 3.9 pCi L^{-1} in

an area with a radon potential of 3 mCi y^{-1}. Average radon concentrations in *actual* houses may differ from those in the reference house because they also depend on house and occupant characteristics. Important house properties include the ventilation and dilution of indoor air, the indoor air pressure, the foundation design and construction, and its susceptibility to radon penetration. Some of these properties also change with time, along with soil water distributions, to alter both the radon potential and its equivalent indoor radon concentration. The temporal variations preclude direct comparisons of indoor radon measurements with soil radon potentials without an adequate definition of long-term average values for all significant soil, house, and occupant parameters.

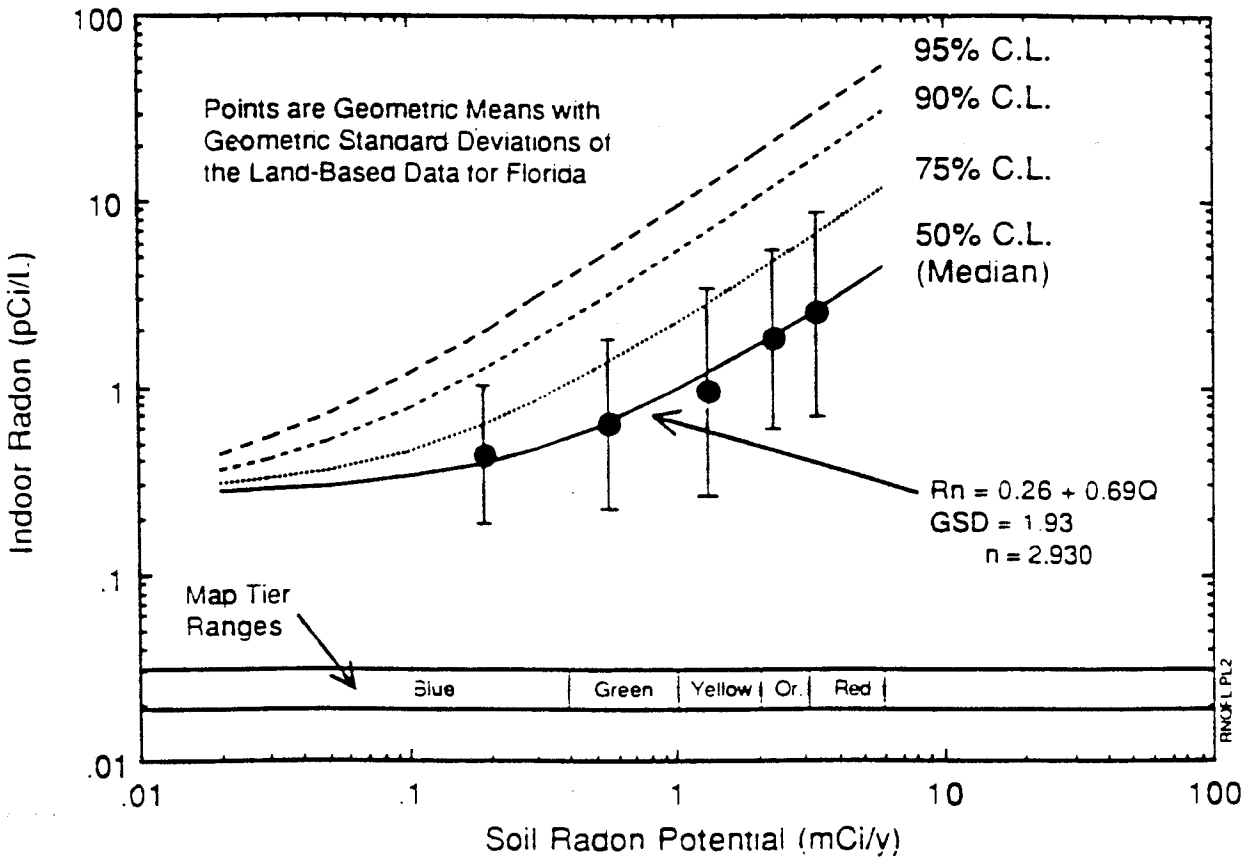

Figure 5-5. Comparison of tier-averaged indoor radon levels with mapped soil radon potentials.

Soil radon potentials, calculated from geometric mean radium concentrations, correspond to the median, or 50% confidence limit for individual locations in a polygon area. This means that

approximately half of the land area represented by a given polygon may have lower radon potentials and half may have higher potentials. Similar interpretations apply to the other maps (i.e., 95% of the land area in the 95% confidence limit map has expectedly lower radon potentials while 5% has higher potentials, etc.). The four maps together give a more complete picture of soil radon potentials than a single map.

The definition of areas that need radon-resistant building features and of areas that do not depends strongly on the margin of safety desired. Houses in areas with low soil radon potentials on all four maps are unlikely to have elevated radon levels. Conversely, houses in areas with high radon potentials on all four maps are very likely to have elevated radon levels. The 50% confidence limit map shows the most likely radon potential for a particular location. However, if an area has a low radon potential on the 50% confidence limit map and a high radon potential on the 95% confidence limit map, the area does not have a uniformly low radon potential. The area will contain both low radon potential and high radon potential sections. In such cases, the four maps help estimate the chances of a particular location having a radon potential that is within the illustrated limits. Housing development in these areas should consider the potential for elevated radon, and possibly increase the level of radon surveillance, incorporate radon-resistant construction features, or take other appropriate precautions.

Differences between actual houses and the reference house will alter the potential radon entry rate for a given soil profile. They also will alter its conversion to an indoor radon concentration, as in equation (31). For example, if house variations are log-normally distributed with a geometric standard deviation of 3.0, approximately 16 percent of the houses in a map unit with a radon potential of 3 mCi y^{-1} would be expected to exceed a radon potential of 9 mCi y^{-1} (corresponding to nearly 12 pCi L^{-1} in the reference house). Additionally, approximately 2.3 percent would be expected to exceed 27 mCi y^{-1} (corresponding to over 35 pCi L^{-1} in the reference house). The same percentages applied to a map unit with a radon potential of 0.3 mCi y^{-1} would indicate lower radon potentials and soil-related concentrations by approximately a factor of ten.

Interpretations of the soil radon potential maps should also recognize other sources of uncertainty. These sources include the extrapolation of NURE data to undefined map polygons, averaging from limited sample analyses to represent geologic radium sources, representing radon map polygons primarily by the STATSGO soil maps, and estimating seasonal water table depths from high water table data. The maps

have the advantage of being independent of particular sets of indoor radon data, however, and therefore they avoid house and occupant variables and biased sampling associated with empirical data sets. Because of the higher uncertainties associated with predicting the upper confidence limits, the median (50% confidence limit) radon potentials should be regarded as more reliable, with progressively greater uncertainty associated with the values computed for higher confidence limits.

Boundaries between map units should be considered approximate because of the gradational nature of many lithologic and geologic contacts, and because of the imprecisions in defining their locations. Although the STATSGO soils map constitutes the most widely available geographic basis for defining soil radon potentials, further variations are inherent within map units. The boundaries between colored map tiers are based on arbitrary cuts at the indicated values of radon potential. The colored zone boundaries therefore could change simply with different tier grouping of the calculated radon potentials into more, less, or different groups. Use of the numerical radon potentials associated with each polygon avoids the tier definition uncertainties.

Section 6
STATE-WIDE VALIDATION OF THE RADON MAPS

There is no cost-effective protocol to directly measure soil radon potentials. The soil radon potential maps were therefore validated on a state-wide basis by comparisons with two surrogates: soil radon flux measurements and indoor radon concentration measurements. The soil radon flux measurements hold the potential to better validate the calculated soil radon potentials because they eliminate the variables associated with house construction and occupancy. However, their advantage is largely offset by large spatial variations and a sensitivity to soil moisture that increases temporal variations. Indoor radon measurements are attractive because they better represent annual-average indoor radon concentrations, which are the parameter of ultimate interest in using the radon maps. However, the indoor radon data may vary from map-calculated values because of differences in house construction and occupancy characteristics compared to the map reference house. Because both radon flux measurements and indoor radon measurements represent only a 1-3 day period, they both introduce uncertainty when used to represent annual-average conditions. Despite the differences between the mapped soil radon potentials and the surrogates, the surrogates provide the best available basis for validating the radon maps.

6.1 STATE-WIDE COMPARISONS WITH RADON FLUX MEASUREMENTS

The RnMAP calculations of soil radon potential included a corresponding calculation of bare-soil radon flux (as shown in Appendix B). For initial validation comparisons, the radon fluxes calculated by RnMAP were compared with radon flux measurements made throughout the state. The radon flux measurements were distributed to include at least several locations in each Florida county. After the initial feasibility measurements in Alachua County, flux measurement sites were selected from criteria that included accessibility, gamma-ray intensity, and calculated radon potentials. Where possible, locations were selected from proximate high-radon-potential and low-radon-potential polygons. A survey of five gamma-ray measurements were then made at 1-m elevations in different

regions of the polygon using a 5 cm x 5 cm scintillation detector (Model 44-10, Ludlum Measurements, Inc., Sweetwater, TX). The location with the highest gamma measurement was used for the radon flux measurements.

Triplicate measurements were made at each location at 10-meter intervals to characterize local site variability, and also to provide backup in the event that any individual samplers were disturbed. The gamma-ray activity and soil moisture content also were measured at the flux measurement sites. Site locations (longitude and latitude) were determined at the time of sampling with a global positioning system (NAV-5000D, Magellan Systems Corp., San Dimas, CA). The locations were later analyzed by the University of Florida GeoPlan Center to confirm which map polygon contained the sampling site.

The protocol for measuring soil radon fluxes is presented in Appendix K, along with supporting quality assurance data on field blanks and duplicate measurements. A total of 1,041 radon flux measurements were performed at 330 unique locations. These site locations covered all 67 counties in Florida. The exact locations and results of the radon flux measurements are presented in Appendix K. Figure 6-1 illustrates the locations of the flux measurement sites. As illustrated, more emphasis was placed on sampling in areas where the calculated radon potential was high or highly variable.

Temporal variations in radon flux were examined in addition to the spatial sampling at the 330 locations by repeating measurements at one site during different seasons of a 17-month period in 1993-94. The site for the repeated measurements was near the FRRP test cell structures at the Florida Institute of Phosphate Research in Bartow. The measurements at this site included individual samples at seven different points around the test cells. Measurements were made at the same point in each set. The results of these measurements are summarized in Table 6-1. The geometric standard deviations among the replicate measurements at each of the seven measurement points were averaged to estimate a time-dependent GSD among the radon fluxes of 1.6.

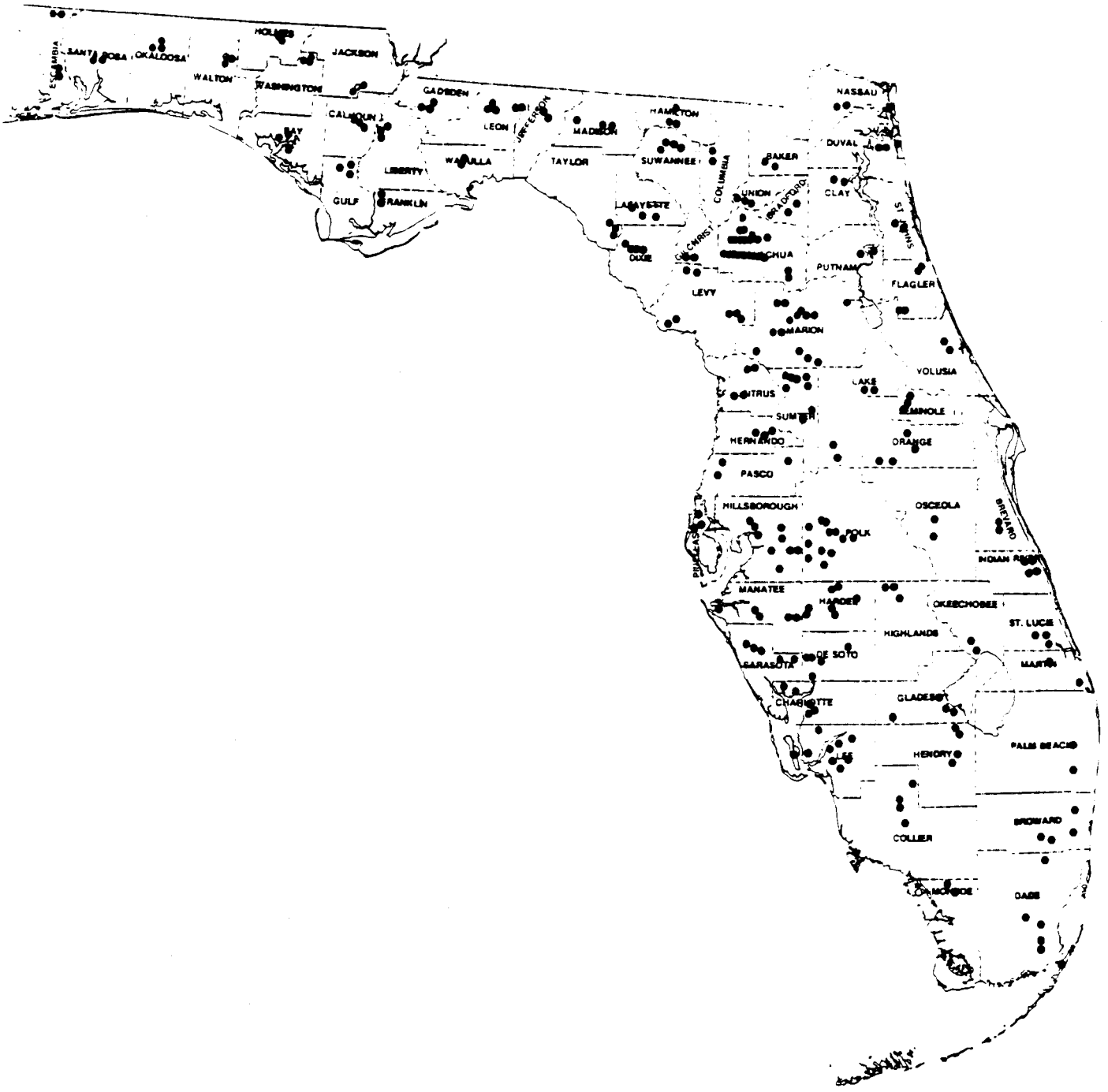

Figure 6-1. Illustration of radon flux sampling locations.

Table 6-1. Radon Flux Measurements Near the FRRP Test Cells in Bartow.

	Soil Radon Flux ($pCi\ m^{-2}\ s^{-1}$)						
Location	3/16/93	6/2/93	10/21/93	2/11/94	6/12/94	8/4/94	GSD
NW	2.3	2.9	2.1	2.7	4.4	0.9	1.7
W	6.1	4.2	6.0	3.4	---[a]	3.5	1.5
SW	5.4	3.4	3.6	4.1	6.4	3.6	1.4
C	4.5	5.6	6.5	3.5	5.2	4.0	1.3
NE	0.6	2.3	1.4	1.7	---[a]	0.7	1.8
E	1.6	7.9	12.5	4.6	---[a]	4.0	2.2
SE	4.3	7.9	9.4	4.8	15.0	14.4	1.7
						Average:	1.6

[a]Not measured.

Considering the temporal variations, site variations (from gamma-ray and replicate flux measurements), and polygon variations in soil radon potential (Table C-1), the measured radon fluxes were compared to the mapped soil radon potentials. Figure 6-2 illustrates this comparison in terms of a bias statistic between the measured and mapped soil radon fluxes. The bias statistic is defined as:

$$Z = [\ln(\text{Meas}) - \ln(\text{Map})] / \sqrt{(\ln G_{Meas})^2 + (\ln G_{Map})^2} \tag{34}$$

where Z = measurement-map bias statistic (standard deviations)

Meas = value of the measured parameter (point in time)

Map = value of the mapped parameter (annual average basis)

G_{Meas} = uncertainty (GSD) in representing annual average by the measured value

G_{Map} = uncertainty (GSD) of the mapped value.

The estimate of G_{Meas} was calculated to include both temporal and spatial uncertainties as:

$$G_{Meas} = \exp[\sqrt{\Sigma_i(\ln G_i)^2}\ ] \tag{35}$$

where G_i = GSD of component i.

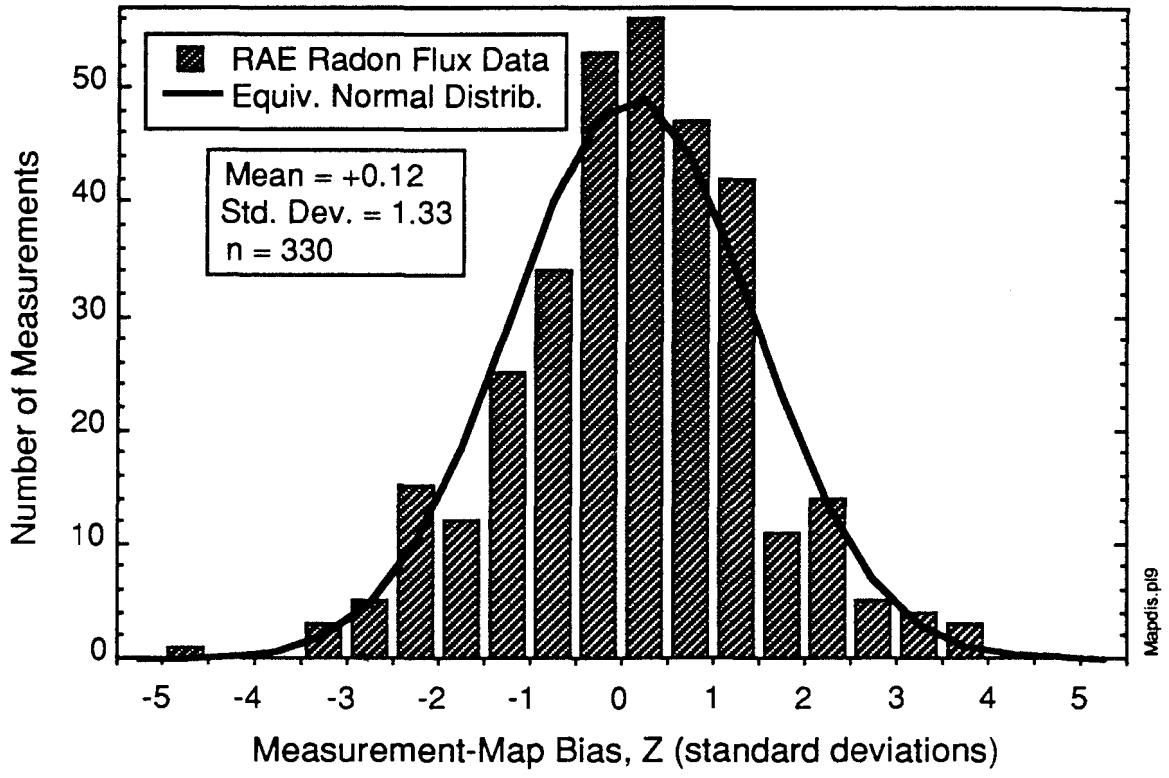

Figure 6-2. Distribution of bias statistics for the radon flux measurements.

The distribution of the bias statistics computed from equation (34) for the measured and mapped radon flux comparisons is illustrated in Figure 6-2. The distribution averaged 0.12, indicating minimal average bias for the overall data set. The standard deviation of the distribution was 1.33, indicating more scatter in the radon flux measurements than was predicted from the radon potential map calculations. With the excess scatter, 16 measurements (4.8%) were below the central 95% range of the distribution, and 18 measurements (5.5%) were above it, compared to 8 measurements (2.5%) expected for each. The extra scatter is attributed primarily to the temporal variations in radon flux, since short-term (24 h) radon fluxes are being compared to annual-average fluxes from the map calculations.

6.2 STATE-WIDE VALIDATION WITH INDOOR RADON DATA SETS

The soil radon potential maps were validated on a general, state-wide basis by comparisons of their predictions for radon in the reference house to radon levels observed in actual houses. Three data sets were used for these validations, all of which were based on short-term charcoal canister measurements of indoor radon. The first, and most representative was the Geomet land-based data set (Nag87), which contained 2,952 radon measurements covering all 67 Florida counties. The second data set was the Geomet population-based data set (Nag87), which contained 2,095 radon measurements in 57 counties. The third data set was the Florida Health and Rehabilitative Services (HRS) residential data set (Form 1750 data), which contained 3,991 radon measurements in 49 counties.

The distributions of measurements by county are shown in Figures 6-3 through 6-5 for the land-based, population-based, and HRS residential data sets, respectively. Their biases are compared in Figure 6-6, which shows the cumulative percentages of measurements in all Florida counties. A nearly-straight line would show the ideal case, in which each county has equal sample representation. Although all of the sets show some bias, the radon flux data and the Geomet land-based data sets have the least bias because they include at least some measurements in every county. The other sets have many more measurements in some counties, but leave many others unrepresented.

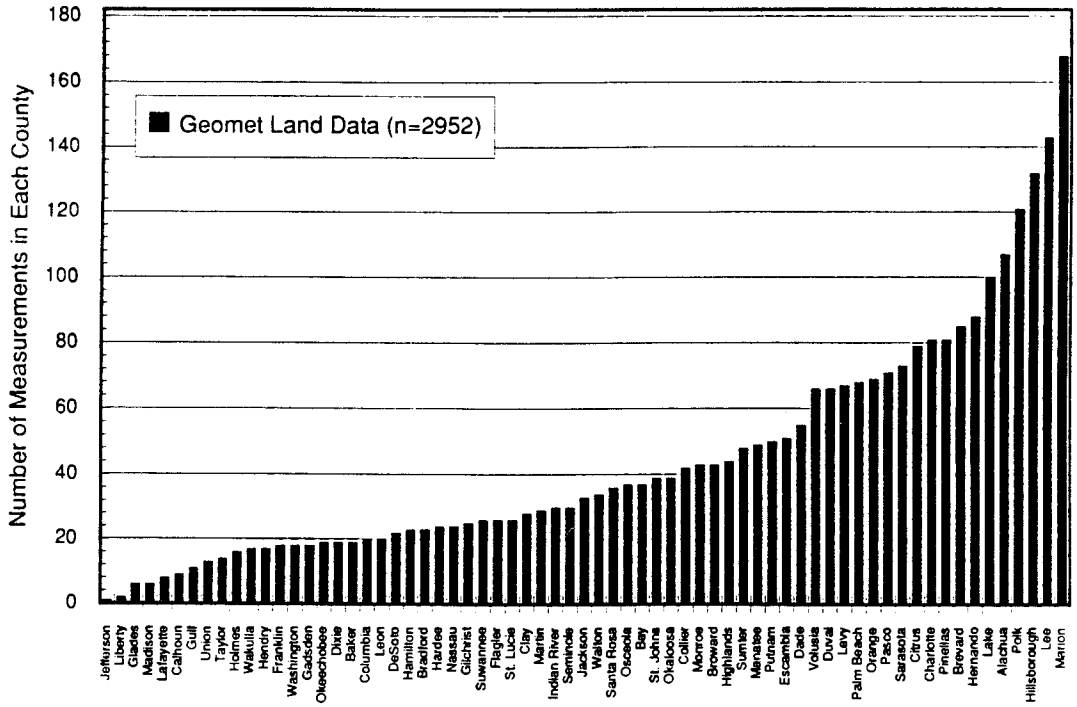

Figure 6-3. Distribution of Geomet land-based radon measurements by county.

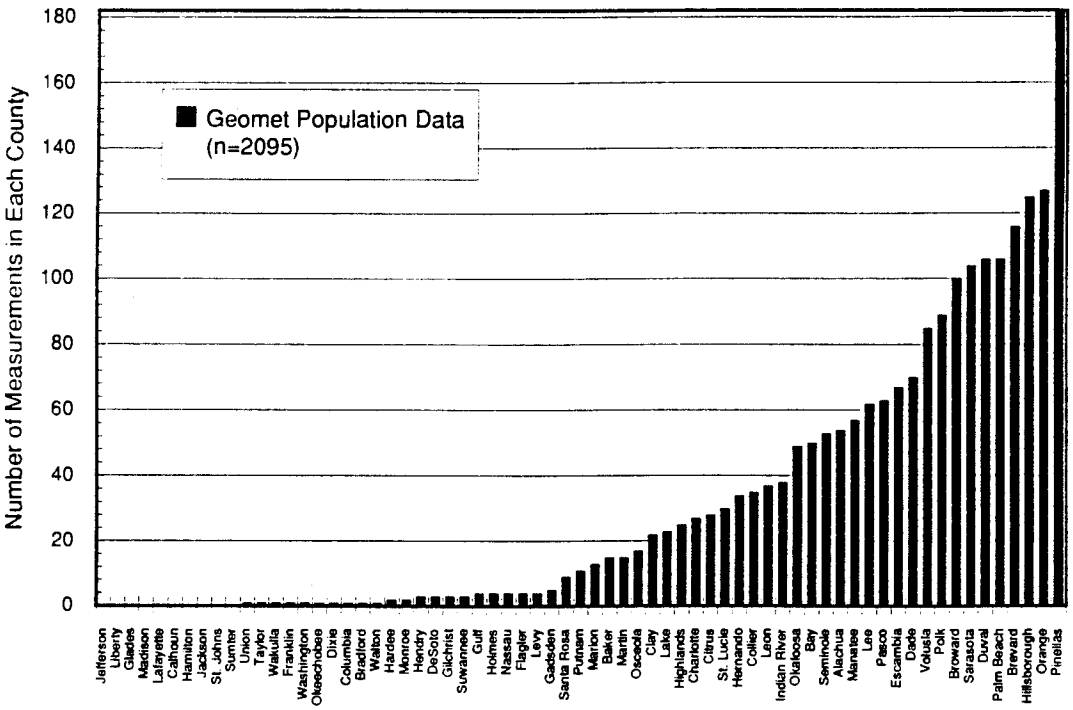

Figure 6-4. Distribution of Geomet population-based radon measurements by county.

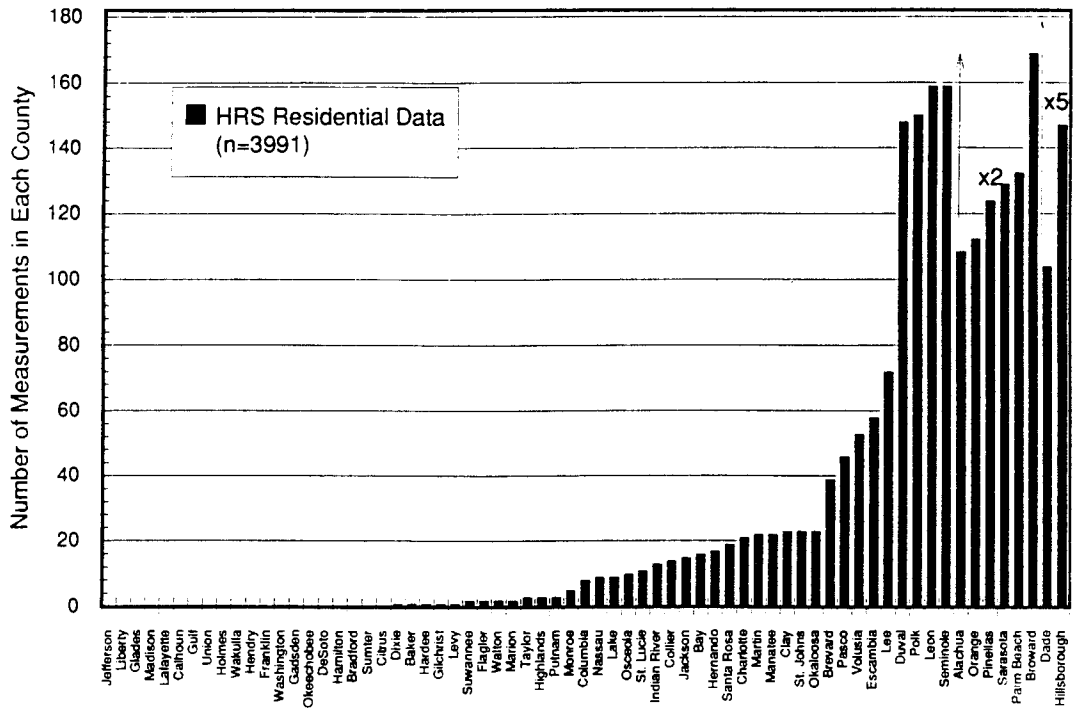

Figure 6-5. Distribution of HRS residential radon measurements by county.

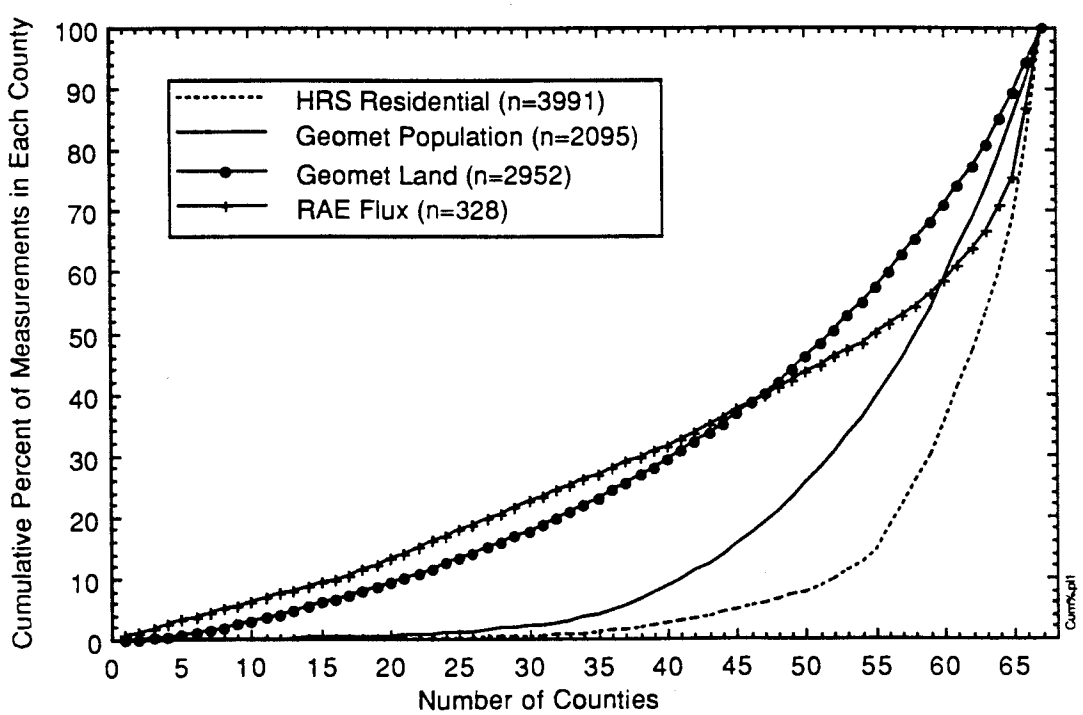

Figure 6-6. Comparison of radon data coverage of Florida counties by data set.

Radon measurements from the Geomet land-based and population-based data sets were compared directly with the numerical predictions for the reference house from the soil radon potential map data. The latitude and longitude associated with each measurement point were associated with their corresponding map polygon by the University of Florida GeoPlan Center using a GIS system. Each measurement was compared with the median annual-average indoor radon calculated for the reference house using C_{out}=0.1 pCi L^{-1} and x=1.3 pCi L^{-1} per mCi y^{-1} in equation (32). The comparison used the bias statistic defined by equation (34) with G_{meas} = 2.083 for the uncertainty in annual-average indoor radon when estimated from a single charcoal canister measurement (Roe90). The value of G_{map} was estimated from the median and 95% confidence limits of soil radon potential as $G_{map}=(Q_{95}/Q_{50})^{1/1.645}$.

The bias statistics calculated for each radon measurement are listed in Appendix L for the Geomet land-based data set, and in Appendix M for the Geomet population-based data set. The bias statistics were summarized on a state-wide basis for each data set by fitting to an equivalent normal distribution. The fitted distribution plot for the land-based data set is illustrated in Figure 6-7. The land-based data showed virtually no bias for the state-wide average, with a mean value of only $\bar{Z}$=-0.04 standard deviations. The standard deviation of the Z distribution was 0.99, compared to an ideal value of 1.00, indicating that the observed variations between measured and mapped values are almost exactly equal to the variations predicted from map and measurement uncertainties.

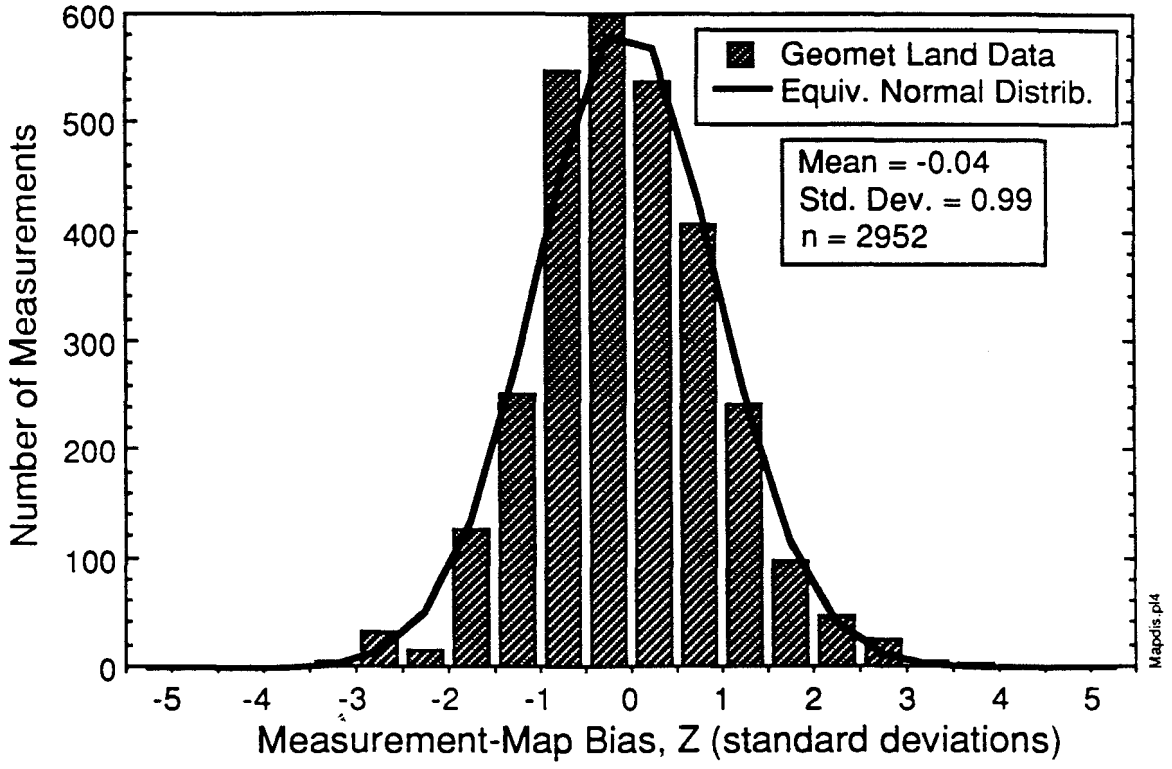

Figure 6-7. Distribution of bias statistics for the Geomet land-based indoor radon measurements.

A corresponding distribution plot of the bias statistics for the Geomet population-based data set is presented in Figure 6-8. The population-based data showed a negative bias of -0.42 standard deviations, indicating that for the state-wide average, the population-based measurements were slightly lower than the values predicted by the map for the reference house. The standard deviation of the Z distribution was 0.99, indicating that the observed variations between measured and mapped values were again almost exactly equal to the variations predicted from map and measurement uncertainties.

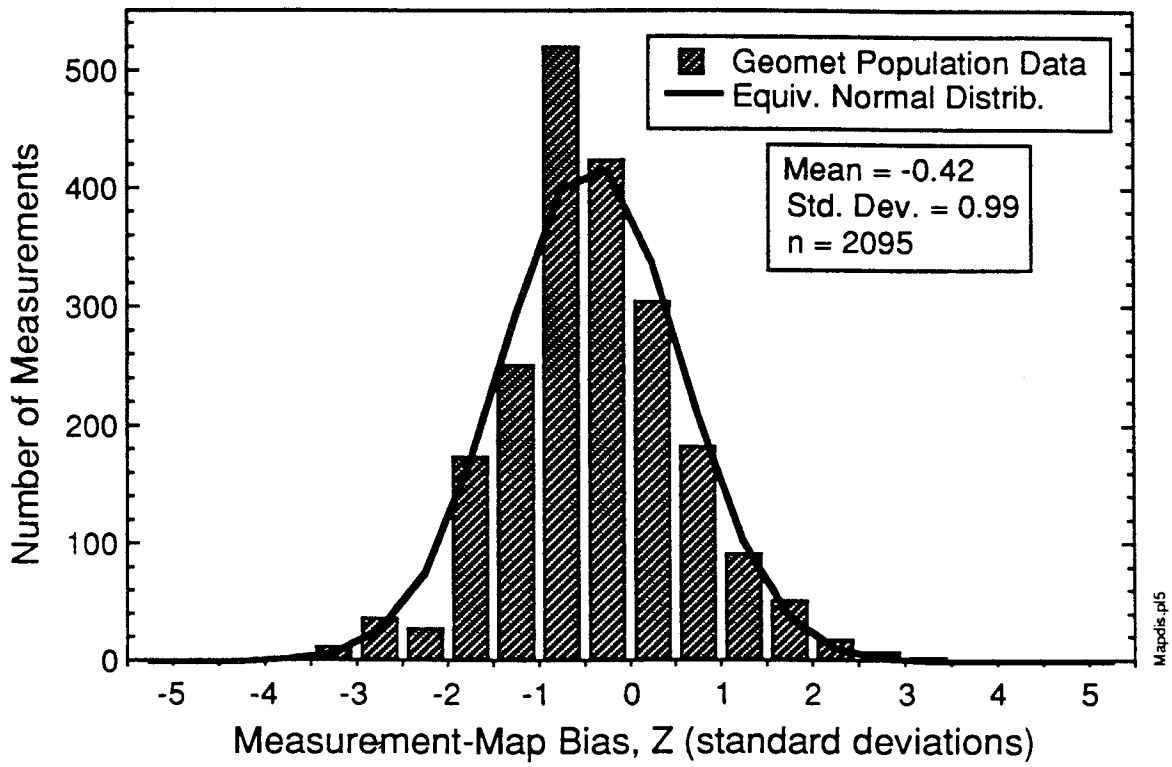

Figure 6-8. Distribution of bias statistics for the Geomet population-based indoor radon measurements.

Radon measurements in the HRS residential data set were listed by address rather than by map coordinates. They therefore could not be directly linked to a map polygon with the GIS system as was done for the Geomet data sets. Although address matching to map coordinates was performed by the U.F. GeoPlan Center for some of the data, it was not generally successful in rural areas or even in urban areas where long roads traverse more than one map polygon. An alternative approach therefore was used to compare the HRS data with map predictions. A digitized state-wide zip-code map was intersected with the radon polygon map to determine the percentages of each polygon that comprised each zip code. The resulting percentages then were used to compute the polygon-weighted average soil radon potentials for each zip code where HRS residential radon data were available. These averages were computed for both the median and 95% confidence limits as:

$$\bar{Q}_{50} = 0.01 \Sigma p_i Q_{50i} \quad (36)$$

$$\bar{Q}_{95} = 0.01 \Sigma p_i Q_{95i} \quad (37)$$

where $\bar{Q}_{50}$ = polygon-weighted average median radon potential for a zip code (mCi y^{-1})
$\bar{Q}_{95}$ = polygon-weighted average 95% C.L. radon potential for a zip code (mCi y^{-1})
p_i = percentage of polygon i in the zip code area.

Comparisons of each measurement in the HRS residential data set were then made with the average map predictions for their zip code area using $\bar{Q}_{50}$ in equation (32) with C_{out}=0.1 pCi L^{-1} and x=1.3 pCi L^{-1} per mCi y^{-1}. The comparisons are reported in Appendix N in terms of the bias statistic defined by equation (34). The uncertainties for use in equation (34) were defined as with the Geomet data sets as G_{meas}=2.083 and $G_{map}=(\bar{Q}_{95}/\bar{Q}_{50})^{1/1.645}$.

The bias statistics calculated for each radon measurement are listed in Appendix N for the HRS residential data set. The statistics were summarized on a state-wide basis by fitting to an equivalent normal distribution. The fitted distribution plot for the HRS residential data set is illustrated in Figure 6-9. The HRS residential data showed a state-wide average positive bias of $\bar{Z}$=0.51 standard deviations. The standard deviation of the Z distribution was 0.96, compared to an ideal value of 1.00, indicating once again that the observed variations between measured and mapped values are nearly equal to the variations predicted from map and measurement uncertainties.

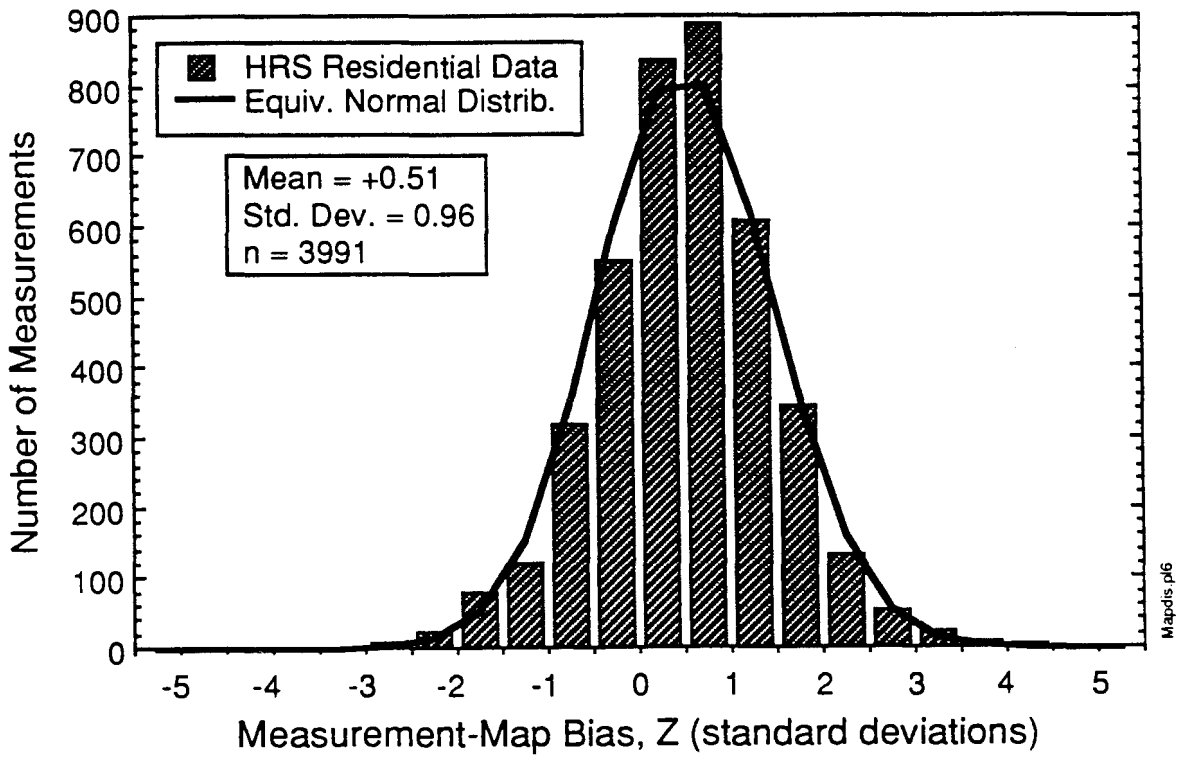

Figure 6-9. Distribution of bias statistics for the HRS residential indoor radon measurements.

6.3 EXAMINATION OF INDOOR RADON ANOMALIES

Indoor radon anomalies are difficult to positively identify because they can not be individually distinguished from the small percentage of houses that are statistically expected to have poor agreement between measurements and map predictions. The approach used here to search for indoor radon anomalies was to calculate from the bias statistics the number of houses expected to exceed a prescribed limit, and then to compare the actual number of houses exceeding the limit with the expected value. If the actual numbers of houses outside the limits significantly exceeds the expected number, then the excess number may constitute an anomaly if all the houses above the limit correspond to the reference house used in developing the radon map. If the potentially anomalous houses have features that

could otherwise explain their disagreement with the map, however, they may not necessarily constitute an anomaly.

The search for possible indoor radon anomalies was conducted on a state-wide basis using all three of the indoor radon data sets. Houses with very large positive or negative Z statistics were flagged as *potential* anomalies, and their locations were compiled from their map coordinates or, in the case of the HRS residential data, from their zip codes. Where the potential anomalies occurred in regional clusters, the houses were investigated by drive-by observations. The observations included building type (single-family detached vs. large building), floor type (slab-on-grade vs. crawl space), wall construction (frame, concrete block, brick, etc.), soil surface gamma-ray intensity, and other pertinent features (such as number of stories, terrain slope, evidence of basements, vents from crawl spaces, fireplace vents, and approximate age). In some regions, the gamma activity near concrete and aggregate materials was also observed, and samples were analyzed to characterize materials of interest.

The house investigations utilized a global positioning system (NAV-5000D, Magellan Systems Corp., San Dimas, CA) to locate houses from map coordinates in the Geomet data sets, and street addresses to locate houses in the HRS data sets. The latitude and longitude coordinates of the HRS houses were also determined with the global positioning system during the house investigations to permit a positive identification of the map polygon where the house was located. To maintain the anonymity and privacy of the data and house occupants, no contacts were made with house occupants, no addresses from the Geomet data sets were recorded, and all observations were made from an automobile during an approximate 1-minute curb-side period, during which a 0.5-minute gamma-ray measurement was made over an exposed soil or sod surface. The gamma-ray measurements utilized a 5 cm x 5 cm scintillation detector (Model 44-10, Ludlum Measurements, Inc., Sweetwater, TX).

Houses were flagged as *potential* anomalies for on-site investigation in two stages. Initially, measurement uncertainties were ignored (G_{meas}=0), and Z statistics calculated by equation (34) were flagged and investigated as potential anomalies if they were below -3 or above +3. After the magnitude of G_{meas} was identified (from Roe90), all of the Z statistics were re-calculated using G_{meas}=2.08 in equation (34), and the potential anomalies were re-

flagged using a $|Z|>1.96$ criterion to define a central range that should contain 95% of the observations. The latter criterion included many additional houses, but in some cases excluded houses that had already been investigated. For completeness, all houses that were investigated are listed in Appendix O with their final Z statistic that includes measurement uncertainty.

The numbers of houses flagged in each of the data sets as potential anomalies are listed in Table 6-2 for comparison with the number of houses expected to randomly vary beyond the $|Z|=1.96$ limit that should include the central 95% of the data. The Geomet land-based data set, which is the most representative and least biased of the sets, shows slightly less than the expected number of random negative anomalies (1.9% vs. 2.5%), and slightly more than the expected number of random positive anomalies (2.7% vs. 2.5%). Compared to the expected numbers of measurements above and below the central 95% range, the observed numbers of potential anomalies are not significantly different from the random variations.

Table 6-2. Statistical Summary of State-Wide Radon Map Validations

Data Set	No. of Comparisons	Potential Negative Anomalies		Potential Positive Anomalies	
		Number	Percent	Number	Percent
Expected:			2.5%		2.5%
Observed:					
Geomet Land-Based Data	2,952	56	1.9%	80	2.7%
Geomet Population-Based Data	2,095	84	4.0%	31	1.5%
HRS Residential Data	3,991	32	0.8%	235	5.9%
HRS Residential Data Excluding Large Buildings	3,938	28	0.7%	185	4.7%

The population-based data set showed a total of 115 measurements outside the expected central 95% range, compared to 105 expected from random variations. This difference is not significant. However, because of the bias noted for this set, most of the measurements outside the central range are on the low side, contributing to a significant excess of potential negative anomalies. Whether or not the excess number of low measurements is caused by actual low-radon anomalies depends on how many of the houses have significant mitigating features that cause them to be more radon resistant than the reference house.

The HRS residential data showed a total of 267 measurements outside the expected central 95% range, compared to 200 expected from random variations. This difference is significant. However, when 53 of the measurements are removed from the comparison because they were observed to come from large buildings instead of detached houses, the number of measurements outside the central 95% range drops to 213. This number is not significantly different from the 200 expected from random variations. The 53 observations removed were among the potential anomalies given follow-up investigation (Appendix O). It is possible that even more large buildings are among the other potential anomalies listed in Appendix O that were not investigated, and that the comparison could become even closer. However, because of the bias noted for this data set, most of the measurements outside the central range are on the high side, contributing to a significant excess of potential positive anomalies. Whether or not the excess number of high measurements is caused by actual high-radon anomalies depends on how many of the houses have significant radon entry routes that cause them to be less radon resistant than the reference house.

In selected regions where potential anomalies were investigated, the gamma-ray activity near concrete and aggregate materials was also observed. Samples were collected for radium and emanation measurements at some of these sites. The results of these observations are listed in Table 6-3. The measurements for the Lee County area suggest higher radium levels in the aggregates and concretes than were observed at the sites in the other two counties. Simple model analyses suggest that this magnitude of radium elevation in concrete could cause incremental increases in indoor radon on the order of 1-2 pCi L^{-1}. In

houses that would otherwise be just under the 4 pCi L^{-1} standard, this increase could cause them to exceed it.

Table 6-3. Gamma-Ray and Radon Measurements of Concretes and Aggregates.

County	Longitude	Latitude	Material	Gamma (uR h^{-1})	Radium (pCi g^{-1})	Emanation (%)
Dade	80°29.211'	25°41.387'	Aggregate	8.7	1.7	1.5
Dade	80°21.633'	25°54.772'	Aggregate	6.3	---[a]	---[a]
Dade	80°22.096'	25°52.159'	Aggregate	5.3	---[a]	---[a]
Dade	80°23.999'	25°46.914'	Aggregate	5.9	---[a]	---[a]
Dade	80°29.216'	25°42.452'	Aggregate	5.7	---[a]	---[a]
Dade	80°24.863'	25°37.883'	Aggregate	4.1	---[a]	---[a]
Lee	81°49.180'	26°29.477'	Concrete	---[b]	4.0	15.5
Lee	81°49.180'	26°29.535'	Concrete	11.6	3.8	3.7
Lee	81°49.180'	26°29.477'	Aggregate	18.2	3.8	4.7
Lee	81°41.658'	26°29.857'	Aggregate	14.5	5.0	4.0
Lee	81°49.519'	26°29.787'	Aggregate	17.4	5.1	3.5
Lee	81°45.592'	26°29.457'	Aggregate	14.8	3.1	4.5
Sumter	82°00.477'	28°39.037'	Aggregate	6.8	1.5	10.1

[a]Not sampled for analysis.
[b]Not measured

Analyses of the slab and wall construction details observed for the potential anomalies in Table O-1 suggests some significant aggravating and mitigating trends may be present in the potential anomaly houses that were investigated. For example, analyses of the 80 houses investigated from the Geomet land-based data set (Fig. 6-10) showed that houses above the 95% mid-range were about four times more likely to use slab-on-grade construction than to have crawl spaces, while the opposite trend was seen for houses below the mid-range. Similarly, houses above the 95% mid-range were over 40% more likely to use hollow-block wall construction than frame walls, while the opposite trend was seen for houses below the mid-range. These trends are consistent with model predictions, which show that crawl spaces dilute sub-floor radon before it enters houses, and that hollow-block exterior walls may provide channels for enhanced soil gas entry.

Similar slab and wall construction trends were observed for the other data sets. When aggregated, all 251 of the houses from the land-based, population-based, and HRS residential data sets in Appendix O showed almost identical trends, as illustrated in Fig. 6-11. In this case, houses above the 95% mid-range were nearly three times more likely to use slab-on-grade construction than to have crawl spaces, while the opposite trend was seen for houses below the mid-range. Similarly, houses above the 95% mid-range were 50% more likely to use hollow-block wall construction than frame walls, while the opposite trend was seen for houses below the mid-range. These state-wide trends are sufficient to explain the potential anomalies that are combined with the expected random measurements that fall outside the central 95% range.

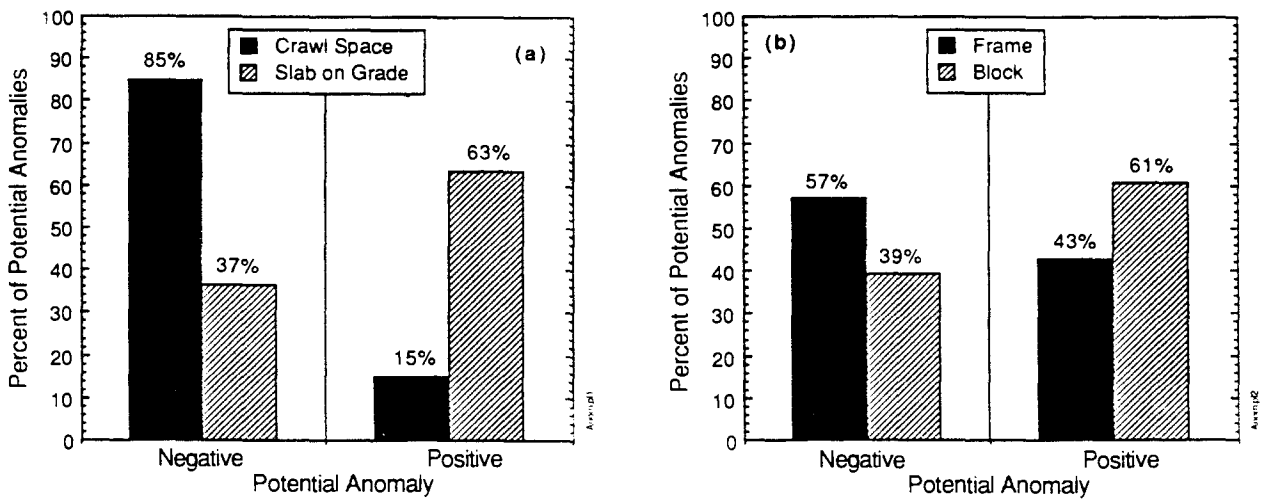

Figure 6-10. Comparison of floor (a) and wall (b) construction features in potentially anomalous houses in the 80 cases investigated from the Geomet land-based data set.

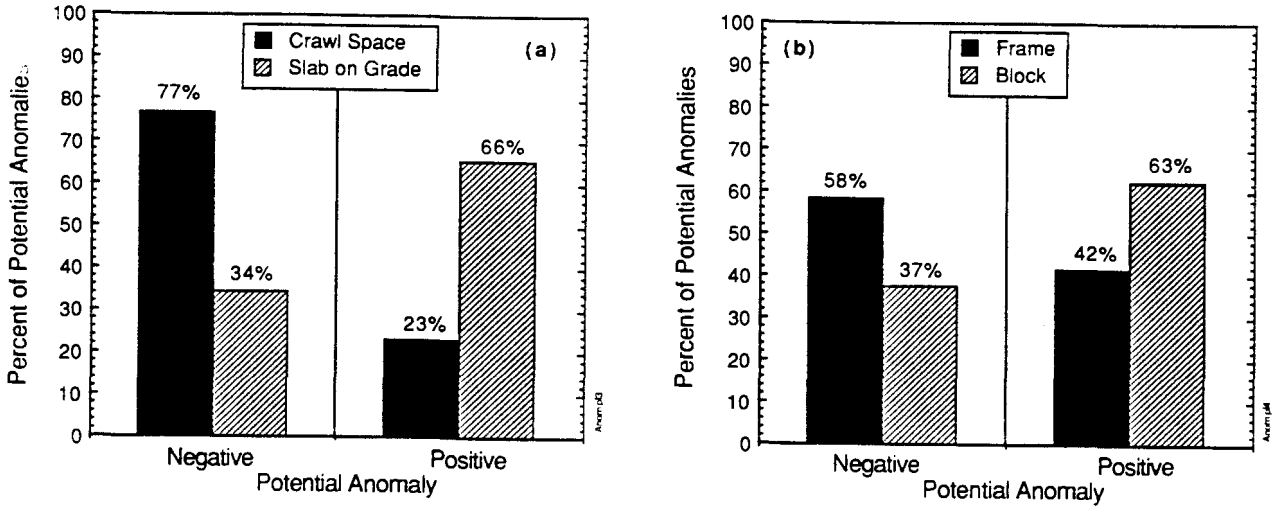

Figure 6-11. Comparison of floor (a) and wall (b) construction features in potentially anomalous houses in the 251 cases investigated from the land-based, population-based, and HRS residential data sets.

6.4 MAP VALIDATION SUMMARY

The maps were validated by state-wide comparisons with over a thousand soil radon flux measurements at 330 locations and with 9,038 indoor radon measurements from three different data sets. The radon flux measurements averaged similar to the map predictions, but were scattered more widely than the map data (16 below and 18 above the central 95% range, compared to eight expected for each). The difference in scatter is caused by inadequate definition of the temporal variations in radon flux that are needed for comparing the 24-hour flux measurements to annual-average calculated values.

The Geomet land-based data set best represents all regions of Florida and agrees very well with the map predictions. The middle 95% of the map range included 95.4% of the 2,952 measurements, with 1.9% below and 2.7% above the mid-range, compared to 2.5% expected for each. The HRS residential and Geomet population data sets do not represent all regions

in Florida, but they were compared with the map predictions anyway. The 2,095 measurements in the Geomet population-based set averaged slightly lower than map values, while the 3,938 measurements in the HRS residential data set averaged slightly higher than map values.

Over 250 houses with the greatest differences between measured and predicted indoor radon concentrations were investigated and found to show trends that offer further explanations. Houses above the 95% mid-range were nearly three times more likely to use slab-on-grade construction than to have crawl spaces, while the opposite trend was seen for houses below the mid-range. Similarly, houses above the 95% mid-range were about 50% more likely to use hollow-block construction than frame construction, and the opposite trend was also seen for houses below the mid-range. These trends are consistent with model predictions, and account for potential anomalies on a state-wide level. Considering the variations in both measurements and map calculations, the measurements give excellent overall state-wide validation of the radon maps.

Section 7

LITERATURE REFERENCES

Acr90 Acres. Measurement of Crack and Opening Contribution to Radon Entry (Feasibility Study). Vol. III of Radon Entry Through Cracks in Slabs-on-Grade, Acres International Corp., report *PO9314,* 1990.

Aus78 Austin, S.R. and Droullard, R.F., Radon Emanation From Domestic Uranium Ores Determined by Modifications of the Closed-Can, Gamma-Only Assay Method. Washington D.C.: U.S. Department of the Interior, Bureau of Mines; *Report of Investigations 8264*, 1978.

Bar76 Barakat, R., Sums of Independent Lognormally Distributed Random Variables, *Journal of the Optical Society of America* **66**: 211-216, 1976.

Bre90 Brennan, T., Clarkin, M., Osborne, M.C., and Brodhead, B., Evaluation of Radon Resistant New Construction Techniques. in Proceedings: the 1990 International Symposium on Radon and Radon Reduction Technology, Vol. 2, *EPA/600/9-91/026b* (NTIS PB91-234450), VIII-1, 1991.

Cla91 Clarkin, M., and Brennan, T., Radon Resistant Construction Techniques for New Residential Construction. Washington D. C.: U. S. Environmental Protection Agency report *EPA/625/2-91/032*, 1991.

Coh86 Cohen, B.L., A National Survey of ^{222}Rn in U. S. Homes and Correlating Factors. *Health Physics* **51**:175-183; 1986.

Cum92 Cummings, J.B., Tooley, J.J., and Moyer, N., Radon Pressure Differential Project, Phase I, FRRP, U. S. Environmental Protection Agency report *EPA-600-R92-008* (NTIS PB92-148519), January 1992.

Dev87 Devore, J.L., *Probability and Statistics for Engineering and the Sciences*, 2nd edition, Monterey, CA: Brooks/Cole Publishing Company, 1987.

EGG81 E G & G Geometrics, Aerial Gamma Ray and Magnetic Survey, Gainesville and Daytona Beach Quadrangles Florida. Grand Junction, CO: U. S. Department of Energy Report *GJBX-101*, March 1981.

EPA86 Environmental Protection Agency, Radon Reduction Techniques for Detached Houses, Technical Guidance. U.S. Environmental Protection Agency, Air and Energy Engineering Research Laboratory report *EPA/625/5-86/019*, 1986.

EPA92a Environmental Protection Agency, Technical Support Document for the 1992 Citizen's Guide to Radon. Washington D.C.: Office of Air and Radiation report *EPA-400-R-92-011* (NTIS PB92-218395), May 1992.

EPA92b Environmental Protection Agency, National Residential Radon Survey Summary Report Washington D.C.: Office of Air and Radiation report EPA-402/R-92-011, October 1992.

Fin89 Findlay, W.O., Robertson, A., and Scott, A.G., Testing of Indoor Radon Reduction Techniques in Central Ohio Houses: Phase 1 (Winter 1987-88). U. S. Environmental Protection Agency, report *EPA/600/8-89/071* (NTIS PB89-219984), July 1989.

Gil93 Gilbert, R.O., personal communication, Richland, WA: Battelle Pacific Northwest Laboratory, 1993.

Has75 Hastings, N.A.J. and Peacock, J.B., *Statistical Distributions*, New York: John Wiley & Sons, 1975.

Lou87 Loureiro, C.O., Simulation of the Steady-State Transport of Radon from Soil into Houses with Basements under Constant Negative Pressure. Berkeley, CA: Lawrence Berkeley Laboratory report *LBL-24378*, 1987.

Lut79 Lutton, R.J., Regan, G.L., and Jones, L.W., Design and Construction of Covers for Solid Waste Landfills. Cincinnati OH: Municipal Environmental Research Laboratory report *EPA-600/2-79-165* (NTIS PB80-100381), 1979.

Mit68 Mitchell, R.L., Permanence of the Log-Normal Distribution, *Journal of the Optical Society of America* **58**: 1267-1272, 1968.

Mur90 Murane, D.M., Model Standards and Techniques for Controlling Radon Levels Within New Buildings. in Proceedings: the 1990 International Symposium on Radon and Radon Reduction Technology. Vol. 3, *EPA/600/9-91/026c* (NTIS PB91-234468), A-I-2, 1991.

Nag87 Nagda, N.L., Koontz, M.D., Fortmann, R.C., Schoenborn, W.A., and Mehegan, L.L., Florida Statewide Radiation Study. Germantown, MD: Geomet Technologies Inc. report *IE-1808*; 1987.

Nat66 Natrella, M.G., *Experimental Statistics*, Washington D.C.: U.S. Department of Commerce, National Bureau of Standards *Handbook 91*, 1966.

Naz87 Nazaroff, W.W., Lewis, S.R., Doyle, S.M., Moed, B.A., and Nero, A.V., Experiments on Pollutant Transport from Soil into Residential Basements by Pressure-Driven Airflow. *Environmental Science and Technology* **21**:459-466, 1987.

Naz88 Nazaroff, W.W., Doyle, S.M., Nero, A.V., and Sextro, R.G., Radon Entry via Potable Water. pp. 131-157 in: *Radon and Its Decay Products in Indoor Air*, W. W. Nazaroff and A. V.Nero, eds., New York: Wiley & Sons, 1988.

Naz89 Nazaroff, W.W. and Sextro, R.G., Technique for Measuring the Indoor ^{222}Rn Source Potential of Soil, *Environmental Science and Technology* **23**:451-458, 1989.

Ner88 Nero, A.V., Radon and Its Decay Products in Indoor Air: An Overview, in *Radon and Its Decay Products in Indoor Air*, W.W. Nazaroff and A.V. Nero, eds., p. 1-53, New York: John Wiley and Sons, 1988.

Nie82 Nielson, K.K., Rogers, V.C., Mauch, M.L., Hartley, J.N., and Freeman, H.D., Radon Emanation Characteristics of Uranium Mill Tailings, in: *Uranium Mill Tailings Management - V*, Ft. Collins, CO: Colorado State Univ., 355-367, 1982.

Nie84 Nielson, K.K., Rogers, V.C., and Gee, G.W., Diffusion of Radon Through Soils: A Pore Distribution Model. *Soil Science Society of America Journal* **48**:482-487, 1984

Nie91a Nielson, K.K. and Rogers, V.C., Feasibility and Approach for Mapping Radon Potentials in Florida. Florida Radon Research Program. Research Triangle Park, NC: U. S. Environmental Protection Agency report *EPA-600/8-91-046* (NTIS PB91-217372), July 1991.

Nie91b Nielson, K.K. and Rogers, V.C., Proceedings of the Workshop on Radon Potential Mapping. Florida Radon Research Program. Research Triangle Park, NC: U. S. Environmental Protection Agency report *EPA-600/9-91-044* (NTIS PB92-115278),November 1991.

Nie91c Nielson, K.K. and Rogers, V.C., Development of a Prototype Map of the Soil Radon Potentials in Alachua County Florida, Salt Lake City, UT: Rogers & Associates Engineering Corp. *RAE-9127/3-1*, October 1991.

Nie91d Nielson, K.K. Rogers, V.C., and Rogers, V., Modeling Radon Generation, Transport, and Indoor Entry for Building Construction Standards, Salt Lake City, UT: Rogers & Associates Engineering Corp. *RAE-9127/3-2*, October 1991.

Nie92a Nielson, K.K. and Rogers, V.C., Radon Transport Properties of Soil Classes for Estimating Indoor Radon Entry. in: *Indoor Radon and Lung Cancer: Reality or Myth?*, F.T. Cross, ed., p. 357-372, 1992.

Nie92b Nielson, K.K., Rogers, V.C., Otton, J.K., Brown, R.B., and Harris, W.G., Soil Radon Potential Mapping and Validation for Central Florida. in Proceedings: the 1992 International Symposium on Radon and Radon Reduction Technology. Vol. 3, EPA/600/R-93-083c (NTIS PB93-196210), 1993.

Nie94a Nielson, K.K., Rogers, V.C., Rogers, V., and Holt, R. B. The RAETRAD Model of Radon Gas Generation, Transport,and Indoor Entry, EPA-600/R-94-198 (NTIS PB95-142030), November 1994.

Nie94b Nielson, K.K., Holt, R.B., and Rogers, V.C., Soil Radon Potential Mapping of Twelve Counties in North-Central Florida, EPA/600-R-94-218 (NTIS PB95-159869), December 1994.

Nit89 Nitschke, I., Radon Reduction and Radon Resistant Construction Demonstrations in New York. U. S. Environmental Protection Agency, Air and Energy Engineering Research Laboratory report *EPA/600/8-89/001* (NTIS PB89-151476), 1989.

Nue90 Nuess, M., and Price, S., Public Policy Considerations and the Development of a Code for the Control of Radon in Residences. in Proceedings: the 1990 International Symposium on Radon and Radon Reduction Technology, Vol. 1, *EPA/600/9-91/026a* (NTIS PB91-234443), I-4, 1991.

Osb88 Osborne, M.C., Radon-Resistant Residential New Construction. U. S. Environmental Protection Agency, Air and Energy Engineering Research Laboratory report *EPA/600/8-88/087* (NTIS PB90-274119), 1988.

Pea90 Peake, R. T., Gundersen, L. C. S., Schumann, R. R., James, J., and Ronca-Batista, M., Determination of Radon Geologic Provinces in the United States, in proceedings: the 1990 International Symposium on Radon and Radon Reduction Technology. Vol. 3, EPA/600/9-91/026c (NTIS PB91-234450), C-VI-1, February 1991.

Rev91 Revzan, K.L., Fisk. W.J., and Gadgil, A.J., Modeling Radon Entry Into Houses with Basements: Model Description and Verification, in Indoor Air, Vol.2, pp. 173-190, 1991.

Roe90 Roessler, C.E., Revell, J.W., and Wen, M.J., Temporal Patterns of Indoor Radon in North Central Florida and Comparison of Short-Term Monitoring to Long-Term Averages. in Proceedings: the 1990 International Symposium on Radon and Radon Reduction Technology, Vol. 1, EPA/600/9-91-026a (NTIS PB91-234443), February 1991.

Rog84 Rogers, V.C. and Nielson, K.K., and Kalkwarf, D.R., Radon Attenuation Handbook for Uranium Mill Tailings Cover Design, Washington D. C.: U. S. Nuclear Regulatory Commission report *NUREG/CR-3533*, 1984.

Rog89 Rogers, V.C., Nielson, K.K., and Merrell, G.B., Radon Generation, Adsorption, Absorption, and Transport in Porous Media. Washington D. C.: U. S. Department of Energy report *DOE/ER/60664-1*; 1989.

Rog90 Rogers, V.C. and Nielson, K.K., Benchmark and Application of the RAETRAD Model, in: Proceedings: the 1990 International Symposium on Radon and Radon Reduction Technology, Vol. 2, *EPA/600/9-91/026b* (NTIS PB91-234450), VI-1, 1991.

Rog91a Rogers, V.C. and Nielson, K.K., Multiphase Radon Generation and Transport in Porous Materials. *Health Physics* **60**:807-815, 1991.

Rog91b Rogers, V.C. and Nielson, K.K., Correlations for Predicting Air Permeabilities and ^{222}Rn Diffusion Coefficients of Soils. *Health Physics* **61**:225-230, 1991.

Rog95 Rogers, V.C., Nielson, K.K., and Holt, R.B., Radon Generation and Transport in Aged Concrete, U. S. Environmental Protection Agency Report EPA-600/R-95-032 (NTIS PB95-181590), February 1995.

San90 Sanchez, D.C., Dixon, R, and Williamson, A.D., The Florida Radon Research Program: Systematic Development of a Basis for Statewide Standards, in Proceedings: the 1990 International Symposium on Radon and Radon Reduction Technology, Vol. 3, EPA/600-9-91-026c (NTIS PB91-234450), A-I-3, 1991.

SBC90 Florida Code for Radon-Resistant Construction and Mitigation, Southern Building Code Congress International, Inc., Rev. 1, January 1990.

Sco88 Scott, A.G. and Robertson, A., Follow-Up Alpha-Track Monitoring of 40 Eastern Pennsylvania Houses with Indoor Radon Reduction Systems (Winter 1987-88), U. S. Environmental Protection Agency, AEERL report *EPA/600/8-88/098* (NTIS PB89-110035), September 1988.

Sco89 Scott, A.G. and Robertson, A., Follow-Up Alpha-Track Monitoring in 40 Eastern Pennsylvania Houses with Indoor Radon Reduction Systems (Winter 1988-89), U. S. Environmental Protection Agency, AEERL report *EPA/600/8-89/083* (NTIS PB90-134172), October 1989.

SCS75 Soil Conservation Service, Soil Taxonomy. A Basic System of Soil Classification for Making and Interpreting Soil Surveys. Washington D. C.: U. S. Department of Agriculture, Soil Conservation Service. *Agriculture Handbook No. 436*, 1975.

SCS91 Soil Conservation Service, State Soil Geographic Data Base (STATSGO) Data Users Guide, Lincoln, Nebraska: National Soil Survey Center, Soil Conservation Service, U. S. Department of Agriculture, report, 1991.

Sul88 Sullivan, T.M., Kempf, C.R., Suen, C.J., and Mughabghab, S.M., Low-Level Radioactive Waste Source Term Model Development and Testing, Washington D. C.: U. S. Nuclear Regulatory Commission report *NUREG/CR-5204*, 1988.

Swe86 Swedjemark, G.A., Swedish Limitation Schemes to Decrease Rn Daughters in Indoor Air, *Health Physics* **51**:569-578, 1986.

Swe90 Swedjemark, G.A. and Makitalo, A., Recent Swedish Experiences in ^{222}Rn Control, *Health Physics* **58**:453-460, 1990.

Tha82 Thamer, B.J., Nielson, K.K., and Felthauser, K. The Effects of Moisture on Radon Emanation. Washington D.C.: U.S. Department of the Interior, Bureau of Mines; Open File Report *OFR-184-82*, 1982.

Tho64 Thornthwaite, C.W. and Mather, J.R. Average Climatic Water Balance Data of The Continents. Part VII: United States. Centerton, NJ: *Publications in Climatology* **17** (3), 485, 1964.

Tho85 Thomas, B.P., Cummings, E., and Wittstruck, W.H., Soil Survey of Alachua County Florida, Gainesville, FL: U. S. Department of Agriculture, Soil Conservation Service, 1985.

Von90 Vonstille, W.T. and Sacarello, H.L.A., Assessment of Health Impacts of Radon Exposures in Florida. in Proceedings: the 1990 International Symposium on Radon and Radon Reduction Technology, Vol. 3, *EPA/600/9-91-026c* (NTIS PB91-234450), A-II-4, 1991.

Wil91 Williamson, A.D. and Finkel, J.M. Standard Measurement Protocols, Florida Radon Research Program, EPA-600/8-91-212 (NTIS PB92-115294), November 1991.

Yeh87 Yeh, G.T., FEMWATER: A Finite Element Model of Water Flow Through Saturated-Unsaturated Porous Media - First Revision, Oak Ridge, TN: U. S. Department of Energy report *ORNL-5567/R1*, 1987.